OXYGEN TRANSPORT IN OXIDES OF FLUORITE STRUCTURE.

A Thesis

presented for the degree of

DOCTOR OF PHILISOPHY

in the

UNIVERSITY OF LONDON

by

JOHN MILLICE FLOYD

Department of Metallurgy,
Royal School of Mines,

November 1969.

Abstract.

Gaseous exchange measurements on the rate of depletion of oxygen - 18 from the gas phase consisting of N_2 - O_2 and CO-CO_2 mixtures in the temperature range 850 - 1150°C were made on single crystal(S) and polycrystalline(P) CeO_2 (S and P), $CeO_{(2-x)}$ (S and P), $Ce_{(1-2x)}\ Y_{2x}O_{(2-x)}$(P), thoria-yttria (P), and zirconia-yttria (S and P) specimens. Results revealed an effect due to a surface exchange reaction as well as diffusion. Arrhenius equations found for diffusion coefficients (D) and surface exchange coefficients (K) were:

CeO_2 (S) - 0.21 atm. oxygen pressure.

$D = 1.9^{+5.7}_{-1.4} \times 10^{-4} \exp(-24.8 \pm 3.5\ \text{k.cal./RT})$

CeO_2 (S) - 0.02 atm. oxygen pressure.

$D = 1.8^{+2.1}_{-1.1} \times 10^{-5} \exp(-17.4 \pm 1.9\ \text{k.cal/RT})$

$CeO_{1.92}$ (S) - CO-CO_2 mixtures.

$D = 1.5^{+6.1}_{-1.2} \times 10^{-5} \exp(-11.9 \pm 3.9\ \text{k.cal/RT})$

$CeO_{1.80}$ (S) - CO-CO_2 mixtures.

$D = 6.2^{+25}_{-5.0} \times 10^{-6} \exp(-3.6 \pm 4.2\ \text{k.cal/RT})$

$K = 6.8^{+334}_{-6.7} \exp(-28.4 \pm 10.0\ \text{k.cal/RT})$

CeO_2 (P) - 0.21 atm. oxygen pressure.

$D = 1.4^{+0.4}_{-0.3} \times 10^{-4} \exp(-21.3 \pm 0.6\ \text{k. cal/RT})$

$Ce_{0.90}Y_{0.10}O_{1.95}$ (P) - 0.21 atm. oxygen pressure.

$D = 1.5^{+1.2}_{-0.6} \times 10^{-4} \exp(-19.2 \pm 1.4\ \text{k.cal/RT})$

$Ce_{0.80}Y_{0.20}O_{1.90}$ (P) - 0.21 atm. oxygen pressure.

$D = 1.7^{+4.1}_{-1.2} \times 10^{-4} \exp(-18.3 \pm 3.0\ \text{k.cal/RT})$

$K = 1.7^{+6.8}_{-1.4} \times 10 \exp(-33.5 \pm 4.1\ \text{k.cal/RT})$

$Ce_{0.60}Y_{0.40}O_{1.80}$ (P) - 0.21 atm. oxygen pressure.

$$D = 5.1^{+5.1}_{-2.5} \times 10^{-3} \exp(-21.3 \pm 1.7 \text{ k.cal/RT})$$

$$K = 4.9^{+150}_{-4.7} \times 10^{2} \exp(-36.5 \pm 8.7 \text{ k. cal/RT})$$

$Th_{0.90}Y_{0.10}O_{1.950}$ (P) - CO-CO_2 mixtures.

$$D = 1.8^{+16}_{-1.6} \times 10^{-4} \exp(-22.0 \pm 5.8 \text{ k.cal/RT})$$

$Th_{0.85}Y_{0.15}O_{1.925}$ (P) - 0.21 atm. oxygen pressure.

$$D = 5.5^{+8.0}_{-3.3} \times 10^{-5} \exp(-18.2 \pm 1.1 \text{ k.cal/RT})$$

$Zr_{0.844}Y_{0.156}O_{1.920}$ (S) - 0.21 atm. oxygen pressure.

$$D = 1.5^{+0.8}_{-0.4} \times 10^{-5} \exp(-11.3 \pm 1.0 \text{ k.cal/RT})$$

$$K = 8.7^{+3.9}_{-2.7} \times 10^{-1} \exp(-27.3 \pm 0.9 \text{ k.cal/RT})$$

$Zr_{0.850}Y_{0.150}O_{1.925}$ (P) - 0.21 atm. oxygen pressure.

$$D = 2.6^{+4.3}_{-1.6} \times 10^{-4} \exp(-21.7 \pm 2.5 \text{ k. cal/RT})$$

$$K = 9.1^{+41}_{-7.1} \times 10^{-2} \exp(-22.1 \pm 3.8 \text{ k. cal/RT})$$

For $CeO_{(2-x)}$ and $Ce_{(1-2x)}Y_{2x}O_{(2-x)}$ the diffusion coefficient increased considerably with x. The increase seemed to be due to different factors in the two systems, and this was explained in terms of proposed structural entities for the two types of solution.

The rate of the surface exchange process was shown to be limited by adsorption or desorption. Results indicated that the adsorption site was produced by the same entity which controlled diffusion. The availability of electrons at the surface did not seem to affect the adsorption-desorption process, and a reaction scheme involving oxygen vacancies was proposed.

Diffusion coefficients in polycrystalline ceria specimens were higher than for single crystals, suggesting more rapid grain boundary diffusion.

For ceria in air this was visually confirmed using a technique of proton activation with autoradiography.

The specimen preparation in this investigation was such that the defects on the cation sublattice were appropriate to a temperature of about 2000°C. An exchange experiment with a zirconia-yttria single crystal annealed in air at 1400°C revealed no significant change in diffusion coefficient or surface exchange coefficient.

TABLE OF CONTENTS.

		Page
CHAPTER 1.	INTRODUCTION	1
1.1.	General Introduction.	1
1.2.	The Fluorite Structure.	2
1.3.	Ceria.	2
1.4.	Experimental Techniques for Studying Oxygen Transport in Oxides.	6
1.5.	Previous Work on Oxygen Transport in Fluorite Structure Oxides.	11
1.6.	Scope of the Present Investigation	14
CHAPTER 2.	EXPERIMENTAL	16
2.1.	Materials.	16
2.2.	Specimen Preparation.	22
2.3.	Gaseous Exchange.	23
2.4.	Proton Activation and Autoradiography	29
CHAPTER 3.	RESULTS	30
3.1.	Gaseous Exchange Results	30
3.2.	Errors in Exchange Experiments.	44
3.3.	Proton Activation and Autoradiography	54
CHAPTER 4.	DISCUSSION	59
4.1.	Introduction.	59
4.2.	Diffusion Coefficients	59
4.3.	Surface Exchange Coefficients.	89
4.4.	Applications.	97
4.5.	Suggestions for Further Work.	98
Conclusions.		99
References.		100

Appendix 1. Treatment of mass spectrometer results. 106
Appendix 2 Computer programs. 111
Appendix 3. Sample calculation. 118
Appendix 4. Tabulated results. 123
Appendix 5 - CeO_{2-x} dissociation pressures 135
Acknowledgements. 136

LIST OF ILLUSTRATIONS.

Figure		Page.
1.	Unit cell of the fluorite structure.	3.
2.	The CeO_2- $CeO_{1.5}$ phase diagram.	4.
3.	"String" of octahedrally co-ordinated Ce^{3+}	7.
4.	Oxygen diffusion in fluorites.	13.
5.	Isotope exchange apparatus.	24
6.	Ceria diffusion coefficients (single crystals)	32.
7.	Ceria surface exchange coefficients (single crystals).	33
8.	Log D vs. log Po_2 for ceria single crystals.	35
9.	Log D vs. x in $CeO_{(2-x)}$ and $Ce_{(1-2x)}$ Y_{2x} $O_{(2-x)}$ at 1100°C	36
10.	Log K vs. x in $CeO_{(2-x)}$ and $Ce_{(1-2x)}$ Y_{2x} $O_{(2-x)}$ at 1100°C.	37
11.	Log D vs. $10^4/T°K$ for CeO_2 - $YO_{1.5}$ solid solutions.	39
12.	Log K vs. $10^4/T°K$ for CeO_2 - $YO_{1.5}$ solid solutions.	40.
13.	Log D vs. $10^4/T°K$ for thoria - yttria and zirconia - yttria.	42.
14.	Log K vs. $10^4/T°K$ for thoria - yttria and zirconia - yttria.	43.
15.	Photomecrograph (x80) of autoradiograph of the grain boundary region of a ceria single crystal aggregate bombarded with 2.8 MeV protons at 20 nanoamps.	55.
16.	Same as figure 15 (x 320)	55.

17. Photomicrograph (x 500) of autoradiograph of grain boundary region of a ceria single crystal aggregate bombarded with 3.1 MeV protons at 100 nanoamps. 57.

18. Same autoradiograph as fig. 17. surface region (x80) 57.

19. Same autoradiograph as figures 17 and 18. Diffusion front of surface region (x 500) 58

20. Oxygen diffusion in ceria based fluorites. 60.

21. Oxygen diffusion in thoria and zirconia based fluorites. 61.

22. Log D vs. log Po_2 for ceria in N_2 - O_2 mixtures at 1100°C. 67.

23. Log D vs. log x for $CeO_{(2-x)}$ and $Ce_{(1-2x)}\ Y_{2x}\ O_{(2-x)}$ at 1100°C. 76.

24. Log D_o vs. x for $CeO_{(2-x)}$ and $Ce_{(1-2x)}\ Y_{2x}\ O_{(2-x)}$ 77.

25. Log D_o vs. log x for $CeO_{(2-x)}$ and $Ce_{(1-2x)}\ Y_{2x}\ O_{(2-x)}$. 78.

26. Q_D vs. x for $CeO_{(2-x)}$ and $Ce_{(1-2x)}\ Y_{2x}\ O_{(2-x)}$. 79.

27. Surface exchange coefficients. 93.

28. Diffusion coefficients. 95.

29. Mass spectrometer trace - N_2 - O_2. 107.

30. Mass spectrometer trace - CO - CO_2. 109.

31. Mt/M_∞ vs. $(Dt/\ell^2)^{\frac{1}{2}}$ for plane sheet geometry. = 0.57. 114.

32. Mt/M_∞ vs. $(Dt/\ell^2)^{\frac{1}{2}}$ for spherical geometry. = 0.19. 117.

117.
33. Dt/ℓ^2 vs. t for run 49. 121.
34. Dissociation pressures vs. x in $CeO_{(2-x)}$ 135.

1. 2. The Fluorite Structure.

The unit cell of the fluorite structure is shown in fig. 1. The cations form a face centered cubic sublattice within which the anions occupy simple cubic positions.

The common binary oxides with this structure are UO_2, ThO_2, CeO_2, PrO_2, and TbO_2. ZrO_2 has a distorted fluorite type structure. A unique property of these oxides is that the oxygen diffusivity is greater than that of the cation [1]. The cation sublattice can be considered as rigid while the oxygen ions are relatively free to move through the oxygen sublattice by means of vacancies or interstitials.

Pure thoria exhibits no appreciable departure from stoichiometry, but the other fluorite oxides have very large ranges of non stoichiometry, with oxygen excess due to interstitials in $UO_{(2+x)}$, and with oxygen deficiency due to vacancies in $UO_{(2-x)}$, $CeO_{(2-x)}$, $PrO_{(2-x)}$, and $TbO_{(2-x)}$. With all of the fluorite oxides very large concentrations of vacancies are shown, by comparison of pycnometric and x-ray densities, to be introduced into the anion sublattice by addition of lower valent cations.

1. 3. Ceria.

The phase diagram for the system CeO_2 - $CeO_{1.5}$, derived by Bevan and Kordis [2] from x-ray (3,4,5,6) and tensiometric (2,7,8) studies, is shown in fig. 2. The phases are:

α	-	fluorite;
β and γ	-	rhombohedral;
TCO	-	ordered type - C rare-earth oxide;
TCD	-	disordered type - C rare-earth oxide;
TA	-	type - A rare-earth oxide.

At high temperatures ceria of disordered fluorite structure exists over the composition range $CeO_{2.00}$ - $CeO_{1.72}$. At lower temperatures a series of ordered phases, related to the fluorite structure by ordered omission of oxygen ions, is formed.

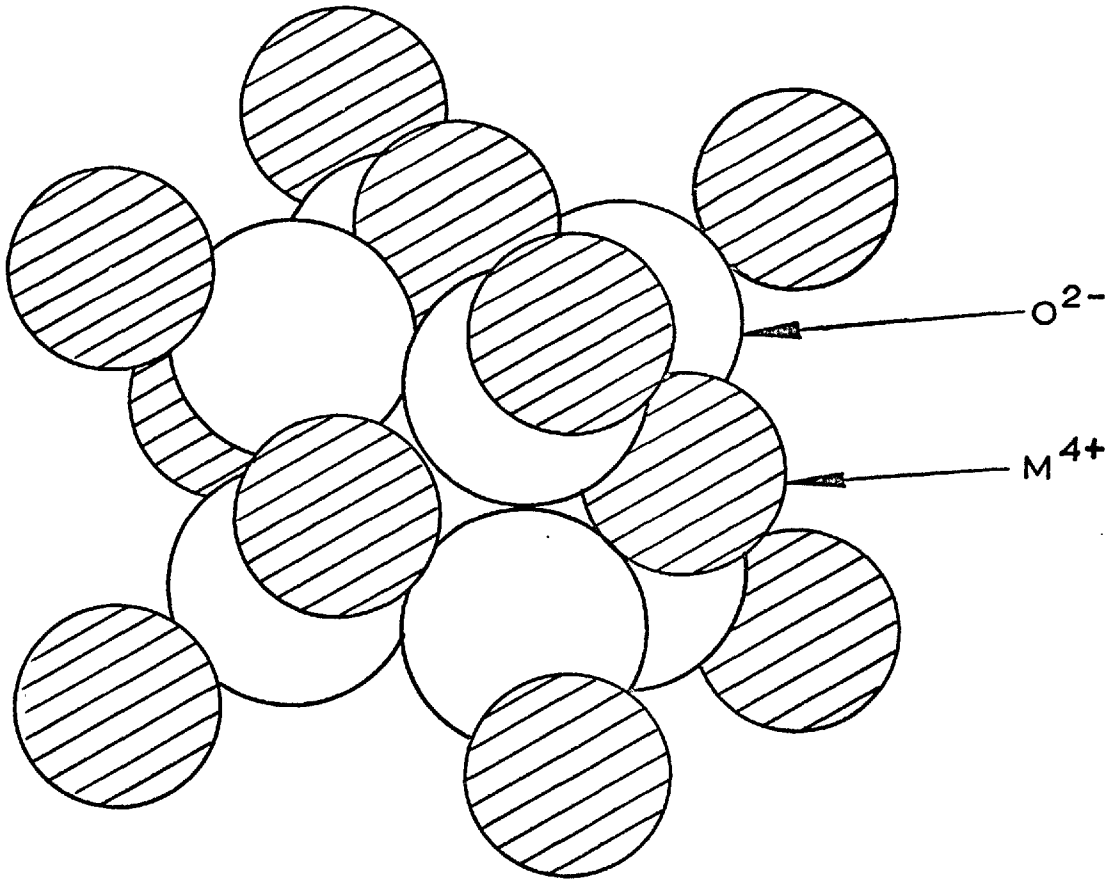

Fig.1. UNIT CELL OF THE FLUORITE STRUCTURE

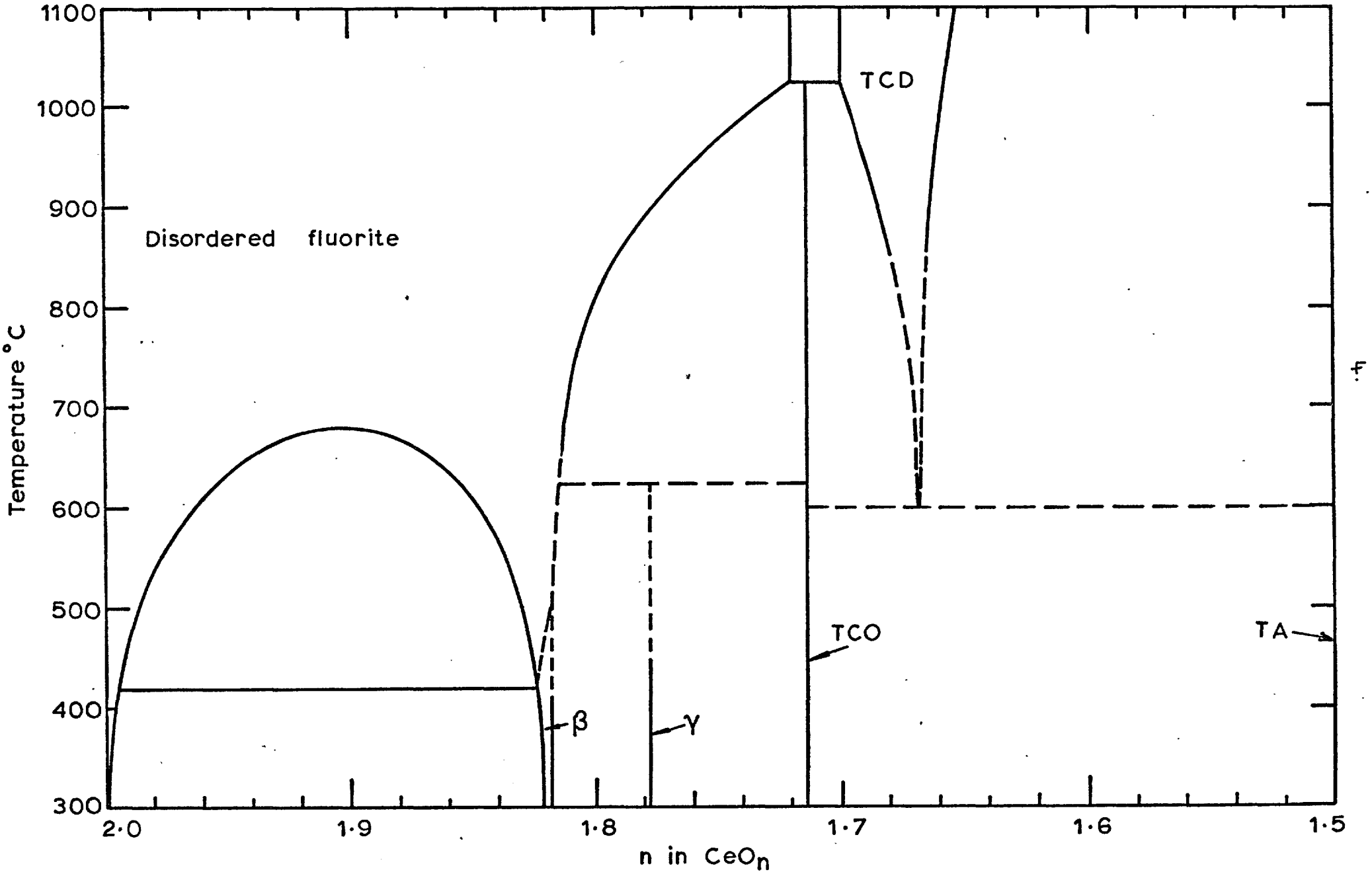

Fig.2. THE $CeO_2 - CeO_{1.5}$ PHASE DIAGRAM.

The other fluorite rare-earth oxides, PrO_2 and TbO_2, have very similar phase diagrams with their sesquioxides, and Hyde and Eyring[9] suggested a homologous series $R_n O_{(2n-2)}$ for the low temperature phases. They suggest that the low temperature phase relations in CeO_2 - $CeO_{1.5}$ should be modified to include ordered phases at $CeO_{1.800}$ and $CeO_{1.818}$, and the existence of $CeO_{1.833}$ is doubted.

Introduction of lower valent cations into the ceria fluorite lattice occurs with charge compensation by oxygen vacancy formation. Very large vacancy concentrations can be introduced in this way. In the ceria-yttria system the fluorite type phase exists to about 50 mole % $YO_{1.5}$ (10, 11, 12), followed by a two phase region and a large range of compositions with C-type rare earth oxide structure.

For large range nonstoichiometric compounds the classical Schottky-Wagner treatment of defects cannot be used because of interaction between defects at the high concentrations implied. For oxides such as $Fe_{(1-x)}O$ and $UO_{(2+x)}$ it is thought that the defects cluster into "microdomains" of the next oxide in the system (Fe_3O_4 and U_4O_9) (13,14).

The ordering of vacancies into microdimains has been invoked in the $CeO_{(2-x)}$ (9) and $Ce_{(1-2x)}$ Y_{2x} $O_{(2-x)}$ systems (9, 10, 12) In the latter it was suggested that for $YO_{1.5}$ contents of less than 12 mole % a random or complexed oxygen vacancy model applied, and that above this the anions or vacancies were ordered into microdomains of essentially C-type rare-earth oxide structure; giving rise to body centered cubic superstructure lines in the x-ray diffraction pattern. It was implied that the lack of mobility in the ceria-yttria system did not allow the formation of the homologous series observed in the RO_2 - $RO'_{1.5}$ systems, and that at low temperatures the solid solution was metastable with respect to these phases[10]

Strings of trivalent cations octahedrally co-ordinated to oxygen ions, with cube diagonals along the strings vacant - as shown in figure 3 - have been postulated as the structural component in microdomains in ceria and its solid solutions[9]. The strings are surrounded by 7- coordinated cations. In the disordered fluorite-type phases it is suggested that strings are randomly oriented and that they align in one or more of the

four ⟨111⟩ directions in the low temperature $R_nO_{(2n-2)}$ phases. (9)

The structure of the two phases apart from the fluorite which are known with any certainty in the RO_2-R_2O_3 systems-C-type rare-earth oxide and rhombohedral R_7O_{12} - comprise these strings, but their presence in the other phases and in the fluorite solution is only hypothetical.

Hyde and Eyring (9) show that in the ceria-yttria solution the intersection of randomly oriented strings would produce C-type rare-earth oxide regions in the fluorite lattice; explaining the body centered cubic x-ray superstructure lines (10, 12).

1. 4. Experimental Techniques for Studying Oxygen Transport in Oxides.

A brief outline is given of the methods available for studying oxygen transport in oxides.

1. 4. 1. Electrical measurements.

The electrical conductivity and transport number for oxygen ions can be used to calculate the diffusion coefficient by means of the Nernst-Einstein equation:

$$D = f \cdot \frac{\sigma \cdot t \cdot k \cdot T}{n \cdot z^2 \cdot e^2} \qquad \ldots\ldots\ldots(1.1)$$

where σ is the electrical conductivity;
t is the transport number;
k is Boltzman's constant;
T is the Absolute temperature;
n is the number of charge carriers per cm^3
z is the charge associated with the ion;
e is the charge of an electron;
f is the correlation coefficient (0.653 for oxygen in fluorites)

1. 4. 2. Oxidation studies.

The oxidation rate of a metal or oxide can be used to obtain transport properties where the rate determining step is the transport of oxygen in

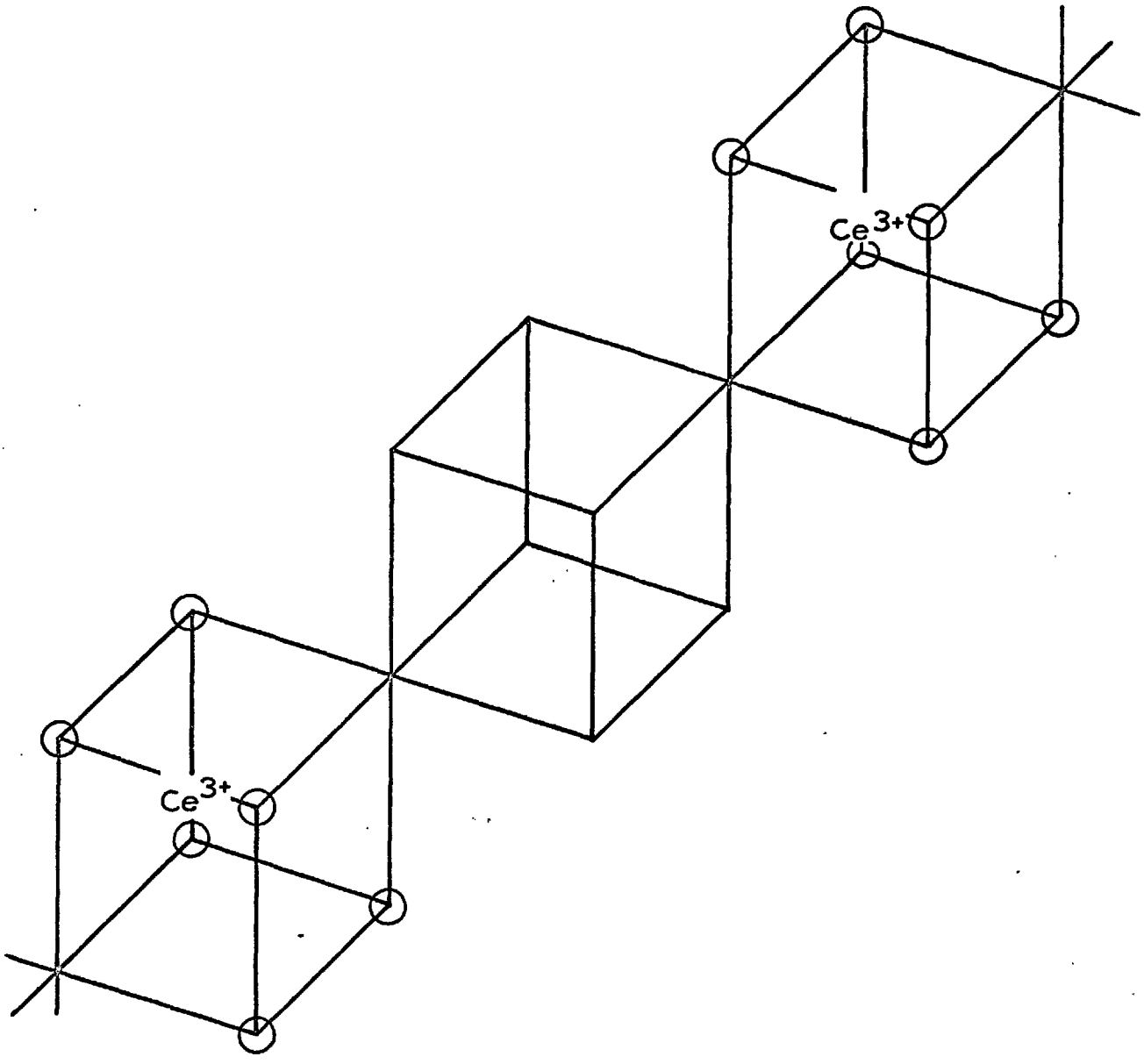

Fig.3. 'STRING' OF OCTAHEDRALLY CO-ORDINATED Ce^{3+}

the oxide. A chemical diffusion coefficient across a concentration gradient is obtained which may involve a flux of electrons or holes as well as ions. If the variation of chemical potential with concentration is known the self diffusion coefficient can be found using a relation such as the Wagner equation for metal oxidation

$$\tilde{D} = \left\{ |Z_1| D_1^* + |Z_2| D_2^* \right\} \cdot \frac{C_{eq}}{\tilde{C}} \cdot \left[\frac{1}{RT} \frac{\partial \mu_O}{\partial \ln C} \right] \qquad \ldots\ldots(1.2)$$

where $\tilde{D}$ is the chemical diffusion coefficient; D_1^* and D_2^* are the self diffusion coefficients of cation and anion of valence Z_1 and Z_2; C_{eq} is the total concentration of anions in equivalents per cm^3 and $\tilde{C}$ is the concentratinn of oxygen defects; μ_O is the chemical potential of oxygen in ergs per gram atom.

1.4.3. Permeability.

The permeability to oxygen may be measured if a high temperature seal can be made. Knowing the dimensions of the oxide, the chemical diffusion coefficient can be calculated from Fick's first law:

$$J = - D \frac{\partial C}{\partial x} \qquad (1.3)$$

where J is the flux and $\partial C / \partial x$ is the change in oxygen concentration with distance across the oxide.

1.4.4. Electrochemical Measurements.

A galvanic cell incorporating a solid oxide electrolyte with the oxide of interest as one electrode can be established with an oxygen potential difference across the cell

$$\text{Fe - FeO} \;(\mu'_{O_2}) \;\Big|\; \text{solid oxide electrolyte} \;\Big|\; \text{oxide, CO-CO}_2 \;(\mu''_{O_2})$$

an imposed e.m.f. depletes the oxide-electrolyte interface of oxygen ions and the resultant change of current with time can be used to find the chemical diffusion coefficient since

$$i = \frac{2F\ (C_b - C_s)\sqrt{D}}{\sqrt{\Pi}\ t} \qquad (1.4)$$

where C_b and C_s are the oxygen ion concentrations in the bulk and at the interface, i is the current and t is the time[15]

1. 4. 5. Isotopic exchange

Experiments involving the isotopic exchange of oxygen with an oxide can be used in several ways to give diffusion coefficients. Since there is no radioactive isotope of oxygen with sufficient half life for normal counting techniques to be used, these methods generally rely on the different masses of ^{16}O, ^{17}O, and ^{18}O to follow the diffusion process.

Two basic methods of gaseous exchange may be used.

a/ The depletion of an enriched isotope from the gas phase during exchange with the solid may be measured as a function of time. These results are fitted to a solution of the diffusion equation for appropriate boundary conditions and solid geometries to yield diffusion coefficients as shown in chapter 2.

b/ After a duffusion anneal the profile of an enriched isotope may be obtained in four ways.

(i) Sections can be ground off the specimen and analysed for isotopes in a mass spectrometer.

(ii) The ionic secondary emission upon sputtering of the sample surface by a primary argan ion beam can be measured continuously with an ion mass analyser.

(iii) A cross section can be proton bombarded to produce the nuclear reaction

$$^{18}_{8}O + ^{1}_{1}H = ^{18}_{9}F + ^{1}_{0}n$$

The positron decay of ^{18}F can be used to determine the ^{18}O profile by autoradiography.

(iv) The surface can be bombarded to produce the nuclear reactions

$$^{17}_{8}O + ^{3}_{2}He = ^{16}_{8}O + ^{4}_{2}He$$

and

$$^{18}_{8}O + ^{1}_{1}H = ^{15}_{7}N + ^{4}_{2}He$$

and α-ray spectroscopy used to determine the profile close to the surface [16]

The profile resulting from these techniques may be treated according to the equations

$$C_{(x,t)} = \frac{Co}{\sqrt{\pi D t}} \exp\left(\frac{-x^2}{4D t}\right) \qquad (1.5)$$

if the concentration at the surface is depleted, and

$$C_{(x,t)} = Co \ \mathrm{erfc}\left(\frac{x}{2\sqrt{D t}}\right) \qquad (1.6)$$

if the surface concentration is constant.

C is the concentration at distance X; C_o is the initial concentration at the surface, D is the diffusion coefficient, and t is the anneal time. More complicated analyses are required when enhanced grain boundary diffusion occurs and when the surface reaction rate is finite.

1. 4. 6. Discussion

Electrical measurements and permeability studies are most reliable for highly doped fluorites where the transport number is known accurately (unity) and where the diffusion coefficient, in permeability measurements, does not change across the specimen.

The electrochemical technique has not, as yet, been used successfully for oxides due to the difficulty of sealing the electrolyte-oxide interface from the gas phase.

Oxidation studies require numerous assumptioss which must be proven before reliable chemical diffusion coefficients can be obtained. The variation of chemical potential with concentration is then required to obtain the self diffusion coefficient.

Isotopic exchange experiments provide the most direct and reliable method for obtaining transport coefficients. The depletion of isotope from the gas phase requires assumptions concerning the diffusion process, cannot separate grain boundary from bulk diffusion, and is less direct than the methods involving profiles. It has the advantage for the present work that it measures the overall rate of oxygen transfer from the gas phase into the solid phase, which is the process occurring in electrochemical cells. Surface exchange coefficients as well as diffusion coefficients can be obtained. This method is generally used in studies of oxygen diffusion in oxides.

The diffusion profile methods can also give surface exchange coefficients as well as diffusion coefficients and can separate the diffusion due to high diffusivity paths from the bulk diffusion. Hence the technique gives more information and requires fewer assumptions than the other methods. Analysis of sections requires a reproducible method for obtaining the ^{18}O from the solid phase in a suitable form for mass analysis, and this has proven a difficulty in the past.

The technique of sputtering and ion mass analysis has very recently been developed[17]. One limitation is that the ionic secondary emission depends on the relative orientation of the bombarding beam and the individual crystals in polycrystalline specimens.

The (p,n) reaction produces a profile and, if autoradiography is used, can provide a visual proof of high diffusion paths.

The (^3He,α) and (p,α) reactions only give profiles to a depth of 5 μ and 0.5 μ respectively, and therefore could be influenced by surface effects. Diffusion depths of this order would also be reached in very short anneals with the high oxygen diffusivities encountered in fluorite oxides.

1.5. Previous work on oxygen transport in fluorite structure oxides.

Fig. 4 shows the oxygen diffusion coefficients calculated from electrical measurements on ceria, ceria-yttria, thoria-yttria, and Zirconia-yttria solid solutions, and obtained by oxidation of reduced ceria.

These are compared with oxygen diffusion coefficients reported in the literature for other fluorite oxides.

1.5.1. Ceria.

Several workers have reported the electrical conductivity of ceria at high oxygen partial pressures[18-23]. These are all in good agreement with the results of Takahashi and Iwahara[23]. As discussed in section 4.2.2. the transport number for oxygen ions is in doubt but if the constant value of 0.3 given by Takahashi and Iwahara above 800°C is used with their electrical conductivity values the line for CeO_2(1) shown in Fig. 4. is obtained.

When the present investigation was almost completed a report of work in which the rate of oxidation of reduced ceria single crystals was used to obtain diffusion coefficients was published by Vinokurov and Ioffe[24]. The ceria was reported to contain 10^{-5} at. % Gd^{3+} for the line shown as CeO_2(2) and 0.3 at. % Gd^{3+} for CeO_2(3).

Neuimin and Pal'guev[21] measured the conductivity of ceria-yttria solutions and determined a transport number of unity for the oxygen ion. $Ce_{0.739}Y_{0.261}O_{1.870}$ had the maximum conductivity of the compositions studied and the diffusion coefficients calculated for this are shown in Fig. 4.

1.5.2. Thoria.

Edwards et. al.[25] studied gaseous exchange of ^{18}O with ThO_2. They found that the surface exchange process contributed to the overall rate of uptake. Their Arrhenius plot of the diffusion coefficients is shown in Fig. 4.

Thoria-yttria solid solutions have an oxygen transport number of unity over a wide temperature and oxygen pressure range. The electrical conductivity has been studied by Lasker and Rapp[26] and Steele and Alcock[27]. The former work gives higher values, and since the most usual fault in high temperature electrical conductivity measurements - poor contacts - lead to lower values, these were used to calculate the diffusion

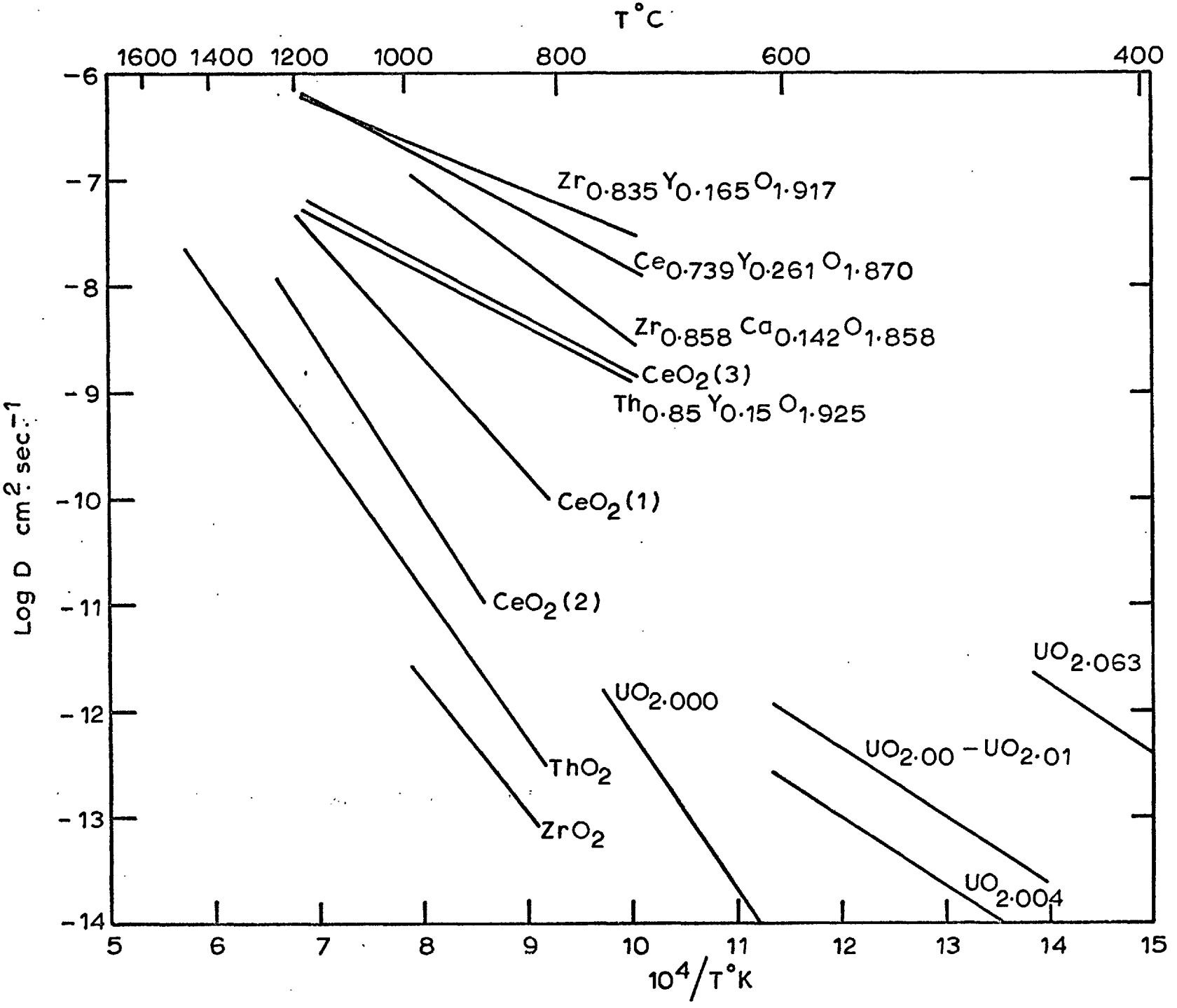

Fig.4. OXYGEN DIFFUSION IN FLUORITES

coefficients shown in Fig. 4.

1.5.3. Zirconia.

The line for ZrO_2 shown in Fig. 4. is from the exchange measurements of Madeyski and Seltzer[28]. The oxidation of metallic zirconium (29,30) and nonstoichiometric zirconia (31) gave diffusion coefficients considerably higher.

The ^{18}O exchange profile results of Simpson and Carter[32] for zirconia-calcia solutions shown in figure 4 were in good agreement with the results of Kingery et. al.[33] An effect due to a slow surface exchange reaction was observed.

The electrical conductivity and transport number of unity found by Strickler and Carlson[34], in good agreement with Dixon et. al.[35], for zirconia-yttria solutions were used to calculate the diffusion coefficients shown for $Zr_{0.835}\ Y_{0.165}\ O_{1.917}$.

1.5.4. Urania.

The diffusion coefficients shown in Fig. 4. for $UO_{(2+x)}$ were obtained from ^{18}O exchange depletion experiments reported by Belle and Lustman[36] for $UO_{2.00}$ - $UO_{2.01}$ and Austern and Belle[37] for $UO_{2.000}$, $UO_{2.004}$ and $UO_{2.063}$.

The recent oxygen diffusion studies at higher temperatures of Roberts et. al[38] by isotope depletion and Marin and Contamin[39] by isotope profile determinations gave good agreement with the work of Belle et. al. for nearly stoichiometric urania. A similar increase of diffusion coefficient with x in $UO_{(2+x)}$ to that found by Belle et. al. was noted in both studies.

1.6. Scope of the Present Investigation.

Examination of Fig. 4. reveals that an enhancement of oxygen diffusion coefficients of several orders of magnitude occurs with addition of lower valent ions to fluorite oxides. In the $UO_{(2+x)}$ system increased nonstoichiometry results in a significant increase in the oxygen

diffusivity. The ceria based system allows a study of the effect of both nonstoichiometry and the addition of lower valent ions on oxygen transport rates over very large ranges of x in $CeO_{(2-x)}$ and $Ce_{(1-2x)}$ Y_{2x} $O_{(2-x)}$.

In some of the previous work the rate of the gas-solid interfacial reaction played a part in the overall kinetics of gas uptake, so that in applications requiring fast transport rates in solid oxide electrolytes this reaction should be considered. The gaseous exchange technique observing depletion of ^{18}O from the gas phase allows both this reaction and diffusion to be studied and this was selected as the method for the present investigation.

In order to check the magnitude of diffusion coefficients obtained, and to observe the effect of grain boundaries, the praton activation technique was also employed.

The effect of gas mixtures, nonstoichiometry, addition of lower valent ions, pores, and grain boundaries on transport properties was to be studied on ceria based materials.

Thoria-yttria was used as a standard since very dense polycrystalline specimens could be prepared, and the ionic conductivity is established.

The availability of large single crystals and dense polycrystalline zirconia-yttria made this material attractive for a further study of the effect of grain boundaries. The ionic conductivity is also well known, allowing this material to be used as a second standard.

Chapter 2.

Experimental.

2.1. Materials.

2.1.1. Polycrystalline specimens.

Table 1 summarises the porosity observed under the microscope, grain size, and density of polycrystalline specimens.

Table 1

Details of polycrystalline specimens.

Specimen	Visual porosity %	Density g/cm^3	Grain size. μ
CeO_2 prep. 1	10	6.40	100
CeO_2 prep 2	20	5.27	50
$Ce_{0.90}Y_{0.10}O_{1.950}$	10	6.50	50
$Ce_{0.80}Y_{0.20}O_{1.900}$	10	5.73	35
$Ce_{0.60}Y_{0.40}O_{1.800}$	5-10	5.56	35
$Zr_{0.85}Y_{0.15}O_{1.925}$	0	5.95	10
$Th_{0.90}Y_{0.10}O_{1.950}$	< 5	9.35	20
$Th_{0.85}Y_{0.15}O_{1.925}$	< 5	9.25	30

(i) Ceria.

Ceria powder was prepared from 99.9% cerric ammonium nitrate by oxalate precipitation from a solution of pH 8.4, followed by calcining and grinding. The powder was mixed with a binder, pressed into discs and pre-fired at 1000°C. Final firing at 1700°C in air for 24 hours produced discs with about 10% unconnected porosity. Discs prepared from

powders produced by evaporation of the nitrate solution and via a sol-gel process [40] had about the same porosity.

The grain size was approximately 100μ. Two types of pores were observed. Half of the pore volume was due to large elongated pores about 20 x 50μ occurring around the grain boundaries, and the rest were spherical pores of 10μ diameter within the grains. The density, measured by the weight change with suspension in water, was 6.40 $\pm$ .03 g/cm^3.

Another series of specimens prepared from powders produced in the same way and fired at 2000°C in air for two hours contained large bubble-like pores, which gave the discs a bloated appearance. In regions away from the large pores the material had about 20% porosity of uniform spherical size approximately 20μ diameter, with at least some pores connected. The grain size was 50μ and density 5.27 g/cm^2.

Exchange experiments were made on both types of specimens, the initial preparation being designated preparation 1 and the latter preparation 2.

No second phase was seen in unetched or etched specimens from either preparation. X-ray fluorescence and spectrographic analysis did not reveal any impurities but both preparations produced slightly straw coloured specimens. X-ray diffraction patterns corresponded to the A.S.T.M. index values for CeO_2 and gave the same lattice parameter; $a_o = 5.4110\text{Å}$.

Cubes of 2 to 3 mm edge length were cut from the discs using a diamond wheel and exchange measurements made on preparation 1 cubes with surfaces ground on 400 mesh silicon corbide paper, and on preparation 2 cubes with surfaces polished on 1μ diamond paste.

The composition of reduced $CeO_{(2-x)}$ was estabilished in CO-CO_2 gas mixtures, using the oxygen dissociation pressures for the CeO_2 - Ce_2O_3 system reported by Bevan and Kordis [2]. The reduced specimens were

black in colour, and were partly reoxidized in air at room temperature to a blue colour.

(ii) Ceria-yttria solutions.

Ceria-yttria solid solutions were prepared from 99.9% cerric ammonium nitrate and 99.9% yttria by taking appropriate quantities into nitrate solution and proceeding in the same way as for preparation 2 ceria. Well sintered discs were produced with the grain sizes, porosities, and densities shown in table 1. The 10 mole % $YO_{1.5}$ specimen had 10 % porosity as uniform spheres of diameter 5-10μ with occasional larger pores of 20μ diameter. The 10% porosity in the 20 mole % $YO_{1.5}$ specimen occurred as uniform spheres of 20μ diameter. In the specimen with 40 mole % $YO_{1.5}$ the 5-10% porosity was produced by elongated pores of size 10 x 20μ. No second phase was observed in the specimens.

X-ray diffraction patterns indexed for a fluorite lattice and gave the parameters:

10%	$a_o = 5.4085$ Å
20%	$a_o = 5.4052$ Å
40%	$a_o = 5.3928$ Å

Good agreement is found with lattice parameters obtained by Barker et.al.[10,12] for these compositions.

For exchange experiments cubes were cut from the discs and the faces polished to 1μ diamond paste.

(iii) Thoria-yttria solutions.

Thoria-15mole % yttria powders were prepared from spectroscopic-purity thorium nitrate and 99.9% yttria by oxalate precipitation at a pH of 3.2 and calcining at 800°C. The powders were mixed with a binder, pressed into discs, pre-fired at 1000°C in air and fired at 2000°C in a tungsten filament vacuum furnace for 3 hours.

The specimens were prepared in two batches under identical conditions and were transparent enough to read figures through the 1 m.m. thick tablets.

The thoria - 10 mole % yttria specimens were prepared by another worker by nitrate evaporation and had the same thermal history during sintering. Their history subsequent to preparation was not known. The specimems were opaque.

Densities, visual porosities, and grain sizes are shown in table 1. The pores in specimens with 15 mole % yttria were elongated and of regular size 1 x 2μ while the specimens with 10% yttria had most of the pores of 10 - 15μ diameter with a small proportion as elongated pores of size 1 x 2μ . No second phase was observed in any of the specimens.

X-ray diffraction patterns indexed with the fluorite structure and gave the lattice parameters:

$$10\% \quad a_o = 5.580\ \text{Å}$$

$$15\% \quad a_o = 5.570\ \text{Å}$$

These agree well with lattice parameters reported by Steele[41] for the same compositions.

For exchange experiments the discs were ground circular and the faces polished to 1μ diamond. Approximate dimensions were 1 x 0.1cm. The dimensions are shown for each exchange experiment specimen in appendix 4, table 11.

(iv) Zirconia-yttria solutions.

The oxide powder used for specimens was prepared by an autoclave technique by Zircoa* who quote a composition of 15 mole % $YO_{1.5}$. The powder was very fine and required no binder in the pressing stage. The disc was fired at 2000°C in a vacuum for 3 hours.

The grain size and density are shown in table 1. No pores were seen but when etched there appeared to be a small amount of a second phase of 1-2μ grain size.

* Zirconium Corporation of America, 31501 Solon Road, Solon 39, Ohio, U.S.A.

The x-ray diffraction pattern indexed with fluorite structure of a_o = 5.134 Å in reasonable agreement with the plot of a_o vs. composition found by Duwez et. al. [42] and Strickler and Carlson [34]. No extra lines due to another phase were seen but the fluorite lines were quite diffuse.

Cubes of edge 2-3 m.m. were cut from the disc and exchange experiments carried out with surfaces polished to 1 μ diamond paste.

2.1.2. Single crystals.

(i) Ceria.

Single crystals of ceria were supplied by the single crystal growing unit of Imperial College. They were grown from a solution of 99.9 % ceria in a flux of lead fluoride and lead borate by slow cooling and by evaporation. There was no difference between the single crystals prepared by the two methods. As well as single crystal cubes, some crystal intergrowth occurred to produce bicrystals and multicrystal aggregates, which were used for proton activation experiments. The aggregates generally contained voids trapped within them.

The cubes from the flux were 1 - 3 mm. in size, black in colour, and electron microprobe analysis revealed 200 p.p.m. lead. Firing in water-saturated oxygen for 24 hours at 1200°C produced translucent pale straw coloured crystals in which lead could not be detected.

Microscopic examination of the single crystals showed that they contained no pores, and were single phase. The x-ray powder pattern indexed with the fluorite lattice with a_o = 5.411 Å, in good agreement with the A.S.T.M. Index for CeO_2. Laué back reflection photographs showed that the cube faces corresponded to the [100] crystal plane The density of the translucent single crystals was 7.2 g/cm^3.

Most exchange experiments were carried out on the translucent cubes but in some experiments spheres prepared by grinding in an air blast of abrasive powder, and by blowing the crystal in a jet of air inside a cylinder lined with 400 mesh silicon carbide paper, were used.

Crystals reduced in the range $CeO_{(2-x)}$ were black in colour. No change in colour occurred in air at room temperature, as was observed in polycrystalline specimens. X-ray patterns for the reduced specimens contained the same lines as for CeO_2 with a change of intensity ratios and doubling of lines. There was also an indication of weak extra lines. No density change was detected as the change in the small crystals used was within the accuracy of the method; $\pm$ 0.1 g/cm^3.

(ii) Zirconia-yttria solutions.

Single crystals of zirconia - 15.6 mole % yttria were prepared by W. and C. Spicer* by arc melting 99.9% zirconia and yttria and slow cooling over six hours. Irregular shaped crystals with conchoidal faces resulted. The crystals were transparent and a pale yellow colour. Firing in air produced translucent white crystals. Single crystal patterns with well defined spots were obtained by the Laué back reflection x-ray technique before and after firing. The powder pattern indexed for the fluorite structure had a lattice parameter of a_o = 5.1378, in reasonable agreement with the lattice parameter for this composition found by Duwez et. al.[42] and Strickler and Carlson[34].

The crystals were single phase under the microscope, and contained no pores. The density was 5.96 g/cm^3.

A series of four 0.2 cm cubes were cut from one single crystal with faces corresponding to the [100] crystal plane; except for the cube for exchange run number 40 which was oriented such that two faces were parallel to the [100] plane and the other four were 30° from this plane.

A further 0.3 cm. cube was cut on the [100] planes for run 60 from another single crystal block. This specimen was fired at 2000°C for a half hour and then annealed for seven days at 1400°C prior to the exchange run. No change in density was observed within the error limits of $\pm$ .03 g/cm^3.

* W. and C. Spicer Ltd., St. Mary's , Winchcombe, Gloucester.

2. 1. 3. ^{18}O enriched gases.

Oxygen, carbon monoxide, and water containing 90% ^{18}O were obtained from the Weizmann Institute, Rehovoth, Israel.

To obtain ^{18}O enriched oxygen gas from the water it was first allowed to react with sodium amalgam under a nitrogen atmosphere to produce a sodium hydroxide solution of approximately 0.2 N. This solution was then electrolysed in a cell under a nitrogen pressure of 150 torr at a current of 50 μA. The cell was constructed so that only a very small quantity of water was required, and the volumes over the two sides of the cell were adjusted to exactly 2:1 by addition or removal of mercury in adjoining glass bulbs. When the pressure of oxygen produced had attained about 150 torr, the gas mixture was passed over sponge platinum, through a liquid gas trap, and then transferred via a Toepler pump into a gas reservoir which could be detached and taken to the exchange apparatus.

2.2. Specimen Preparation.

Except for preparation 1 polycrystalline ceria specimens, which were left roughly ground an 400 mesh paper, the cubic or disc shaped specimens were ground on 320, 400, and 600 mesh silicon carbide papers and polished on 3 μ and 1 μ diamond paste.

The natural cube surfaces of the single crystals of ceria were generally used for exchange, since they were flat and of high reflectance. In some early experiments specimens were used which had been air blasted with abrasive, or ground to spheres on 400 mesh silicon carbide paper.

Prior to exchange experiments the prepared specimens were cleaned successively in boiling 1 N potassium hydroxide solution, distilled water, and absolute alcohol.

To anneal out defects caused by cutting and grinding, specimens were prefired at 1200°C in air for a half hour before equilibrating at the oxygen pressure and temperature of the exchange run.

2.3. Gaseous Exchange

2.3.1. Apparatus.

Figure 5 shows the ^{18}O exchange apparatus. The Pt - 10% Rh reaction tube is soldered to the top brass head, which contains a viewing window, and is connected to the bottom assembly via an O-ring seal. Incorporated in this bottom assembly is an expansion bellows and a Wilson seal, through which passes a thermocouple sheath which is also used to raise and lower the specimen contained on a Pt - 10% Rh sample holder (figure 5). The reaction tube is heated in a Pt - 10% Rh wire wound furnace, controlled to $\pm$ 1°C by a "Eurotherm" proportional, integral, derivative, temperature control unit.

The gas circulating system is connected to the water cooled brass head via quick fit joints, and gas is pumped around the system at a maximum rate of 160 ml. of gas at S.T.P. per minute using an electromogmetic pump. Samples of gas of a fixed small volume can be obtained by means of the three way stop cock (figure 5).

The gas handling system is all glass and incorporates gas reservoirs, Toepler pump, mercury manometer, and a Penning vacuum gauge.

The volume of the gas circulating system is 165 ml. and the volume of the gas handling system is 180 ml.

2.3.2. Equilibration.

Prior to an exchange run specimens were fired in the apparatus in the same gas mixture, at the same temperature as the diffusion run, for sufficient time to establish equilibrium on the anion sublattice. This time varied from four days for ceria single crystals in air at 850°C to three hours for ceria - 40% yttria polycrystalline specimens in air at 1150°C, calculated using the rough guide [43] that diffusion into a slab or sphere of half-thickness or radius 1 will be substantially complete when $Dt/l^2 = 1$. The equilibration times were shown to be sufficient in exchange experiments where nearly complete exchange had occurred.

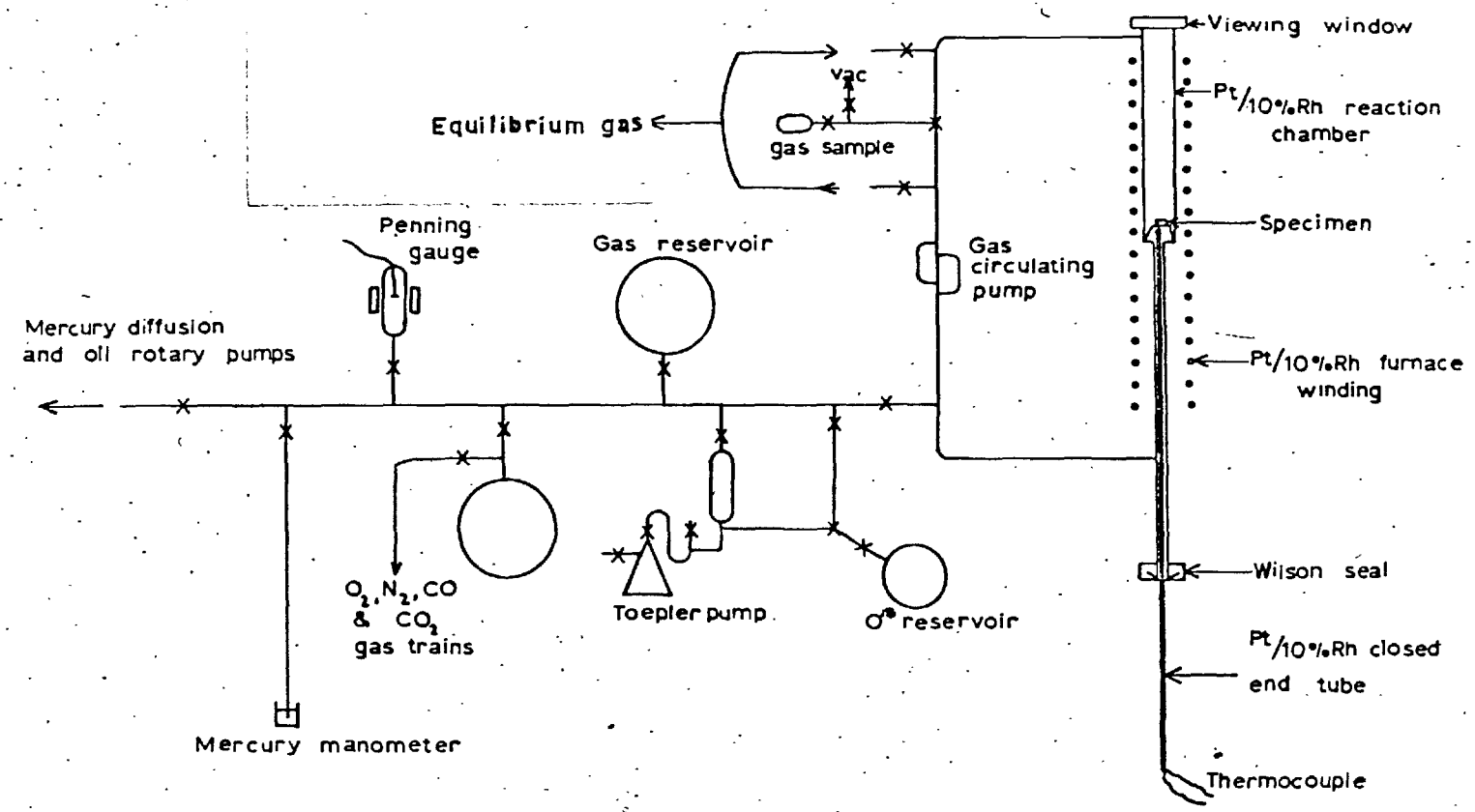

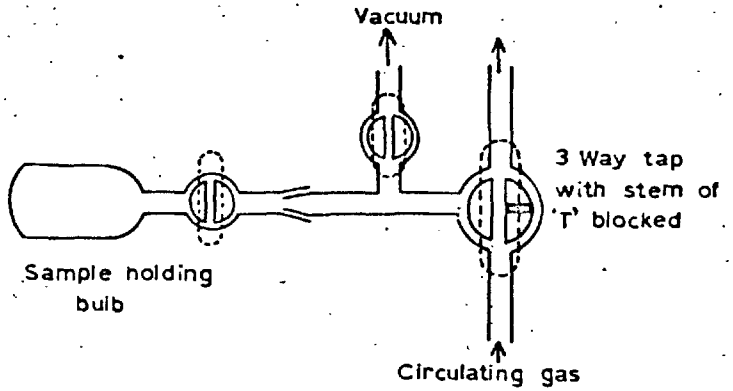

FIG. 5 ISOTOPE EXCHANGE APPARATUS

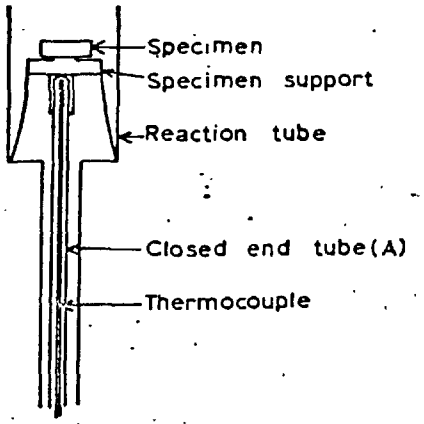

2.4.

Commercial CO_2, CO, N_2, and O_2 gases were dried by passing over silica gel and magnesium perchlorate. CO_2 was removed from CO gas by passing over "sofnolite" Capillary flow meters were used to establish the appropriate mixture of $CO-CO_2$ or N_2-O_2. The oxygen partial pressures of the $CO-CO_2$ mixtures were checked with a galvanic cell utilizing a thoria-yttria electrolyte and a Fe-FeO reference electrode.

At the end of equilibration the sample was pushed out of the hot zone and cooled rapidly in the vicinity of the brass head.

It should be noted that this equilibration of the anion sublattice would not affect the cation sublattice, since the cation diffusivities are generally several orders of magnitude lower than the anion diffusivities for oxides with the fluorite structure[44]. The cations are virtually immobile below 1400°C and consequently the cation sublattice is likely to possess frozen-in high temperature defects. For the ternary oxides the distribution of trivalent and quadravalent cations must be considered as well as the number and distribution of vacancies and/or interstitials, while in the case of CeO_2 the distribution of Ce^{3+} and Ce^{4+} can easily be altered by electron switching.

The polycrystalline specimens were all rapidly cooled from 2000°C so that their cation sublattice should be appropriate to that temperature. The single crystals of ceria were formed at low temperatures and would have poorly defined cation defect concentrations. The zirconia-yttria single crystals were cooled from a melt well above 2000°C and would have a cation sublattice corresponding to a temperature of the order of 2000°C.

In order to see what effect this had on oxygen exchange results, a zirconia-yttria single crystal was fired at 2000°C for a half hour in argon, and then at 1400°C for seven days in air. Using the approximate relation $\bar{S}^2 = 2.D.t$ given by Kubaschewski and Hopkins[45] where $\bar{S}$ is the distance diffused, and the cation diffusion data of Rhodes and Carter[44] for zirconia-calcia, the cations would have travelled a distance of the order of 5 Å in these treatments. Subsequent equilibration and exchange were carried out in the normal way in run 60.

2.3.3. Exchange.

With the equilibrated sample out of the hot zone the temperature was lowered to 500°C and the system evacuated. A gas mixture of appropriate oxygen partial pressure and ^{18}O content was prepared in the gas handling system and expanded into the circulating system. The quantity of gas transferred to the circulating system was known from the volume of the handling system, and the pressure change due to expansion. The furnace temperature was increased to that required and two gas samples taken before lowering the sample into position. This momentarily lowered the temperature, but the original set point was reached in about two minutes after the start of the experiment and maintained to ± 1°C, measured with a Pt - 13%Rh thermocouple.

Further gas samples were taken at intervals during the exchange run. Immediately after taking the final gas sample the specimen was pushed out of the hot zone. The gas pressure of the system was remeasured to ensure that no leakage had occurred into the apporatus during the run. The gas mixture was transferred via the Toepler pump to a gas reservoir and was available for further exchange measurements.

The mass fractions in the gas samples were analysed in an A.E.I. M.S. 3 mass spectrometer by measuring the peak heights of the various mass numbers as shown in appendix 1.

2.3.4. Treatment of Data.

The exchange experiments give the rate at which ^{18}O is removed from the gas phase and we require to know D, the diffusion coefficient for oxygen in the solid phase defined by Fick's diffusion equation

$$\partial c / \partial t = D \nabla^2 C \qquad \ldots\ldots \qquad (2.1)$$

where C is the concentration of ^{18}O at a point in the solid. Crank[46] gives solutions to the diffusion equation in terms of Mt/M_∞, the ratio of the amount of solute taken up at time t to that taken up at infinite time during diffusion into solids of various geometry from a limited fluid.

The solution for a sphere is:

$$Mt/M\infty = 1 - \sum_{a=1}^{\infty} \frac{6\alpha(1+\alpha)\exp(-q_a^2 Dt/r^2)}{q_a^2\alpha^2 + 9\alpha + 9} \qquad \ldots(2.2)$$

where: α = the ratio of the number of moles of solute in the gas to the number in the solid.

t = elapsed time, sec.

r = sphere radius, cm.

D = diffusion coefficient, $cm^2/sec.$

q_a = one of the non-zero, positive roots of $\tan q_a = 3 q_a / (q_a^2\alpha + 3)$

The solution for an inifinite plane sheet is:

$$Mt/M\infty = 1 - \sum_{a=1}^{\infty} \frac{2\alpha(1+\alpha)\exp(-q_a^2 Dt/\ell^2)}{q_a^2\alpha^2 + \alpha + 1} \qquad \ldots (2.3)$$

where ℓ = half-thickness of the slab, cm

q_a = one of the non-zero, positive roots of $\tan q_a = -q_a\alpha$

Crank presents graphs of $Mt/M\infty$ vs. $\sqrt{Dt/\ell^2}$ for different values of the final practional uptake, $\lambda = 1/(1+\alpha)$.

Using the graphs for analysis of the present results plots of Dt/ℓ^2 vs. t were found which were curved, as shown in appendix 3. This curvature occurs when the rate of exchange of gas at the interface contributes to the overall kinetics of exchange [25, 32].

Edwards et. al.[25] and Haul et. al.[47] derived expressions for the uptake of gas by solids of plane sheet and spherical geometry, assuming that the gas-solid interface reaction contributes to the overall rate.

The equation for a sphere is:

$$Mt/M\infty = 1 - \frac{2(1+\alpha)}{3\alpha} \sum_{a=1}^{\infty} \frac{q_a^2 \exp(-q_a^2 Dt/r^2)}{F(q_a^2 Q/9 + 1/\alpha) + F^2 + q_a^2 E^2 - 2E/\alpha} \ldots(2.4)$$

where q_a = one of the non-zero, positive roots of $\tan q_a = q_a E/F$

$E = 1/\alpha - Q q_a^2/9$

$F = 1/\alpha + Q q_a^2 (3/Q - 1)/9$

$Q = DS/K$

K = surface exchange coefficient, cm/sec.

$= k.d.$

k = rate constant of surface reaction, sec^{-1}

d = thickness of solid surface layer in contact with the gas.

S = surface to volume ratio of solid. For a sphere = $3/r$

The equation for a plane sheet is:

$$M_t/M_\infty = 1 - \frac{2(1+\alpha)}{\alpha} \sum_{a=1}^{\infty} \frac{\exp\left(-q_a^2 Dt/\ell^2\right)}{T^2 + q_a^2 + T + 2/\alpha} \qquad \ldots (2.5)$$

where q_a = one of the non-zero positive roots of $\tan q_a = q_a/T$

$T = Q q_a^2 - 1/\alpha$

The computer programs given in appendix 2 were developed to obtain plots of M_t/M_∞ vs. $\sqrt{Dt/\ell^2}$ and $\sqrt{Dt/r^2}$ for appropriate values of λ and a series of Q values such as those shown in figures 31 and 32 of appendix 2. These plots were in agreement with those of Crank for Q = 0 and with those produced by Edwards et. al. for three λ values, each having four Q values.

O'Keefe[48] has shown that the equation for the infinite plane sheet geometry can be used to obtain the solution for a finite rectangular parallelepiped. For the special case of a cube this reduces to

$$m_I = 1 - (1 - m_{III})^{\frac{1}{3}} \qquad \ldots.(2.7)$$

where m_I = M_t/M_∞ for the infinite plane sheet.

m_{III} = M_t/M_∞ measured for the cube.

Exchange experiments for cubes were analysed in this way using the M_t/M_∞ vs $\sqrt{Dt/\ell^2}$ graphs for plane sheets.

A sample calculation of D and K from percent ^{18}O results in the gas phase as a function of time is shown in appendix 3.

2.4. Proton Activation and Autoradiography.

Gaseous exchange experiments measure the overall rate of uptake of ^{18}O from the gas phase but provide no direct information about the oxygen diffusion profile within the specimens. Since there is no radioactive isotope of oxygen with a long enough half life for determining diffusion profiles using the normal counting technique a recently developed proton activation technique was adopted[49,50, 51]. This technique employs the nuclear reaction

$$^{18}_{8}O + ^{1}_{1}H = ^{18}_{9}F + ^{1}_{0}n$$

to produce the ^{18}F isotope, which is a positron emitter with a half life of 112 minutes. The distribution of ^{18}F (and thus ^{18}O) may be determined by taking an autoradiograph of the activated crystal, and examining variations in the density of silver grains in the exposed film. Oxygen diffusion profiles can thus be observed together with fast diffusion paths associated with grain boundaries.

Ceria single crystals and aggregates of two or more crystals, containing grain boundaries which had been exchanged with ^{18}O containing gases were cut in half and polished. The specimens were mounted in a tantalum covered brass holder and bombarded with protons above the threshold energy of 2.6 Mev at a current of 20 to 200 nanoamps for one hour in a linear accelerator at the Nuclear Physics Division, A.E.R.E., Harwell. A neutron detector placed behind the target indicated that the (p,n) reaction was accurring. The surface of the specimen was counted immediately after irradiation and Kodak AR10 stripping film exposed on the surface for 2 to 10 hours and developed in situ. Counts of the surface at intervals of time indicated that the reaction being observed had a half life correspnnding to positron emission from ^{18}F.

With the film on the specimen no variation of silver grain density could be identified under the microscope, but when the film was stripped from the specimen and examined on a glass slide variations in density could be seen.

Chapter 3.

Results.

3.1. Gaseous Exchange Results.

Experimental details are described in appendix 4. Not all experiments gave K values as well as D values. The contribution of the surface exchange reaction to the overall kinetics of gas uptake was greater at lower temperatures and the higher temperature CeO_2 and $CeO_{1.92}$ runs had straight line plots of Dt/ℓ^2 vs t for Q = 0 in equation (2.4) or (2.5). In addition the runs on preparation 1 polycrystalline ceria with roughly ground surfaces contained no effect due to the phase boundary reaction.

The results have been fitted to Arrhenius equations of the form

$$D = D_o \exp(- Q_D /RT) \qquad ....(3.1)$$

and

$$K = K_o \exp(- Q_K/RT) \qquad ....(3.2)$$

using least squares analysis.

Values of $\log D_o$, Q_D, $\log K_o$ and Q_K are summarized in table 2.

3.1.1. Ceria.

Figures 6 and 7 show the Arrhenius plots of diffusion coefficients and surface exchange coefficients for ceria single crystals and bicrystals. Regression lines and most probable error limits are:

Table, 2 Log D_o, Q_D, Log K_o, and Q_K for the Arrhenius Equations.

Specimen	Log D_o $cm^2/sec.$	Q_D k. cal.	Log K_o cm/sec.	Q_K k. cal.
CeO_2(S)-0.21 atm.	-3.72 ± 0.60	24.8 ± 3.5		
CeO_2(S)-0.02 atm.	-4.75 ± 0.34	17.4 ± 1.9		
$CeO_{1.92}$(S)	-4.82 ± 0.70	11.9 ± 3.9		
$CeO_{1.80}$(S)	-5.21 ± 0.70	3.6 ± 4.2	+0.83 ± 1.7	28.4 ± 10.0
CeO_2(P), prep.1, 0.21atm	-3.84 ± 0.10	21.3 ± 0.6		
$Ce_{0.9}Y_{0.1}O_{1.95}$ (P)	-3.82 ± 0.25	19.2 ± 1.4		
$Ce_{0.8}Y_{0.2}O_{1.90}$ (P)	-3.77 ± 0.53	18.3 ± 3.0	+1.22 ± 0.71	33.5 ± 4.1
$Ce_{0.6}Y_{0.4}O_{1.80}$(P)	-2.29 ± 0.30	21.3 ± 1.7	+2.69 ± 1.5	36.5 ± 8.7
$Th_{0.90}Y_{0.10}O_{1.950}$(P)	-3.75 ± 1.0	22.0 ± 5.8		
$Th_{0.85}Y_{0.15}O_{1.925}$(P)	-4.26 ± 0.39	18.2 ± 1.1		
$Zr_{0.844}Y_{0.156}O_{1.920}$(S)	-4.81 ± 0.17	11.3 ± 1.0	-0.06 ± 0.16	27.3 ± 0.9
$Zr_{0.950}Y_{0.150}O_{1.925}$(P)	-3.58 ± 0.42	21.7 ± 2.5	-1.04 ± 0.67	22.1 ± 3.8

(S) - single crystals

(P) - polycrystalline specimens.

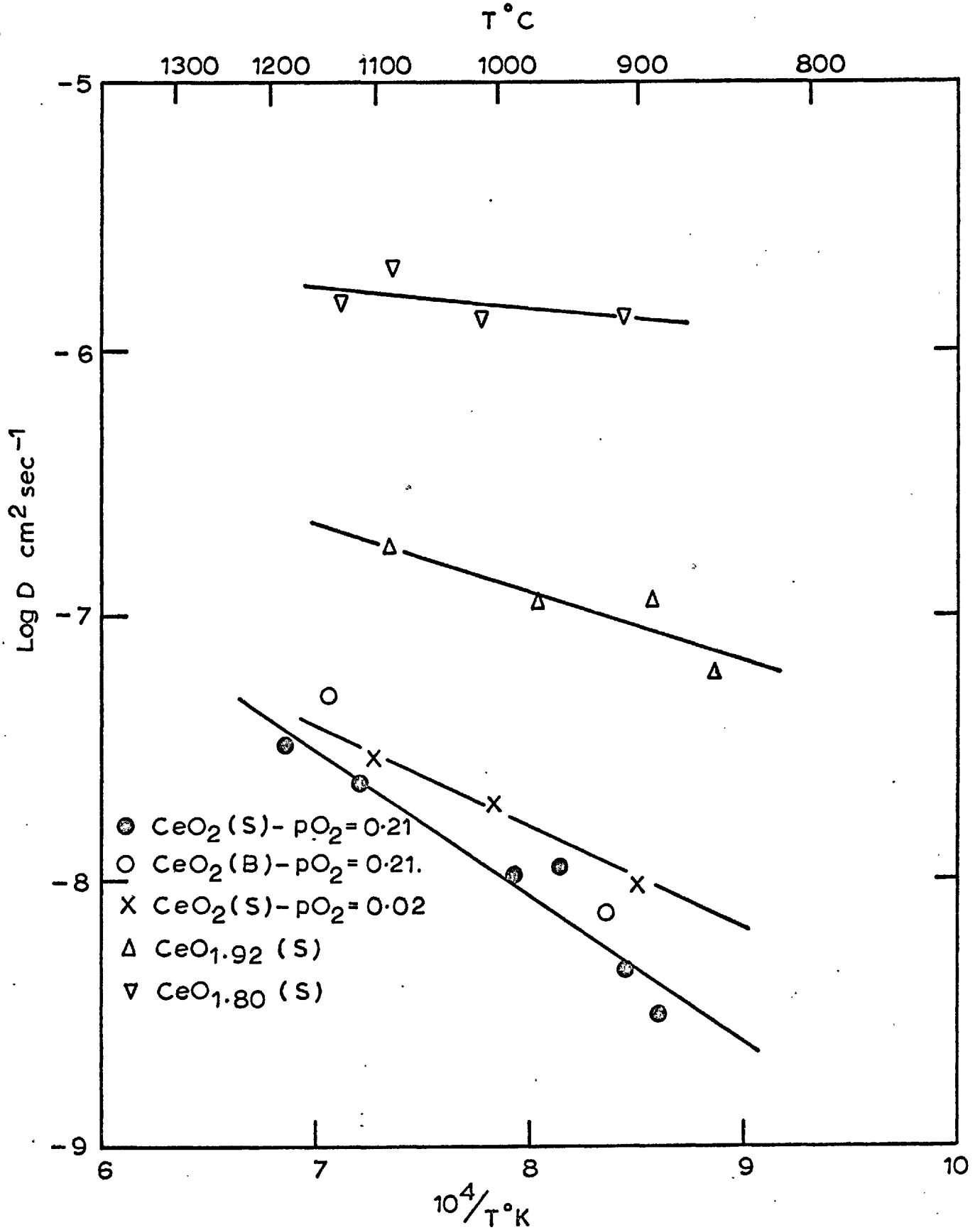

Fig. 6 CERIA DIFFUSION COEFFICIENTS (Single crystals)

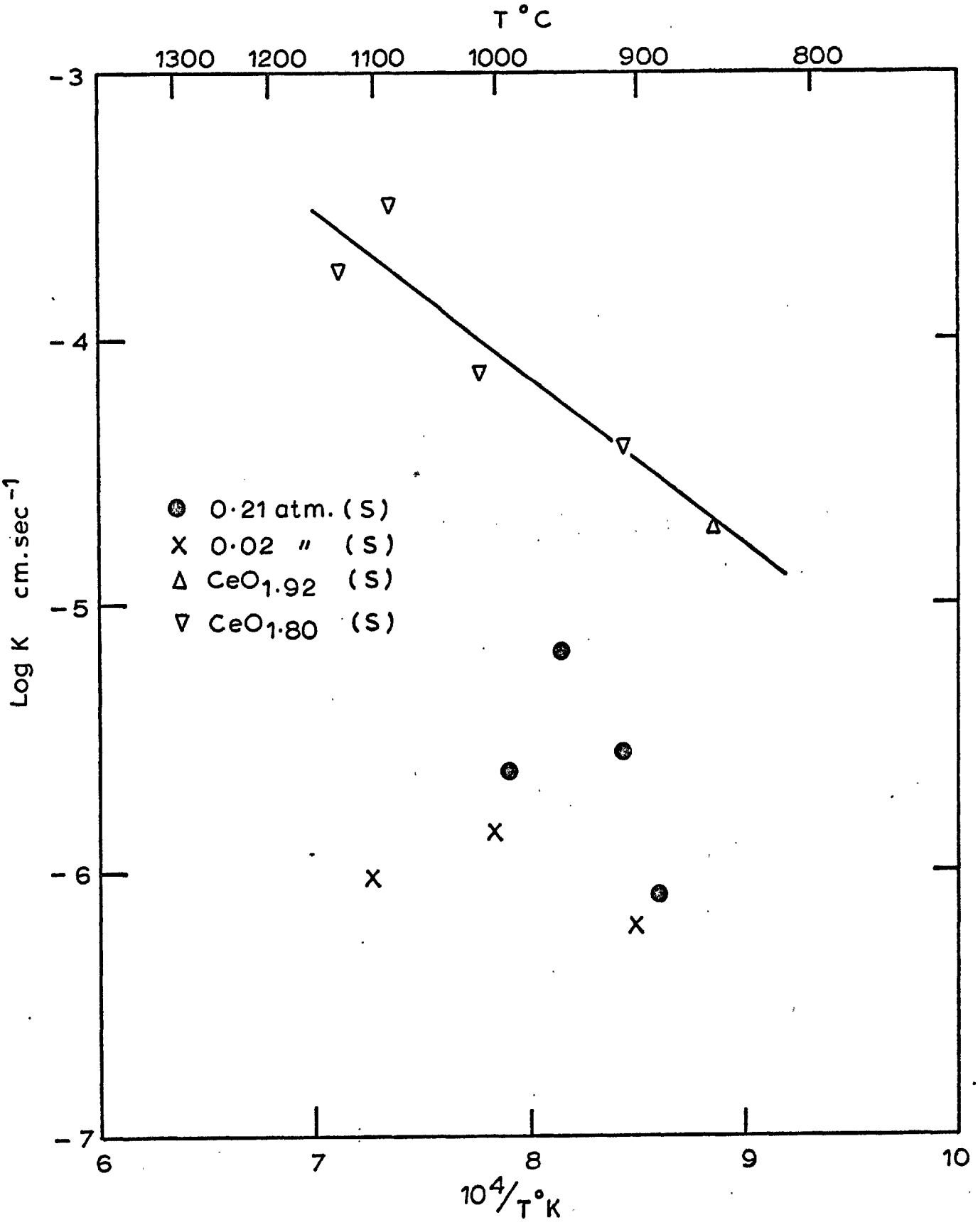

Fig. 7 CERIA SURFACE EXCHANGE COEFFICIENTS (Single-crystals)

CeO_2(S) - 0.21 atm. oxygen partial pressure:

$$D = 1.9\ ^{+5.7}_{-1.4} \times 10^{-4} \exp(-24.8 \pm 3.5 \text{ k. cal /RT}) \quad ....(3.4)$$

CeO_2(S) - 0.02 atm. oxygen partial pressure:

$$D = 1.8\ ^{+\ 2.1}_{-\ 1.1} \times 10^{-5} \exp(-17.4 \pm 1.9 \text{ k. cal/RT}) \quad ....(3.5)$$

$CeO_{1.92}$(S) - CO -CO_2 mixtures:

$$D = 1.5\ ^{+\ 6.1}_{-\ 1.2} \times 10^{-5} \exp(-11.9 \pm 3.9 \text{ k. cal./RT}) \quad ....(3.6)$$

$CeO_{1.80}$(S) - CO -CO_2 mixtures:

$$D = 6.2\ ^{+\ 25}_{-\ 5.0} \times 10^{-6} \exp(-3.6 \pm 4.2 \text{ k. cal/RT}) \quad ....(3.7)$$

$$K = 6.8\ ^{+\ 334}_{-\ 6.7} \exp(-28.4 \pm 10.0 \text{ k. cal/RT}) \quad ....(3.8)$$

The measured surface exchange coefficients for ceria single crystals in 0.21 and 0.02 atmospheres oxygen partial pressures showed a great deal of scatter.

As explained in section 2.1.2 (i) some of these specimens had roughened surfaces while others had the natural cubic crystalline faces. As shown in appendix 4, table 9 spherical specimens for runs number 3, 9, 11 and 12, and cubic specimens for runs number 4 and 10 had surfaces air blasted with abrasive powder. In addition specimens for runs number 11 and 12 had been rolled over 400 mesh silicon carbide paper. The specimens with roughened surfaces gave K values appreciably lower than those with natural surfaces.

Ceria single crystal results for D are shown as a functuon of log p_{O_2} and x in figures 8 and 9 respectively. Surface exchange coefficients are shown as a functuon of x in figure 10. Arrhenius plots of polycrystalline ceria results at 0.21 atmospheres oxygen pressure are shown in figures 11 and 12. The Arrhenius equation for the diffusion coefficient in preparation 1 specimens is

$$D = 1.4\ ^{+\ 0.4}_{-\ 0.3} \times 10^{-4} \exp(-21.3 \pm 0.6 \text{ k. cal/RT}) \quad .....(3.9)$$

The specimens had surfaces ground only on 400 mesh silicon carbide paper. Surface exchange coefficients were not found since Q = 0 for all three runs. For preparation 2 ceria with surfaces polished to 1 μ diamond, both D and K values were found as shown in figures 11 and 12.

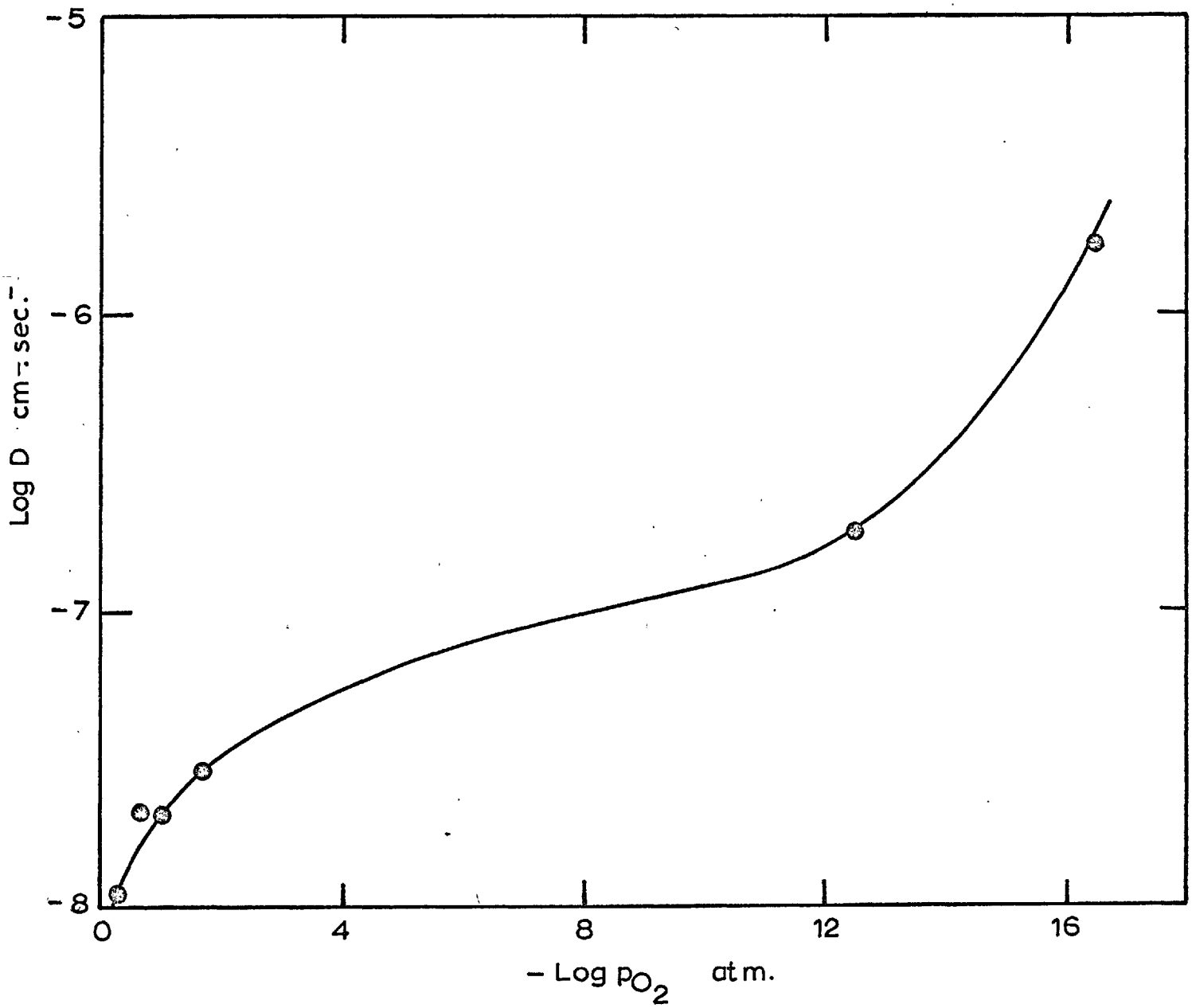

Fig.8. LOG D vs. LOG pO_2 FOR CERIA SINGLE CRYSTAL

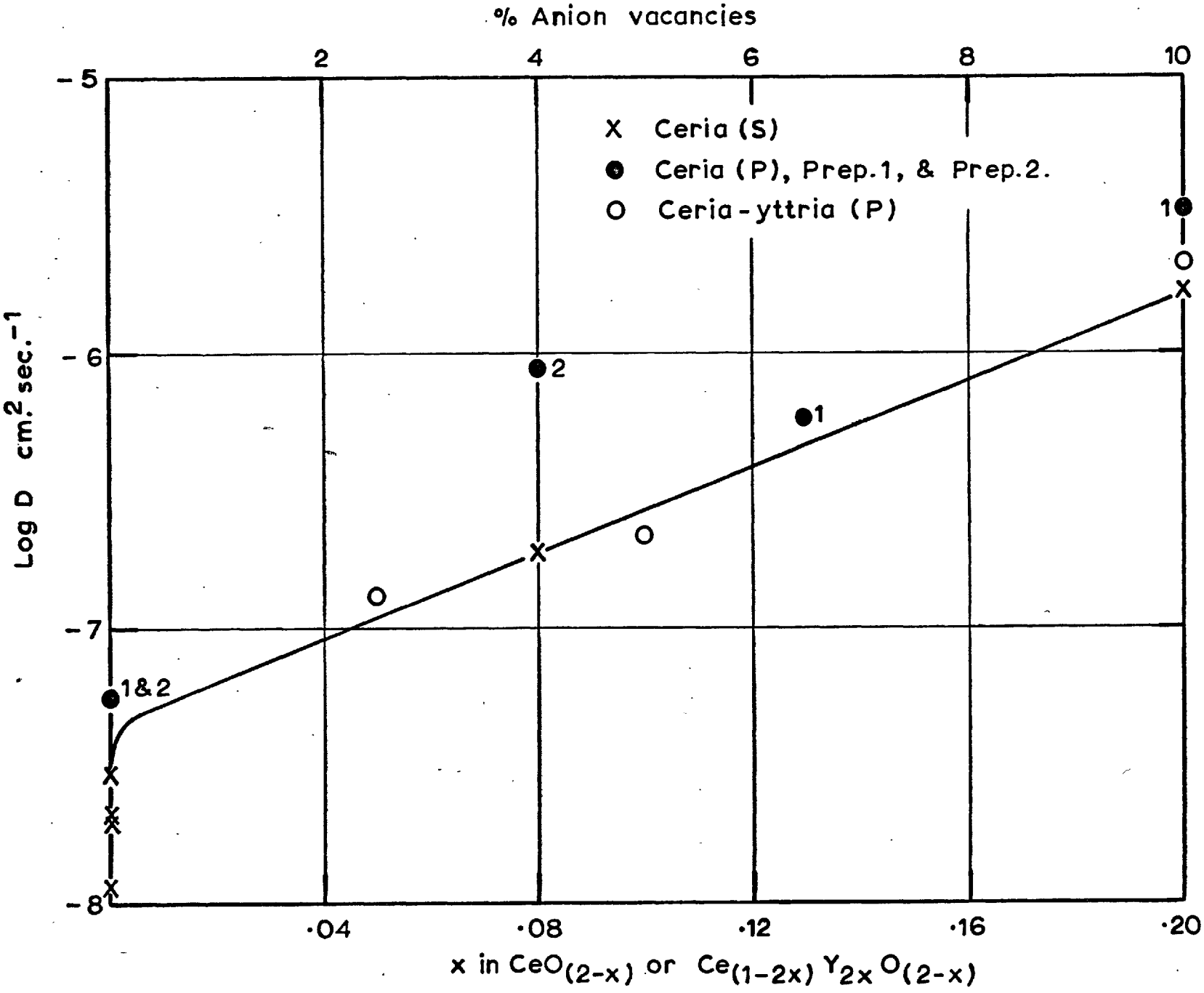

Fig. 9 LOG D vs. x in $CeO_{(2-x)}$ or $Ce_{(1-2x)}Y_{2x}O_{(2-x)}$ AT 1100°C

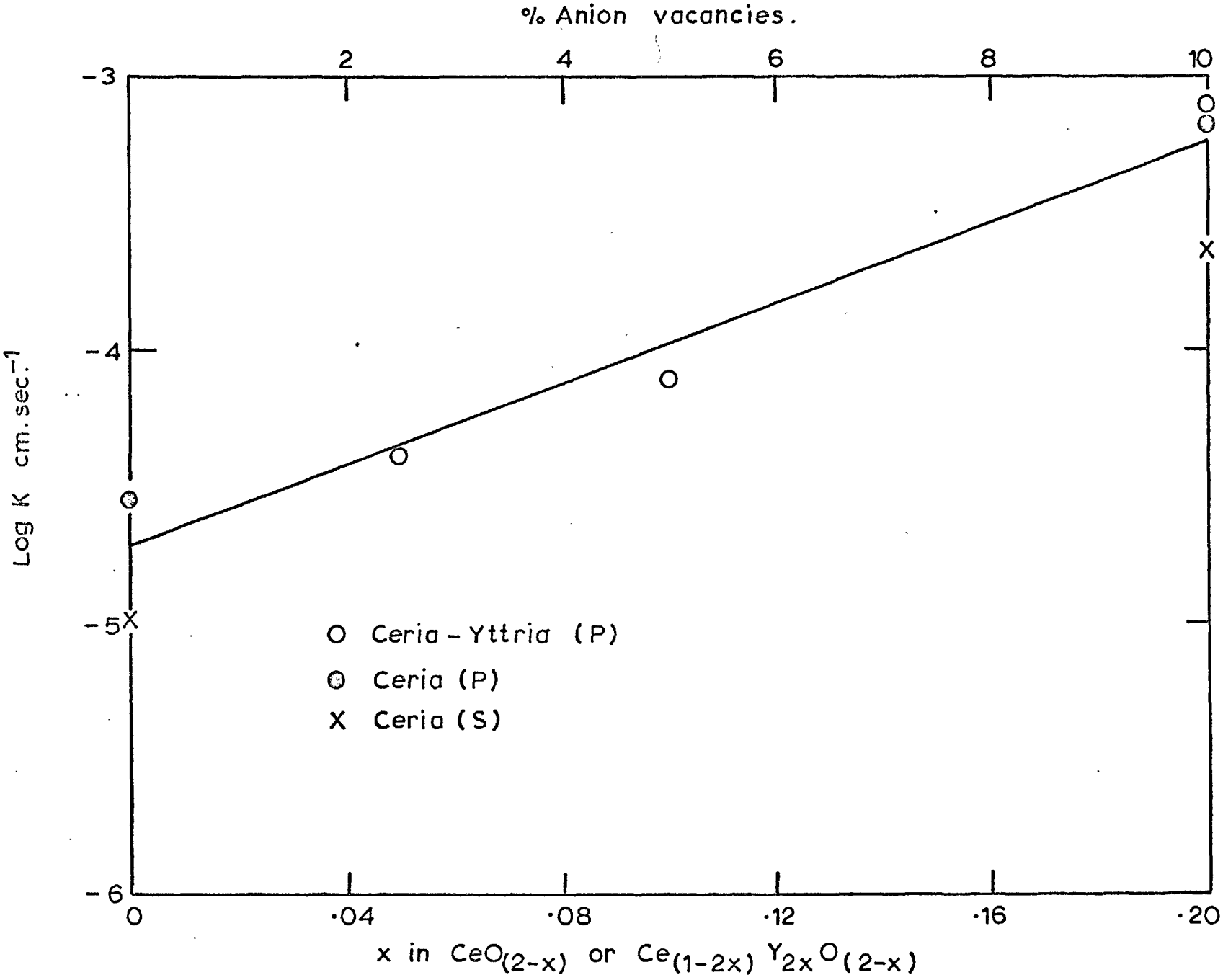

Fig.10. LOG K vs. x IN $CeO_{(2-x)}$ AND $Ce_{(1-2x)}Y_{2x}O_{2-x}$ AT 1100°C

Diffusion coefficients are shown for reduced ceria polycrystalline specimens at 1100°C in figure 9. The $CeO_{1.92}$ value is obtained by extrapolation from two lower temperatures results, assuming the same activation energy as for the single crystal results. Considerable scatter in the results is evident from the figure.

3.1.2. Ceria-yttria solutions.

Arrhenius plots of D and K results for polycrystalline specimens with 10, 20, and 40 mole% $YO_{1.5}$ are shown in figures 11 and 12. These were obtained at an oxygen partial pressure of 0.21 atmospheres.

Regression lines and most probable error limits are:

$Ce_{0.9} Y_{0.1} O_{1.95}$ (P) :

$$D = 1.5^{+\ 1.2}_{-\ 0.6} \times 10^{-4} \exp(-19.2 \pm 1.4 \text{ k. cal/RT}) \quad \ldots.(3.10)$$

$Ce_{0.8} Y_{0.2} O_{1.90}$ (P) :

$$D = 1.7^{+\ 4.1}_{-\ 1.2} \times 10^{-4} \exp(-18.3 \pm 3.0 \text{ k. cal/RT}) \quad \ldots..(3.11)$$

$$K = 1.7^{+\ 6.8}_{-\ 1.4} \times 10 \exp(-33.5 \pm 4.1 \text{ k cal/RT}) \quad \ldots..(3.12)$$

$Ce_{0.6} Y_{0.4} O_{1.80}$ (P) :

$$D = 5.1^{+\ 5.1}_{-\ 2.5} \times 10^{-3} \exp(-21.3 \pm 1.7 \text{ k. cal/RT}) \quad \ldots..(3.13)$$

$$K = 4.9^{+\ 150}_{-\ 4.7} \times 10^{2} \exp(-36.5 \pm 8.7 \text{ k. cal/RT}) \quad \ldots..(3.14)$$

The ceria - 10 % $YO_{1.5}$ specimen in run 48 gave a surface exchange coefficient very much lower than expected from other results. and consequently no regression line could be obtained.

D and K are plotted against x in $Ce_{(1-2x)} Y_{2x} O_{(2-x)}$ for 1100°C in figures 9 and 10.

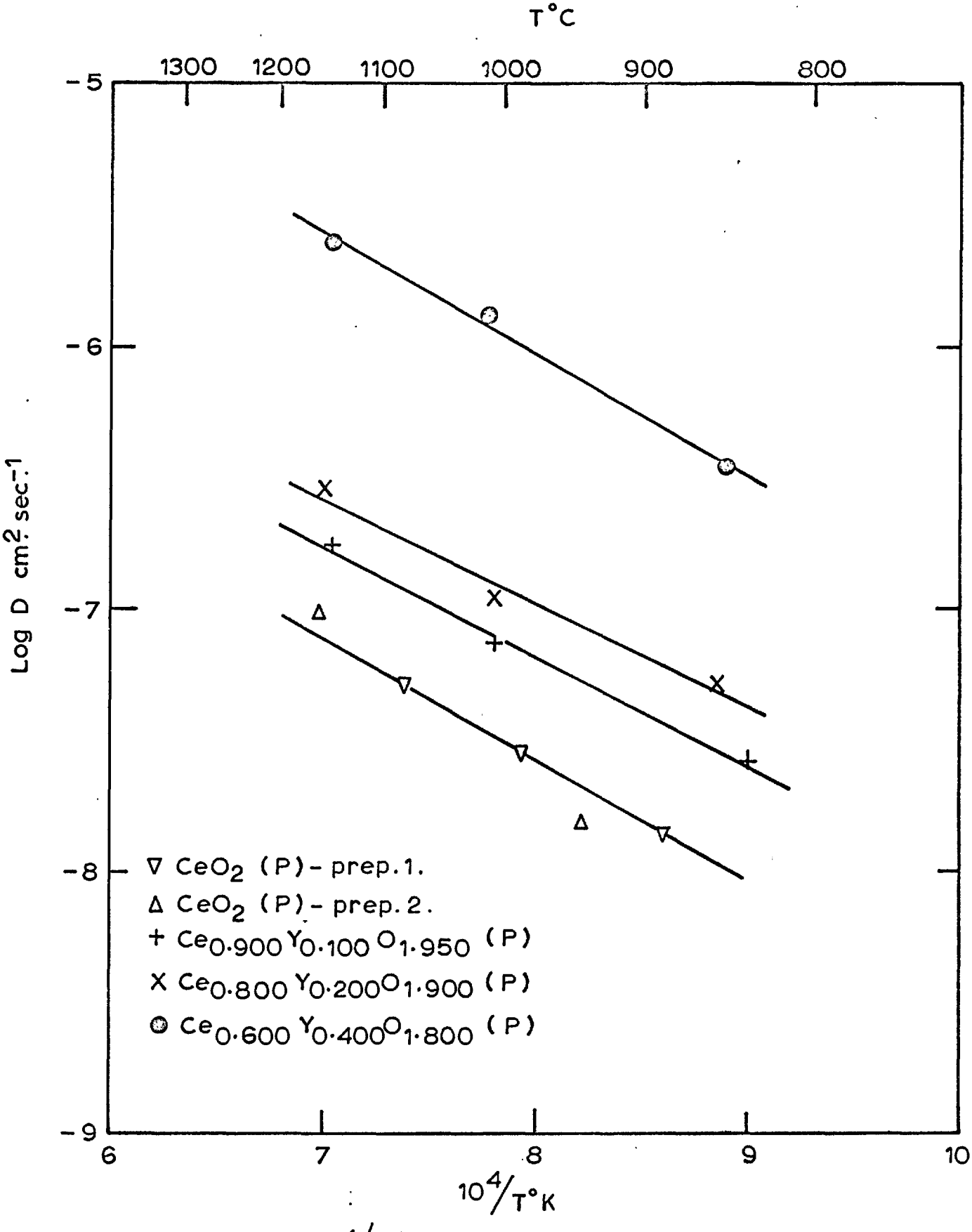

Fig. 11. LOG D vs. $10^4/T°K$ FOR CeO_2-$YO_{1.5}$

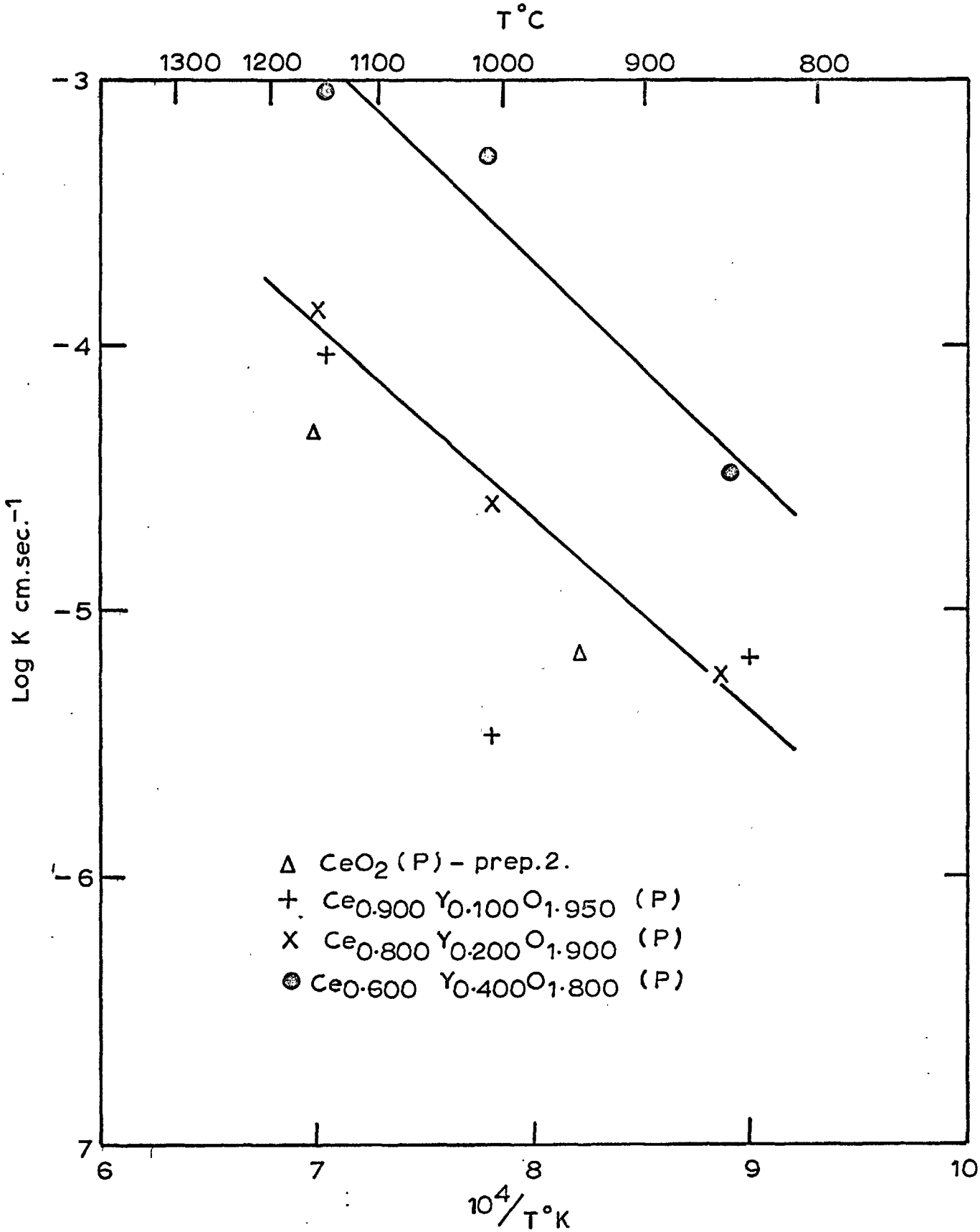

Fig.12. LOG K vs. $10^4/T°K$ FOR $CeO_2 - YO_{1.5}$

3.1.3. Thoria-yttria.

Arrhenius plots for the D and K results of thoria - 10% $YO_{1.5}$ and thoria - 15% $YO_{1.5}$ polycrystalline specimens are shown in figures 13 and 14.

Regression lines and most probable error limits are:

$Th_{0.90} Y_{0.10} O_{1.950}$ (P) - CO-CO_2 mixtures:

$D = 1.8^{+\ 16}_{-\ 1.6} \times 10^{-4} \exp(-22.0 \pm 5.8$ k. cal/RT) .....(3.15)

$Th_{0.85} Y_{0.15} O_{1.925}$ (P) - 0.21 atm. oxygen:

$D = 5.5^{+\ 8.0}_{-\ 3.3} \times 10^{-5} \exp(-18.2 \pm 1.1$ k cal /RT) .....(3.16)

Considerable scatter of K values was observed and no Arrhenius equations were obtained. A factor which may contribute to the scatter of the D and K results for the 10% $YO_{1.5}$ specimens was that the history of the specimens after preparation was not known. The results for 15% $YO_{1.5}$ specimens from runs 1 and 6, with nearly identical conditions, indicated good reproducibility in both D and K values.

3.1.4. Zirconia-yttria.

Arrhenius plots for the polycrystalline and single crystal zirconia -yttria diffusion and surface exchange coefficients are shown in figures 13 and 14.

Regression lines and most probable error limits are:

$Zr_{0.844} Y_{0.156} O_{1.920}$ (S)

$D = 1.5^{+\ 0.8}_{-\ 0.4} \times 10^{-5} \exp(-11.3 \pm 1.0$ k cal /RT) .....(3.17)

$K = 8.7^{+\ 3.9}_{-\ 2.7} \times 10^{-1} \exp(-27.3 \pm 0.9$ k. cal /RT) .....(3.18)

$Zr_{0.850} Y_{0.150} O_{1.925}$(P):

$D = 2.6^{+\ 4.3}_{-\ 1.6} \times 10^{-4} \exp(-21.7 \pm 2.5$ k. cal/RT) .....(3.19)

$K = 9.1^{+\ 41}_{-\ 7.1} \times 10^{-2} \exp(-22.1 \pm 3.8$ k. cal/RT) .....(3.20)

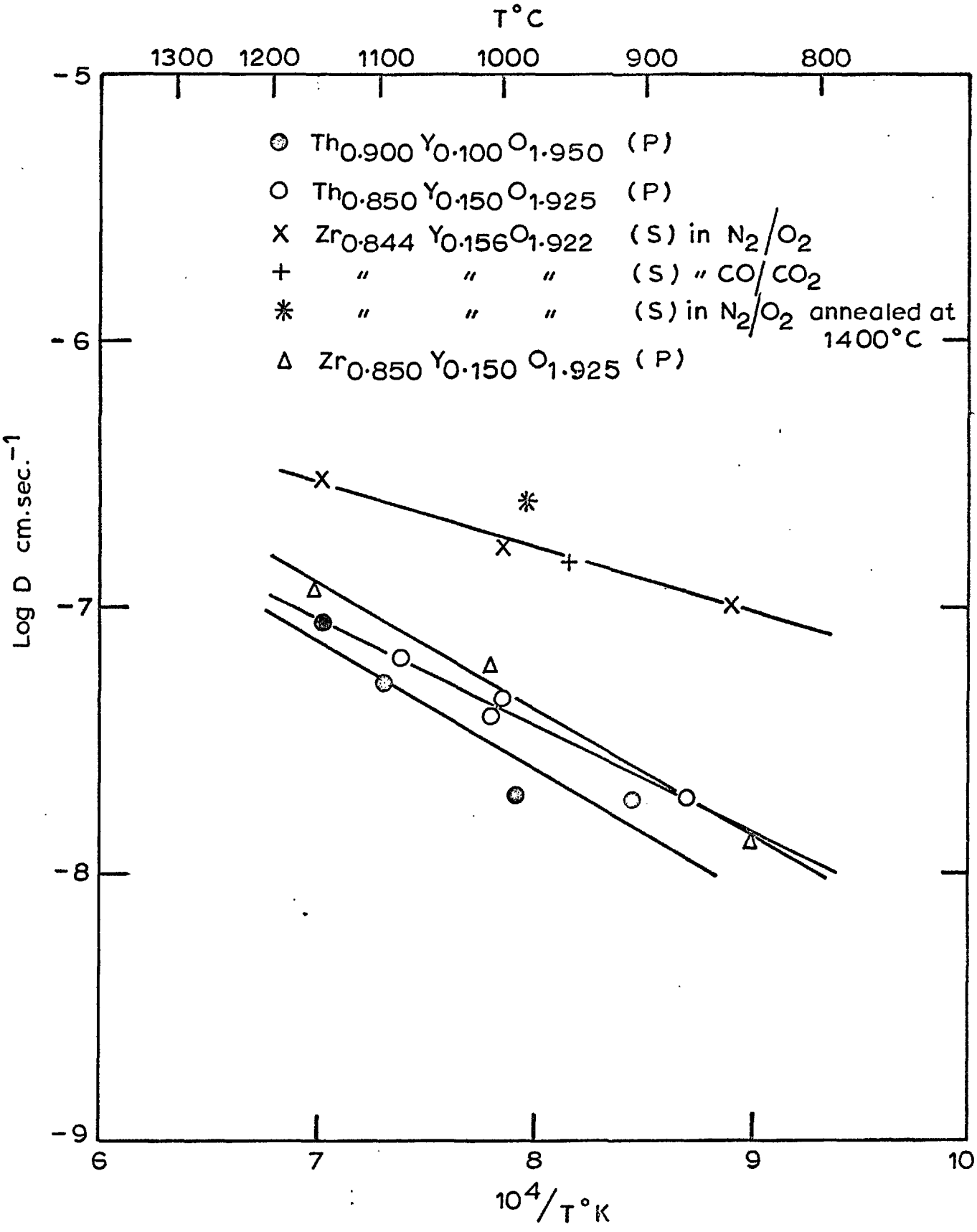

Fig.13. LOG D vs $10^4/T°K$ FOR THORIA-YTTRIA AND ZIRCONIA--YTTRIA

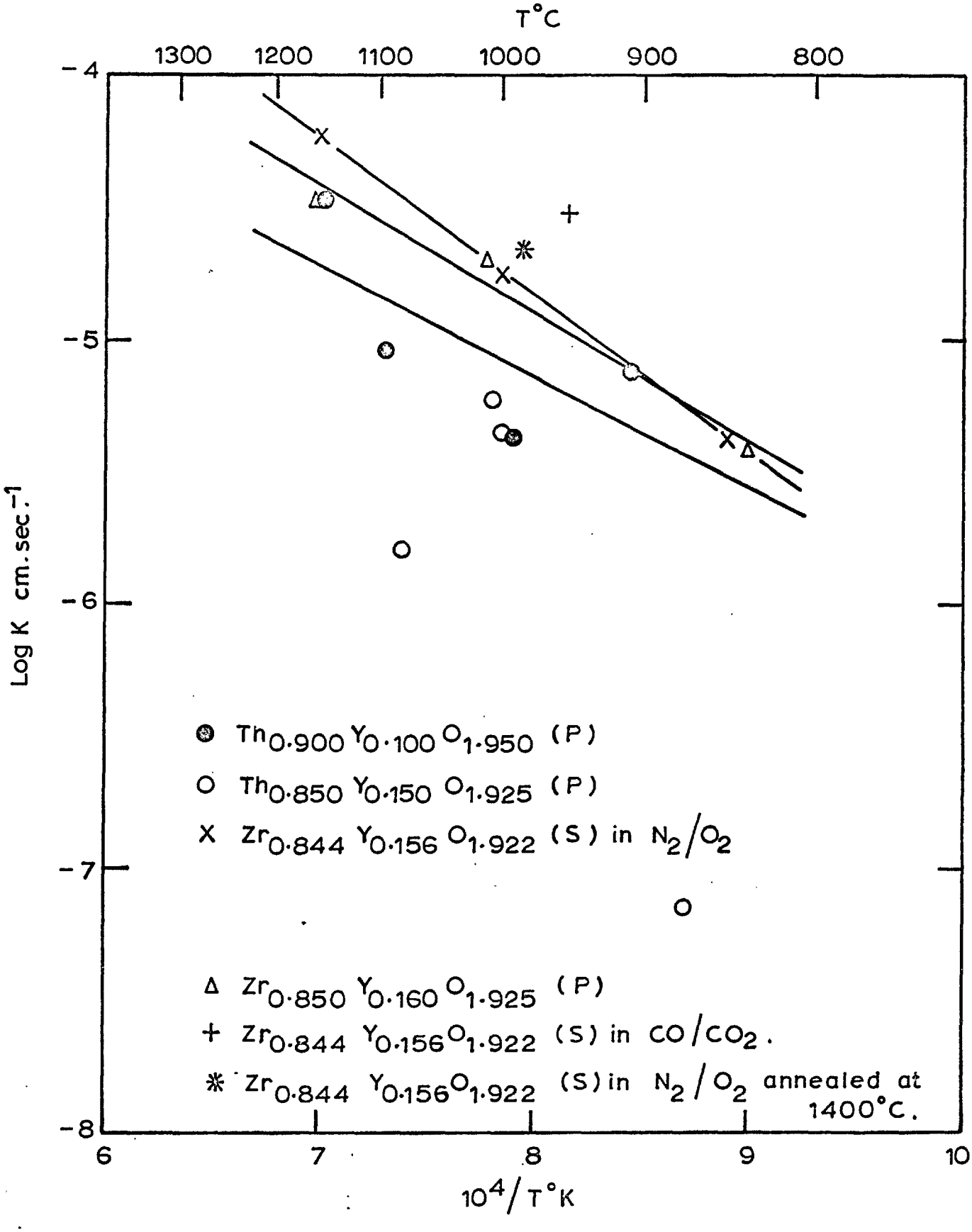

Fig.14. LOG K vs. $10^4/T°K$ FOR THORIA-YTTRIA & ZIRCONIA--YTTRIA

The zirconia - yttria single crystal cubes were all cut from one crystal, with faces oriented on the [100] plane except for run 40 which had two faces parallel to the [100] plane and the other four rotated 30° to this plane. Three of the crystals were exchanged in N_2 - O_2 mixtures but run 41 was exchanged in a CO - CO_2 mixture. Before the exchange run number 38, the specimen had developed a fine crack. All four specimens had D values agreeing very well with the Arrhenius equation, and the three K values for N_2 - O_2 mixtures lay on a good straight line while that in CO - CO_2 was slightly higher.

A further zirconia-yttria cube was cut with [100] faces from another crystal of the same batch. This specimen was fired at 2000°C for a half hour, then at 1400°C for seven days, before exchanging with N_2 - O_2 mixtures in run 60. Slightly higher D and K values are shown in the figures.

3.2. Errors in Exchange Expariments.

Possible sources of error in the exchange results are set out in the following:

(i) Uptake or exchange of gas with material other than the specimen.

Platinum - rhodium alloy was used as the construction material for the exchange apparatus because it is impervious to oxygen up to 1425°C [52], is only slightly oxidized in air to form a volatile oxide[53], and has been used successfully for this application up to 1250°C in previous work[54]

Nevertheless, as a check, a blank run (number 17) was carried out at 1100°C with no sample in the tube. During the 96 minutes of the run no reduction in ^{18}O content of the gas occurred.

(ii) Determination of n_g.

n_g, the number of moles of oxygen in the gas phase is known from. the pressure and volume of the gas handling system, room temperature, and the fraction of oxygen in the gas mixture.

The pressure was measured to within . 1mm. with a mercury monometer, leading to a typical error of 0.5%.

The uncertainty in the volume of 180 $\pm$ 1 ml leads to an error of 0.6%. The room temperature was measured to $\pm$ 0.5°C giving an error of 0.2%

The fraction of oxygen in the gas mixture was found initially from the gases added, and in later experiments from the ratio of the mass spectrometer peak heights, compared with the ratio for known gas mixtures. This was typically 0.5 $\pm$ .005 - giving an error of 1%.

Thus the total error in n_g is approximately 2.3%

The effect of an error in n_g is to produce an error in the value and in the calculation of M_t and M_∞ (see appendix 3). A small error in n_g will affect M_t and M_∞ in the same way, and so will be effectively cancelled in the calculation of M_t/M_∞. With a λ value of 0.54 the error is about $\pm$ .01. A calculation has been carried through using values of 0.54 and 0.53 with Q = 0.1. The difference between the two diffusion coefficients is 2%

(iii) Sample weight.

The sample weight is required to calculate the number of moles of oxygen in the solid and the dimension of the cubic and spherical specimens. The typical sample weight of 0.1000 $\pm$ .0001 g. would give nigligible errors compared with other sources.

(iv) Densities.

The error is greatest for small ceria single crystals where the density is 7.2 $\pm$ .1g/cm^3. For zirconia-yttria single crystals the density is 6.95 $\pm$ .03g/cm^3. For ceria the error is thus 1.4% leading to the same error in ℓ, and an error of 2.8% in ℓ^2 and hence in D. The effect will be the same on all specimens of the same composition and will thus be systematic.

(v) Temperature.

There was a constant temperature zone to within $\pm$ 1°C for two inches around the position of the specimen in the furnace. The temperature was controlled to $\pm$ 1°C but at the start of an experiment the temperature was reduced by introduction of the cold thermocouple tube and sample into the hot zone. About two minutes were required to regain the set temperature.

The temperature of the equilibration process was generally within 10°C of the exchange temperature. The former could be adjusted accurately but the latter was not measured until the exchange had commenced, and consequently exact correspondence of temperatures was not attained. This was generally not important, but in the case of $CeO_{(2-x)}$ it could affect the composition significantly - see (vii).

(vi) Oxygen pressures.

The oxygen pressures of the equilibrium gas mixtures were established from the flowrate of appropriate gases through dibutyl-pthalate capillary flow meters. The flow meters were calibrated against a soap bubble flow meter. The height of dibutyl-pthalate could be measured and controlled to $\pm$ 1mm and for typical heights of 50mm this introduces an error of 2% into the pressure. The total gas flow rate was maintained in the range 300 to 500 ml./min.

To prepare $CeO_{1.80}$, gas mixture with small amounts of CO_2 were required and a finer capillary was used. The minimum height of 18mm. dibutyl-pthalate gave a flow rate of 2ml./min. CO_2 so that the error from this source is 6%.

The $CO-CO_2$ gas mixtures were found to be correct to within these errors by passing over one electrode of a galvanic cell.

Using the data of Bevan and Kordis[2] a change in composition from $CeO_{1.80}$ to $CeO_{1.81}$ requires a change in the CO/CO_2 ratio of about 30% at 900°C so that the error of 6% will mean in the extreme case a composition

error of $\pm$ .002 for x in $CeO_{(2-x)}$.

The exchange gas composition was fixed from the pressures of gases added to the gas handling system. The same ^{18}O-containing gas was used many times by recovering the gases via a Toepler pump after exchange experiments. Additions were made as necessary to adjust the ^{18}O and N_2/O_2 or CO/CO_2 ratio of the exchange gas, but the same oxygen partial pressure as the equilibration run was not always attained as shown in table 3. This would not affect exchange with doped oxides significantly but for ceria it would imply a flux of oxygen into, or out of, the specimens in addition to ^{18}O into the specimen.

As shown in table 9 of appendix 4 the oxygen partial pressures for the N_2-O_2 exchange mixtures were close to those for equilibration mixtures the difference between equilibration and exchange mixtures is significant for high CO/CO_2 ratios. The effect of these differences is discussed in the next section.

(vii) Composition of specimens.

The lattice parameters of the solid solutions were consistant with the nominal compositions. For thoria-yttria and zirconia-yttria this is quite a sensitive test since the lattice parameter changes by 0.02 Å with 10% compositional change. For ceria-yttria with up to 20% yttria the lattice parameter changes by only about 0.006 Å while the accuracy of measurement is .001 Å. Thus the composition could be in error by $\pm$ 3%.

The composition of CeO_{2-x} specimens is fixed by the CO/CO_2 ratio of the gas mixture and the temperature. Both of these varied between the equilibrium stage and the exchange run in some experiments. Table 3 summarizes the temperatures, CO/CO_2 ratios, and composition for equilibrium and exchange with single crystal ceria. The composition shown for the exchange process is that assuming equilibrium with the CO-CO_2 mixture. The exchange will commence with solid of the composition of the equilibrium stage and will be affected by the change of composition in two ways. when the exchange gas is oxidizing to the solids:

a) There will be a flux of total oxygen as well as ^{18}O into the crystal,

Table 3

Comparison of $CeO_{(2-x)}$ compositions for equilibrium and exchange with single crystals.

Run No.	Equilibrium			Exchange		
	$T^{o}C$	CO/CO_2	x	$T^{o}C$	CO/CO_2	x
18	1100	1	0.08	1089	1	0.08
19	1000	2	0.08	974	2	0.06
20	900	7	0.08	895	9	0.09
21	840	13	0.08	855	13	0.08
22	1100	50	0.20	1130	42	0.20
23	1000	120	0.20	1015	52	0.18
24	900	310	0.20	912	110	0.17
25	1080	60	0.20	1086	46	0.19

tending to enhance the rate of exchange.
b) Since the oxide formed by the gas has lower diffusion coefficients the rate of exchange will tend to be lower.

As exchange proceeds the first effect will decrease and the second will increase so that the slope of Dt/ℓ^2 vs time would decrease with time. Thus a Qvalue lower than that for constant composition would be chosen, resulting in lower K and D values.

The difference in composition is greater at lower temperature for $CeO_{1.80}$, so that if the D value measured is low the activation energy measured would be higher than for constant composition. As the activation energy is already as low as 4 k. cal. the error introduced from this source cannot be very great.

If, however, the D values are higher than for no flux, then the activation energy is too low. If the activation energy is assumed the same as for $CeO_{1.92}$, then the D values are too high by 0.1 in log D at low temperatures where x is .03 to .02 low. For $CeO_{1.92}$ results there is no systematic change of D with Δx ($\Delta x = x_{Eq} - x_{Ex}$) about the Arrhenius line so that the effect of Δx on the diffusion results must be within the random experimental errors.

It should be noted that the ordering reactions occurring in the CeO_2-Ce_2O_3 system on cooling from the fluorite phase region are very rapid and cannot be arrested by quenching[2]. Consequently the specimens would contain the ordered low temperature phases before the exchange run, and the disordering process must occur while the initial exchange takes place. The effect should not be very great since the disordering process should be at least as rapid as ordering.

Possibly a more important source of error is that the reduced oxides have been reported to be pyrophoric[55,56,57]. Ignition did not take place with specimens in air, but the polycrystalline specimens did become lighter in colour indicating that some oxidation had occurred. When the specimens were pushed out of the hot zone after equilibration, the CO-CO_2 gas was oxidizing to them and could result in oxidation before the apparatus

was evacuated. If this has occurred then on lowering the specimen into the hot zone for the exchange run the initial exchange will be occurring in an oxidized specimen, and thus the rate of uptake will be low. The specimen would be reduced during the exchange run, and so movement of ^{18}O into the specimen occurs against a flux of oxygen ions out of the specimen. This counter-flow would reduce the rate of diffusion into the specimen. The reduction of the specimen would increase the concentration of ^{16}O in the gas phase, and so effectively increase the rate of reduction of $\%^{18}O$ in the gas phase.

The effect of the addition of ^{16}O to the gas phase can be calculated. For run number 23, $n_g = 7.47 \times 10^{-4}$ and $n_s = 3.46 \times 10^{-4}$. The number of moles of ^{16}O transferred from solid to gas during reduction is $3.46 \times 10^{-4} \times 0.17/1.99 = 0.30 \times 10^{-4}$ moles assuming the specimen had been oxidized to $CeO_{1.99}$. Before exchange the gas possessed 0.800% ^{18}O, or 0.060×10^{-4} moles. The ^{16}O transferred from the solid thus changes the ^{18}O content of the gas to 0.771%. During exchange the ^{18}O content was reduced to 0.626 so that the reduction can only contribute about one sixth of this. Thus any oxidation of the quenched specimen that did occur has not affected the uptake by a great amount.

If the reduction did contribute oxygen to the gas phase during exchange then the reaction $CO + O_2 = CO_2$ would result in a decrease in the CO/CO_2 ratio during the run. In run 23 the total number of moles of CO and CO_2 in the gas was 1.47×10^{-3} and the ratio CO/CO_2 was 52. The addition of $.037 \times 10^{-3}$ moles of oxygen from the solid would reduce this ratio to 14. The ratios measured from the peak heights of mass numbers 28 and 44 in run 23 showed no systematic variation with sampling time, but was constant at 52 ± 5.

(viii) Time.

The time of commencement of exchange was not well defined since the cold specimen was lowered into the hot zone at zero time and required some finite time to achieve the exchange temperature. From the observed rate of quenching this time could not have been greater than fifteen seconds. Where Q = 0 the straight line plots of Dt/ρ^2 vs t did go through zero

time, indicating that errors from this source were not significant.

The time required for sampling was about three seconds. The samples were taken at different time intervals depending on the rate of exchange, but the most frequent was two minutes so that the uncertainty in time for the first samples was about 2%, but this figure decreases with each sample.

(ix) Air leakage.

Air leakage into the partly evacuated gas could occur either during exchange, or after taking the sample, while transferring to the mass spectrometer.

The first of these leakages was shown to be absent in two ways. Firstly the total gas pressure was measured before and after the exchange runs. In a typical experiment the pressure decreased by 0.5-1% due to removal of gas samples. Secondly the ratio of the peak heights for mass numbers 28 and 32 + 34 + 36 (or 28 and 44) was measured for each sample and showed that the N_2/O_2 (or CO/CO_2) ratios were constant throughout the run.

The measurement of peak height ratios also readily indicated whether any air leakage into the samples had occurred during transfer, and when this had occurred the result was discarded.

The mass number 32 peak in samples of $CO-CO_2$ gas mixtures was not significantly above the back ground of the instrument, confirming that no leakage had occurred into sample holders during transfer to the mass spectrometer.

If air leaked into the reservoir of CO^{18}/CO_2 then there would be a contribution due to both N_2 and CO to the mass number 28 peak, which could not be separated. No change in the CO/CO_2 ratio from the reservoir was seen on standing, and the diffusion coefficients obtained for zirconia-yttria single crystals in $CO-CO_2$ were compatible with those in N_2-O_2 mixtures so that any error from this source must be negligible.

(x) Mass analysis.

The mass spectrometer did not function perfectly for each run. Sometimes an air leak developed leading to high background peaks, and at other times electronic instability occurred leading to an unsteady base line on the recorder. Several experimental runs were lost due to these faults, as shown in appendix 4, tables 9 and 10.

Generally three or four mass scans were made on each gas sample. The reproducibility of the analyses obtained in this way varied from experiment to experiment due to the above causes. The reproducibility was generally $\pm$ 0.05% ^{18}O, although better than $\pm$ 0.01% ^{18}O was obtained at times and the worst was $\pm$ 0.1% ^{18}O. Thus with a 5% sample the greatest error from this source was 2%. As shown in table 10 of appendix 4 much lower ^{18}O contents were used in runs 11, 23 and 25. The reproducibility in each of these was better than $\pm$ 0.01 % ^{18}O, leading to errors of less than 2%

For all runs the gas samples taken several minutes before and just before starting had the same ^{18}O content, to within the sample reproducibility. The scatter of experimental points about the straight lines for Dt/ℓ^2 vs t using the appropriate Q value (appendix 3) was within this error source for all experiments. The effect of mass analysis errors on the diffusion coefficients depended on the change in ^{18}O content rather than on the actual ^{18}O level. With an ^{18}O level of 5% this change was typically about 1%, so that taking the greatest irreproducibility of 0.1% an error of 10% could have been introduced into D. In the extreme case of run 11 the ^{18}O content changed by 0.065% and the reproducibility was 0.005% so that the error in D was less than 10%

(xi) Calculations.

An error is introduced where a selection of a Q value is made on the basis of the plot of Dt/ℓ^2 vs. t being a straight line when the surface exchange coefficients is accounted for. In appendix 3 a selection on this basis was made between Q values of 0.00, 0.05, and 0.1 giving an estimated possible error of 15%. In the range Q = 0.2, 0.5, 1, 2 and 5 the difference

in D values calculated is greater-as is shown in figures 31 and 32 of appendix 2, by the difference in plots of Mt/M_∞ vs. Dt/ℓ^2. This greater difference is counteracted to a large extent by the more positive identification of the correct Q value owing to the more pronounced curvature of the plot for the "wrong" Q value.

In practice it was found that the error from this source was always greater than the scatter due to random experimental errors so that $\pm$ 15% is a reasonable estimate of the total error in the diffusion coefficient results. Where calculation errors of this type were not present, since Q = 0 (CeO_2 (P), prep 1), a very good straight line Arrhenius plot resulted.

As shown in the appendix 3 calculation, the error in the surface exchange coefficients from this source is much greater than that estimated above for the diffusion coefficient, and may be as great as 50%.

(xii) Specimen shape.

A further source of error in the results arises from irregularities in the specimen shape. The spheres produced by air blasting were rather irregular in shape, while those produced by grinding still contained elements of the original cube surfaces, since to continue the grinding to perfect spheres gave specimens too small to be used. The "cubes" had side lengths differing by as much as 10% and the disc thickness could vary by 10% due to non parallel faces.

The dimensions, used for diffusion calculations on the spheres and cubes, were calculated from the weight and density in order to mimimize the effect of these irregularities. The dimensions calculated always agreed with the approximate mean of measured dimensions.

Some idea of the effect of these irregularities can be obtained by comparing the variation about the Arrhenius plot for ceria single crystals in air, where the irregular spheres were used as well as cubes, with the variations about the Arrhenius plots for polycrystalline specimens ground to cubes. In the latter the variation is within the $\pm$ 15% error of calculations. while the former has some points outside these limits.

(xiii) Summary.

a) Diffision coefficients.

Where specimens were of the same shape and composition, Arrhenius plot scatter was within the $\pm$ 15% error due to selection of a Q value (zirconia-yttria (P and S),ceria-yttria (P), and thoria-15% yttria(P)). Where Q = 0 there was very little scatter (ceria (P) - prep. 1.). Where the shape (ceria (S) in air) or the composition ($CeO_{(2-x)}$ (S)) were not well defined, scatter was as great as $\pm$ 30%.

b) Surface exchange coefficients.

Where specimens were of well defined shape and composition, the scatter about the Arrhenius plots was again generally within the errors due to selection of a Q value - $\pm$ 50% (ceria-yttria (P) and zirconia-yttria (P and S)). Some widely differing results were obtained, however, which indicates that the preparation procedure used had given insufficient control of the surface conditions.

3.3. Proton Activation and Autoradiography.

Enhanced activity at edges of specimens and at grain boundaries was observed in autoradiographs of cross sections of ceria specimens bombarded with protons.

Figure 15 is a photomicrograph, at magnification x 80, of the autoradiograph produced by exposing Kodak AR10 stripping film for 10 hours on the cross section of a ceria multicrystal exchanged in 0.21 atmospheres oxygen in run number 27. This specimen had been bombarded with 2.8 MeV protons at a current of 20 nanoamps for one hour. Unfortunately exchange results were not obtained from this run because the mass spectrometer was not functioning correctly. The enhanced activity along the grain boundary can be seen extending from the surface well into the specimen. The same autoradiograph is shown in figure 16 at a maginfication of X 320 The individual silver particles of about $\frac{1}{2}\mu$ diameter can be seen, and the width of exposed film at the grain boundary can be estimated as about 10μ. The resolution of the film using this technique is about 5μ so that very little penetration has occurred into the grain from the boundary. The activity at the specimen surface cannot be seen in figure 15

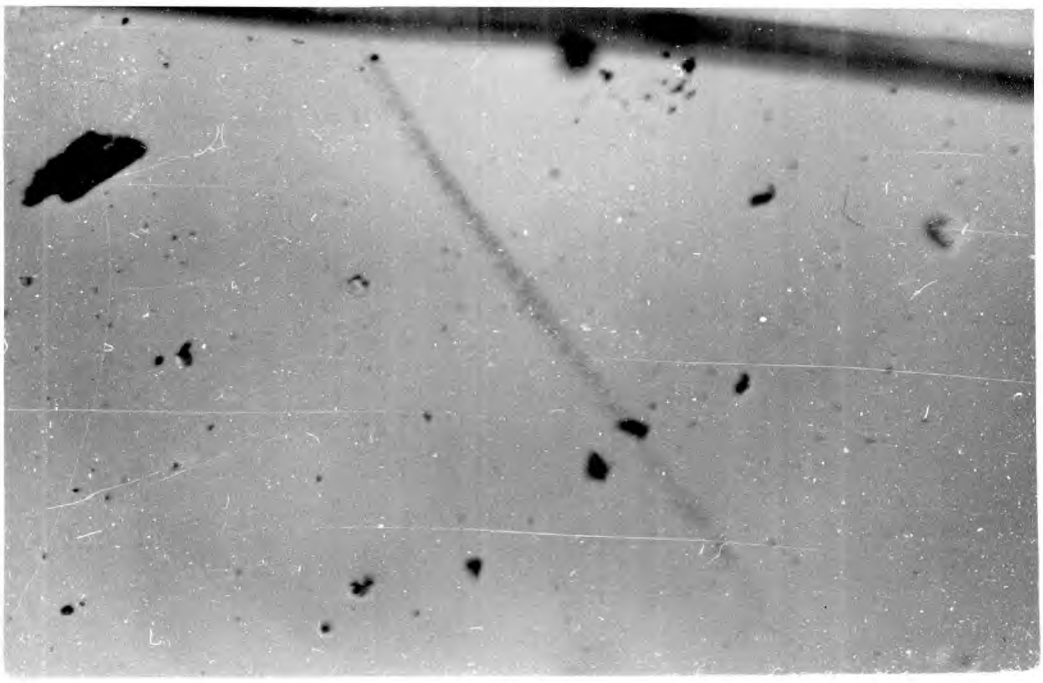

Fig. 15. Photomicrograph (x 80,) of autorodiograph of the grain boundary region of a ceria single crystal aggregate exchanged with ^{18}O at P_{O_2} = 0.21 atm., sectioned, and bombarded with 2.8 MeV protons at 20 nano amps (enlarged x 3).

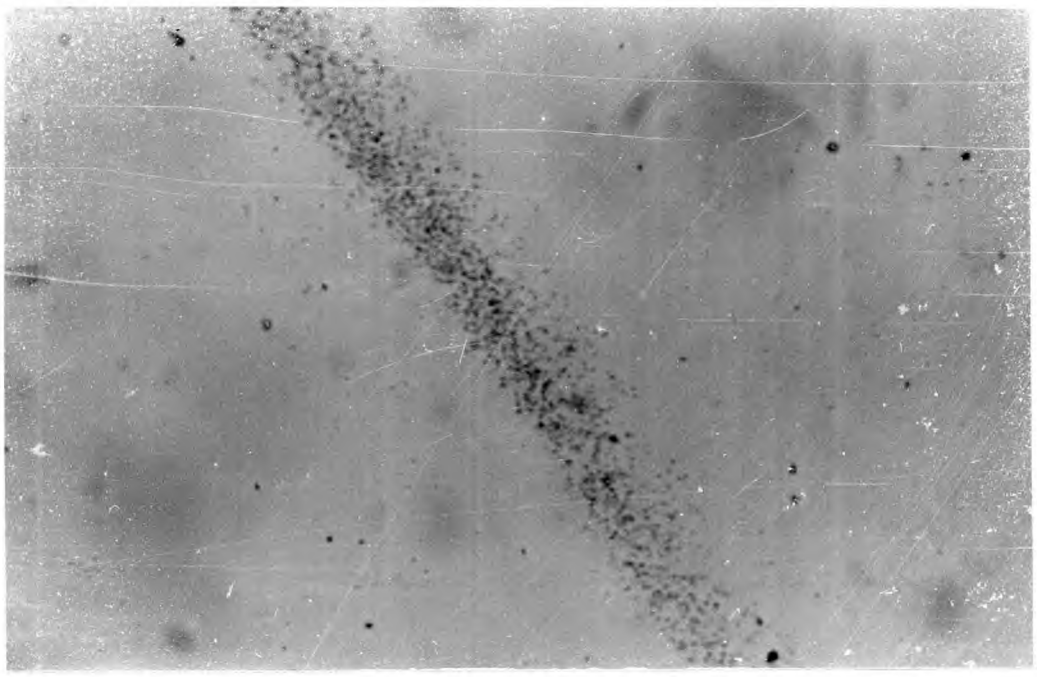

Fig. 16. Same as figure 15 (x 320, enlarged x 3)

because the film was crinkled along the specimen edge after stripping and placing on a glass slide. Surface activity could, however, be seen at the corner where crinkling did not occur, and was similar in extent to that along the grain boundary.

Figure 17 is a photomicrograph at a magnification of X500 of a grain boundary area of an autoradiograph from a ceria multicrystal exchanged at 0.21 atmospheres oxygen pressure and 924°C in run 32. This crystal had been sectioned and irradiated with 3.1 MeV protons at a current of 100 nanoamps for one hour and the autoradiograph exposed for 2¼ hours. The surface enhancement in this autoradiograph is shown at a magnification of X80 in figure 18.

Figure 19 shows the edge of this surface region (X500) representing the diffusion front which has a very rapid reduction of activity going into the crystal. The granular appearance of these exposed regions is not understood, and the observed rapid reduction in activity in the crystal would not be expected from the profile equation

$$C_{(x,t)} = \frac{Co}{\sqrt{\pi Dt}} \exp \left(\frac{-x^2}{4Dt}\right) \qquad \text{.....(3.22)}$$

where $C_{(x,t)}$ is the concentration of diffusing species at distance x for diffusion time t; Co is the concentration at the surface.

In order to obtain diffusion coefficients, the decrease in silver grain density into the crystal is required, and a plot of log C/Co vs x^2 should give a straight line of slope 1/4Dt. The granular appearance of the surface region shown in figure 18 precludes an optical density study such as that of Holt[58]. If it is assumed that the inside edge of the high density silver grain region corresponds to an ^{18}O content equivalent to the natural abundance of 0.2%, then the concentration is about one hundredth of that at the surface. The depth of penetration shown in figure 18 is 0.2mm and exchange had proceeded for 4 hours so that a diffusion coefficient of 1.4×10^{-8} is obtained. This agrees very well with the diffusion coefficient for single crystal ceria at 0.21 atmospheres oxygen pressure obtained from exchange measurements at the same temperature.

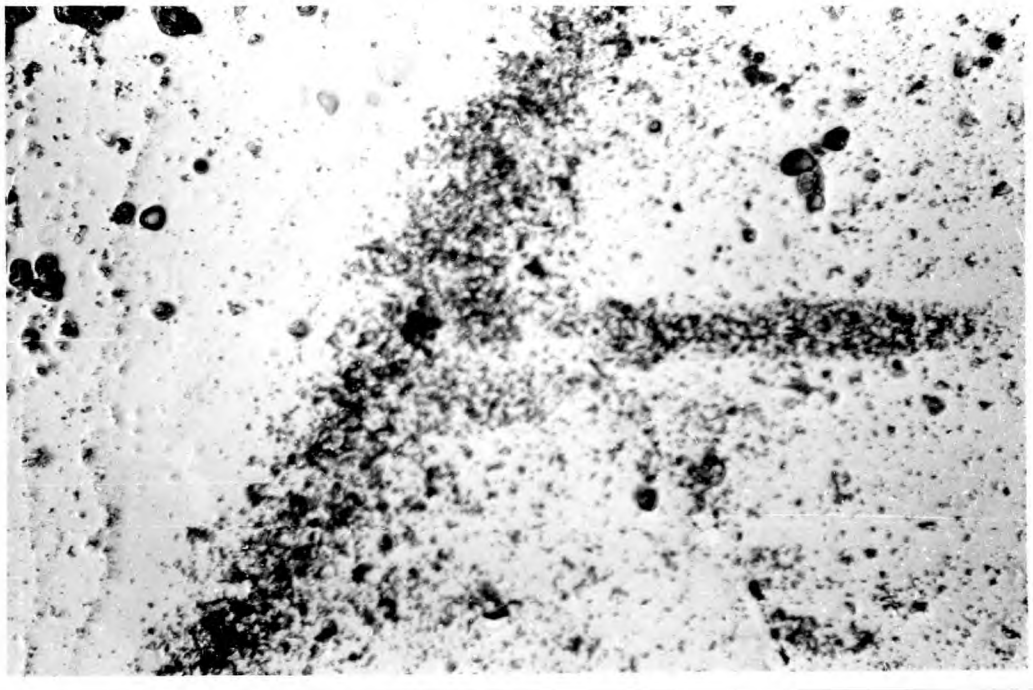

Fig. 17. Photomicrograph (x 500) of autoradiograph of the grain boundary region of ceria single crystal aggregate exchanged with ^{18}O at P_{O_2} = 0.21 amt., sectioned, and bombarded with 3.1 MeV protons at 100 nanoamps (enlarged x 3).

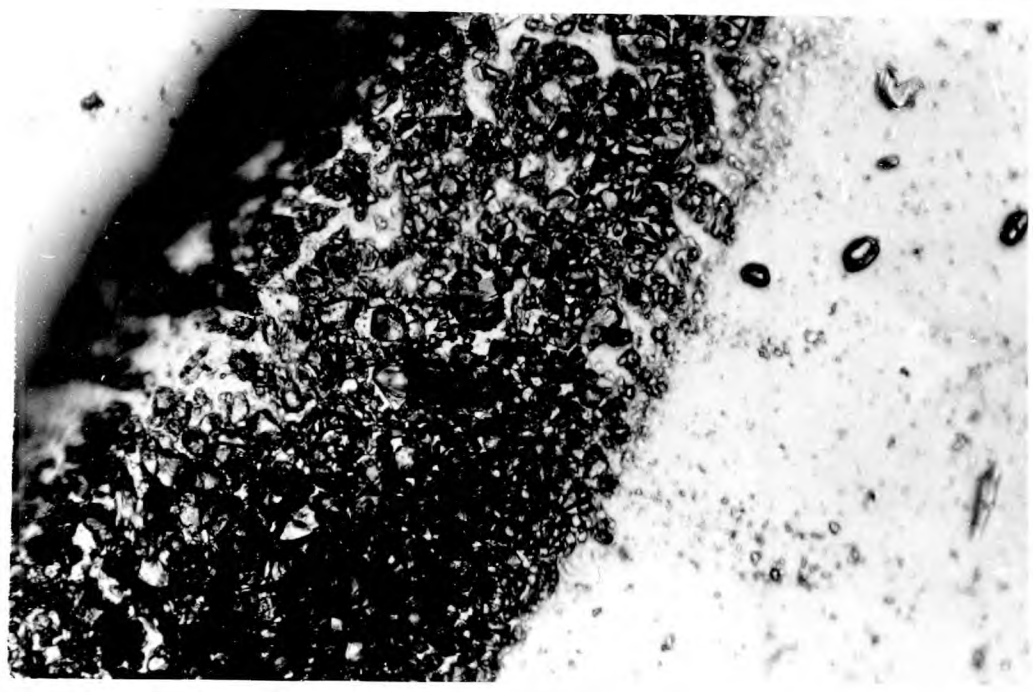

Fig. 18. Same autoradiograph as figure 17. Surface region (x 80, enlarged x 3)

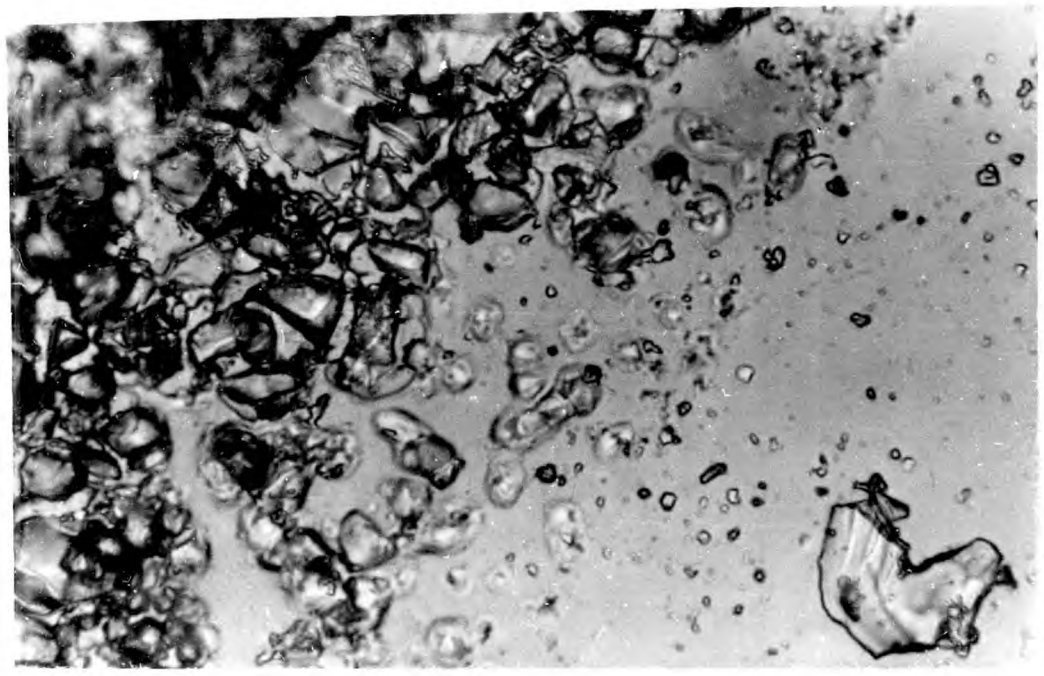

Fig. 19. Same autoradiograph as figure 17 and 18. Diffusion front of surface region (x 500, enlarged x 3).

Chapter 4.

Discussion.

4.1. Introduction.

In this chapter experimental results will be compared with other work on transport in oxides. As noted by Birchenall[60] a better estimate of the reliability of diffusion results is obtained by comparing actual magnitudes of diffusivities rather than activation energies. The variation of transport coefficients with gas composition, non stoichiometry, and concentration of lower valent cation will be examined with a view to elucidating the defect structure and transport mechanisms in the systems studied.

4.2. Diffusion Coefficients.

In the following discussion ^{18}O diffusion results are sometimes compared with results involving the transport of ^{16}O. Heavier isotopes generally do not diffuse as fast as lighter isotopes, and the magnitude of this isotope effect for ^{17}O and ^{18}O was shown by Koros and King[61] to be $D_{17}/D_{18} \simeq 1.25$ for a lime silica slag. Thus, other factors being equal, the isotope effect would predict that the ^{18}O diffusion results should be about 50% lower than results involving ^{16}O.

Figures 20 and 21 show the results of the present work compared with Arrhenius plots for diffusion coefficients obtained from the results of other workers in similar oxides. Generally the plots show order of magnitude agreement between this work and published data for ceria-yttria, zirconia-yttria, and thoria-yttria solutions. There is a large range of results available for CeO_2, perhaps indicating impurity control.

4.2.1. Models for Diffusion.

The random walk approach[62] describes the macroscopic diffusion coefficient D in terms of the jump distance S and jump frequency of the

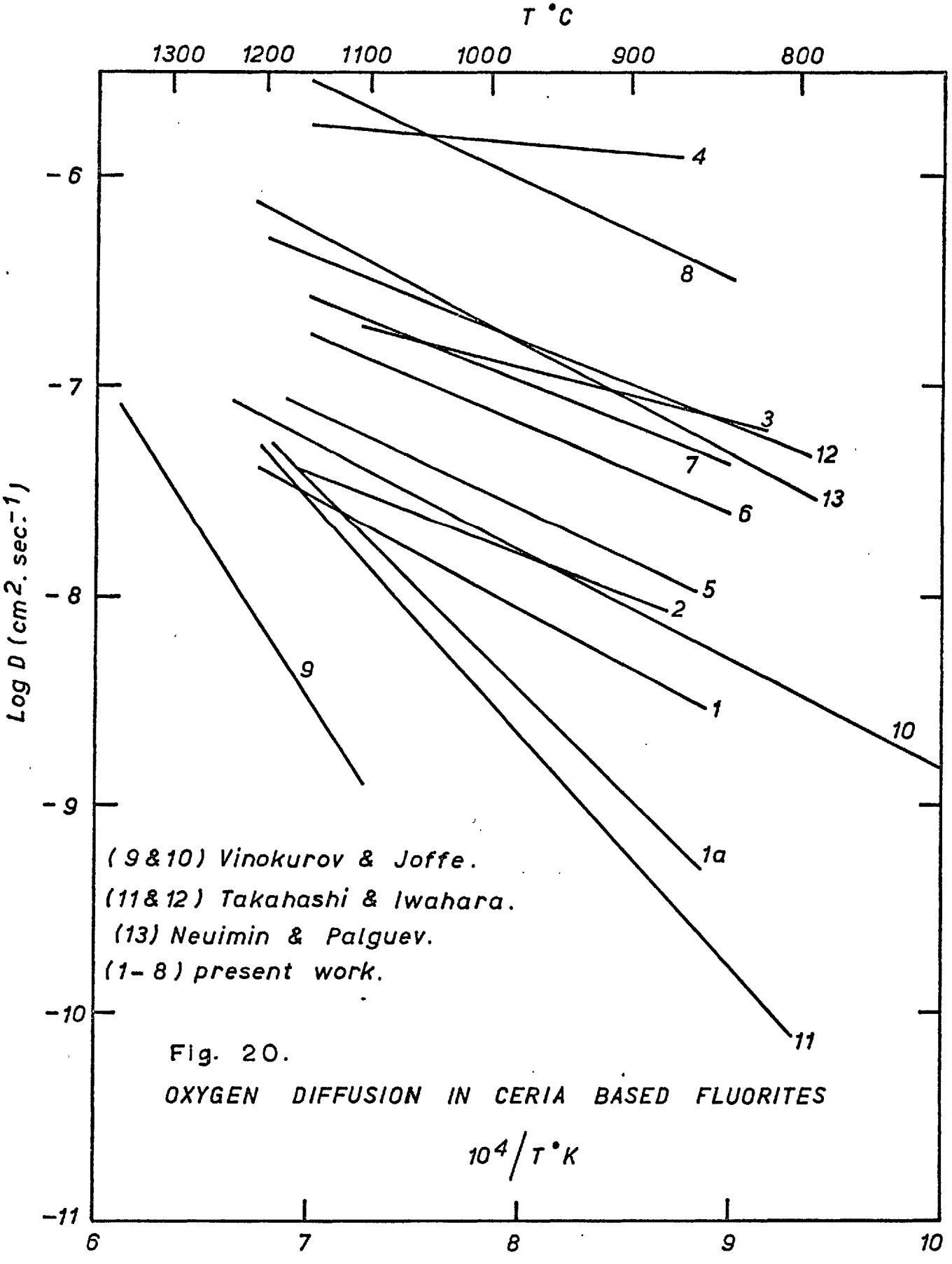

Fig. 20.

OXYGEN DIFFUSION IN CERIA BASED FLUORITES

Key: (1) CeO_2 (S) 0·21 atm. (1a) CeO_2 (S) 0·21 atm. Q = 0. (2) CeO_2 (S) 0·02 atm. (3) $CeO_{1.92}$ (S). (4) $CeO_{1.80}$ (S). (5) CeO_2 (P) 0·21 atm. (6) $Ce_{0.90}Y_{0.10}O_{1.95}$ (P). (7) $Ce_{0.80}Y_{0.20}O_{1.90}$ (P). (8) $Ce_{0.60}Y_{0.40}O_{1.80}$ (P) (1-8 present work). (9) $CeO_2 + 10^{-5}$% Gd (S) (10) CeO_2 + 0·3% Gd (S) (11) CeO_2 (P) (12) $Ce_{0.80}La_{0.20}O_{1.90}$ (P). (13) $Ce_{0.739}Y_{0.201}O_{1.870}$

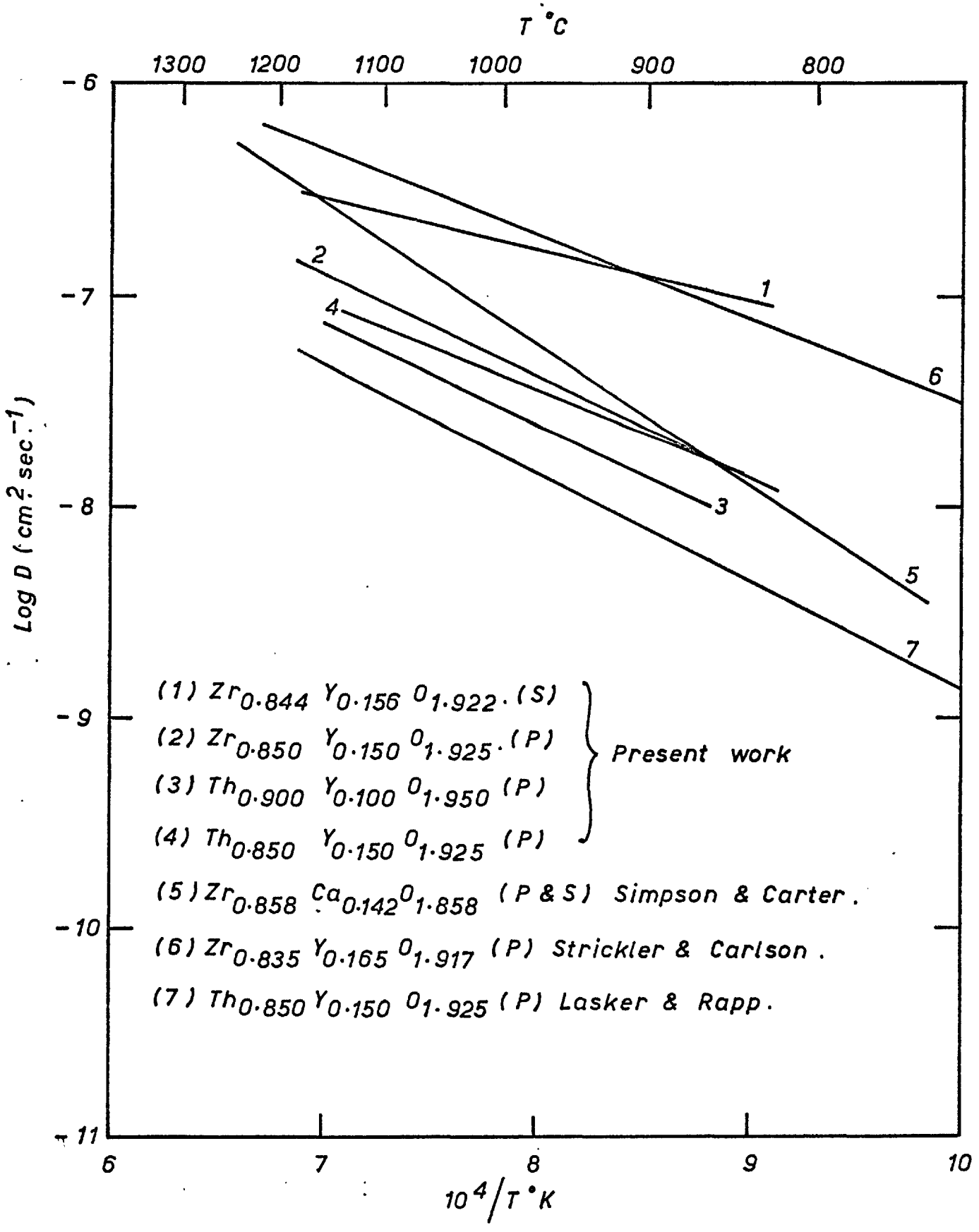

Fig.21. OXYGEN DIFFUSION IN THORIA & ZIRCONIA BASED FLUORITES

diffusing species.

$$D = \frac{1}{6} \quad \gamma \quad S^2 \qquad \text{.....(4.1)}$$

For tracer diffusion by a vacancy mechanism the most likely second jump of the tracer is back into the position it left vacant in the first jump. Consequently a correlation factor, f, must be introduced to allow for the correlation of jumps in this way. Thus

$$D = \frac{1}{6} f \gamma S^2 \qquad \text{.....(4.2)}$$

(For the simple cubic oxygen sublattice of the fluorite structure f = 0.653)

The jump distance for oxygen in the fluorite lattice is a/2 where a is the lattice parameter. The jump frequency is given by

$$\gamma = 6. \omega_v N_v$$

where N_v is the probability that a nearest neighbour site is vacant, ω_v is the probability that the atom will have sufficient energy to jump into the vacant site, and the number of nearest neighbours on the simple cubic oxygen sub-lattice is 6.

Substituting these in equation (4.2)

$$D = \tfrac{1}{4} . f. a^2 . \omega_v .N_v \qquad \text{.....(4.3)}$$

The jump probability is a function of the vibration frequency and the energy barrier to movement of the diffusion species;

$$\omega_v = \nu \exp \quad (- \Delta G_m/RT)$$

ν is usually taken as the Debye frequency and ΔG_m is the free energy to move defects. Thus equation (4.3) leads to

$$D = \tfrac{1}{4}. f. a^2. \nu . N_v. \exp (- \Delta G_m/RT) \qquad \text{.....(4.4)}$$

One may write an equilibrium reaction for completely ionized oxygen vacancy formation in ceria (using the defect notation of Kroger and Vink[63])

$$O_o = \tfrac{1}{2} O_{2(g)} + V_o^{\cdot\cdot} + 2e' \qquad \text{.....(4.5)}$$

The equilibrium constant K for this reaction is

$$K = \frac{P_{O_2}^{\frac{1}{2}} \cdot [V_o^{\cdot\cdot}] \cdot [e']^2}{[O_o]}$$

assuming no interaction of defects.

With $[O_o] = 1$ and $[V_o^{\cdot\cdot}] = \tfrac{1}{2}[e']$ and if ΔGf is the free energy to form defects according to equation (4.5)

$$[V_o^{\cdot\cdot}] = (\tfrac{1}{2})^{\frac{1}{3}} P_{O_2}^{-\frac{1}{6}} \cdot \exp(-\Delta Gf/3RT) \qquad \text{....(4.6)}$$

Putting $N_v = [V_o^{\cdot\cdot}]$ in equation (4.4) gives

$$D = (\tfrac{1}{8}) \gamma f \cdot a^2 \nu \cdot P_{O_2}^{-\frac{1}{6}} \cdot \exp((\Delta Sm + \Delta Sf/3)/R) \cdot \exp(-(\Delta H_m + \Delta H_f/3)/RT) \qquad \text{....(4.7)}$$

In common with other fluorites, the addition of lower valent cations to ceria has been shown[64] to result in substitution of the cation for Ce^{4+} in the cation sublattice, with charge compensation by oxygen vacancy formation. For M^{3+} addition the reaction is

$$O = M_{Ce}' + \tfrac{1}{2} V_o^{\cdot\cdot} \qquad \text{....(4.8)}$$

Assuming no defect interaction

$$[V_o^{\cdot\cdot}] = \tfrac{1}{2}[M_{Ce}'] \qquad \text{.....(4.9)}$$

Substituting in equation (4.4) yeilds

$$D = \tfrac{1}{8} \cdot f \cdot a^2 \nu \cdot [M_{Ce}'] \exp(\Delta S_m/R) \exp(-\Delta H_m/RT) \qquad \text{...(4.10)}$$

A coulombic attractive force between $V_o^{\cdot\cdot}$ and M_{Ce}' would be expected, and if the M^{3+} ion is larger than Ce^{4+} than the presence of a vacancy next to an M^{3+} ion would reduce the mechanical strain associated with the presence of both these defects. Hence a complex could be formed according to the reaction

$$V_O^{\cdot\cdot} + M_{Ce}' = (V_O^{\cdot\cdot} M_{Ce}')^{\cdot} \qquad .....(4.11)$$

with the equilibrium constant

$$K' = \frac{[(V_O^{\cdot\cdot} M_{Ce})^{\cdot}]}{[V_O^{\cdot\cdot}][M_{Ce}']}$$

Condition (4.9) still holds so that

$$[V_O^{\cdot\cdot}] = (\tfrac{1}{4})^{\frac{1}{3}} [V_O^{\cdot\cdot} M_{Ce}']^{\frac{1}{3}} \exp(\Delta Gc/2RT) \qquad ....(4.12)$$

where ΔG_c is the free energy for complex formation according to reaction (4.11)

Substituting in equation (4.4) yeilds

$$D = (\tfrac{1}{4})^{\frac{5}{2}} \cdot f \cdot a^2 \cdot \nu \cdot [V_O^{\cdot\cdot} M_{Ce}']^{\frac{1}{2}} \exp\left((\Delta S_m - \Delta S_c/2/R) \exp(-(\Delta H_m - \Delta H_c/2)/RT) \right.$$

$$\left. \qquad .....(4.13) \right.$$

It should be noted that ΔG_m and ΔG_f are positive quantities while ΔG_c is negative so that equation (4.13) predicts an increase in slope of the Arrhenius plot when complex formation occurs.

In these derivations concentration terms have been used where activity coefficients of unity have been assumed. As shown by Libowitz[14] these equations therefore will not apply at high defect concentrations.

4.2.2. CeO_2

The oxygen diffusion coefficients of Vinokurov and Ioffe[24] shown in figure 20 were obtained from the rate of colour change of black reduced single crystals to clear oxidized crystals. Since the diffusion coefficients for specimens with 10^{-5} at % Gd^{3+} were much lower than with 0.3 at. % Gd^{3+} it is apparent that small departures from stoichiometry will greatly affect the diffusion coefficients. The chemical diffusion coefficients measured by this technique should thus be considerably higher than the self diffusion coefficient obtained from ^{18}O exchange.

If the exchange of oxygen at the surface of the single crystals is effective in slowing down the overall exchange rate, as found in the present work, then a higher diffusion coefficient with lower activation energy than that shown by the work of Vinokurov and Ioffe would be expected. To assess the importance of this, diffusion coefficients from the present work for ceria in air were recalculated by assuming Q = 0 in the diffusion equation solution and drawing a straight line through the curved Dt/ℓ^2 vs. t plot (appendix 3). The effect is shown by line 1a in figure 20.

The conductivity results of Takahashi and Iwahara[23] on ceria are in good agreement with several other workers' results as stated in chapter 1. Mixed conduction due to electrons and oxygen ions, with a constant transport number for oxygen ions of 0.3 above 800°C was found by Takahashi and Iwahara by incorporating ceria as an electrolyte in a galvanic cell. The diffusion coefficients shown in figure 20 as line 11 were calculated from these results.

The oxygen ion transport number in ceria has been the subject of considerable disagreement in the literature. Pal'guev et. al[65,66] determined the transport number in ceria by the e.m.f. technique and by measuring the gas electrolysed during d.c. conduction. They found that with increasing temperature the transport number increased to a maximum of 0.2 at 800°C and then decreased to 0.078 at 1100°C. Noddack and Walch[67] quote oxygen transport numbers of less than 0.002 from 600 to 1300°C based on the ohmic behaviour of d.c. current voltage measurements. No effect due to ionic transport during conduction in pure ceria from 300°C to 1000°C in oxygen could be detected by Blumenthal and Pinz[68] In their work lower conductivity values, of greater temperature dependence than found by other workers were reported for pure ceria. In ceria with 1 wt. % CaO, ionic transport was noted in an argon atmosphere, but not in oxygen. Holverson and Kevane[69] observed discolouration due to oxygen depletion during the passage of d.c. currents through single crystals of ceria with as little as 0.1% Ca^{2+} at 450°C from 1.0 to 10^{-4} atmosphere oxygen pressure.

The fact that Takahashi and Iwahara found a constant transport number of 0.3 over a wide temperature range in itself argues for impurity control of the defect concentration, although they interpreted it as being due to reduction according to reaction (4.5). Alcock[70] pointed out that any departure from stoichiometry involving the creation of electron carriers will make a solid become a semi conductor, since the mobility of electrons is several orders of magnitude greater than the mobility of oxygen ions. Thus as the temperature is raised at constant oxygen partial pressure, reaction (4.5) would produce electrons and oxygen vacancies, and the oxygen ion transport number should decrease. If, however, oxygen vacancies are produced by impurities as shown in reaction (4.8) then the concentration would be independent of temperature, and if the concentration of electrons is constant a constant transport number could result.

From these considerations, and from the comparison of diffusion results of this work with other data, it seems possible that the diffusion coefficients measured were due to the presence of lower valent impurity cations in ceria. It was noted in chapter 3 that all the ceria specimens were slightly yellow coloured. Linares[70] found that ceria single crystals grown from a similar flux to that used for the crystals in the present work contained colour centres due to Ca^{2+}, Pb^{2+}, and F^{-}, while smaller crystals grown from a flux of $Na_2O.B_2O_3$ were transparent. The addition of 0.1 % Ca^{2+} to the crystals resulted in an orange colour. Optical properties of ceria single crystals used in the present work were examined by Griffiths[71]. He concluded that the lack of a broad absorption band in the visible region (found when Ce^{3+} was present due to 50 to 100 p.p.m. W^{5+} in other crystals) indicated the absence of F^{-}; but the presence of lower valent cations was inferred from the yellow colour. Warmkessel and Kevane[57] found that contamination of ceria by platinum after reduction in hydrogen above 1300°C decreased the rate of reduction of ceria. Bevan and Kordis[2] also noted platinum attack after repeated reduction and oxidation of ceria. Chemical analysis of the single crystals in the present work failed to reveal the presence of any impurity.

If the diffusion results of the present investigation for CeO_2 were due only to impurities, no variation with oxygen partial pressure would be expected, as shown by equations (4.10) and (4.13). Figure 22 shows the

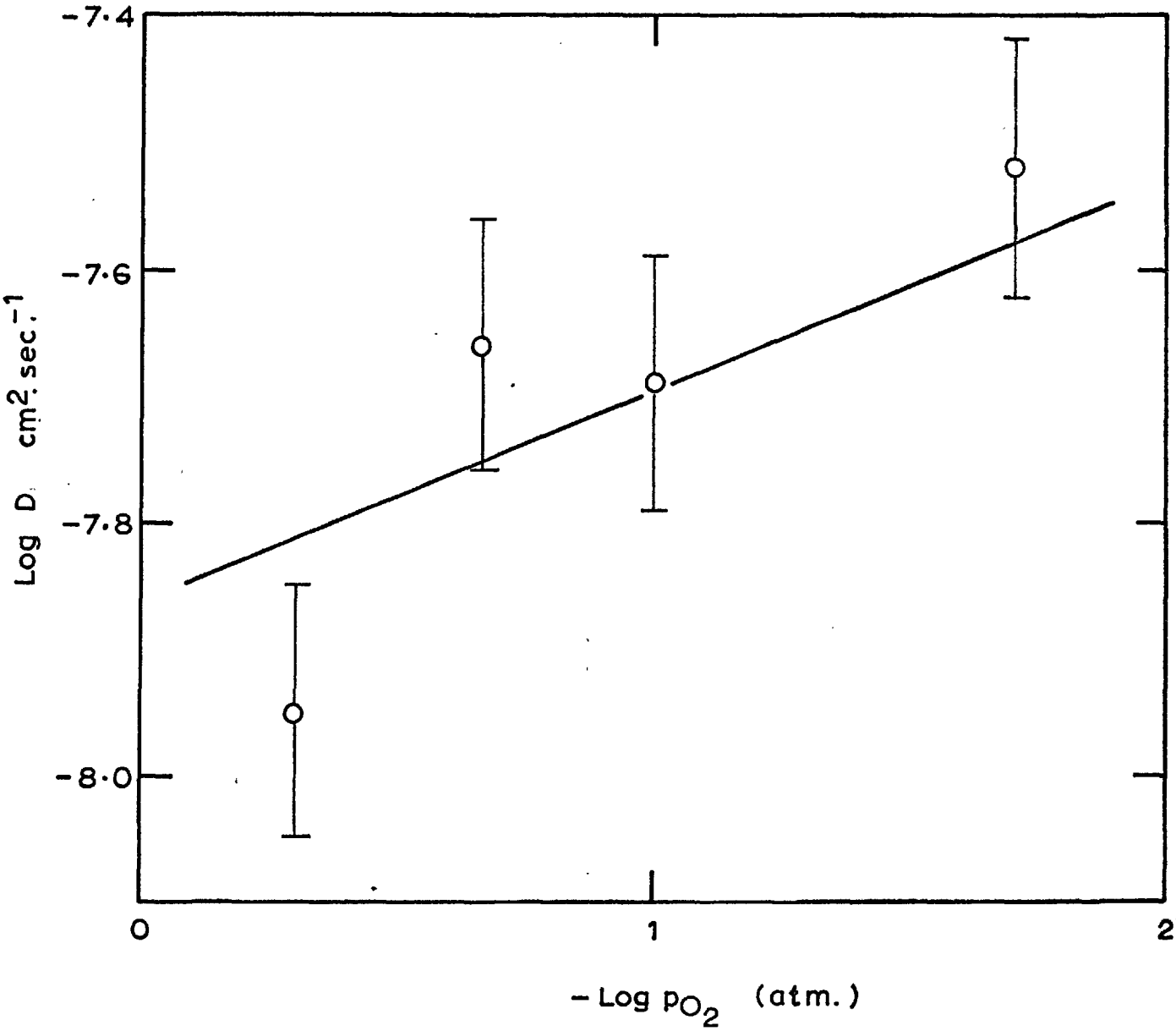

Fig.22. LOG D vs. LOG pO_2 FOR CERIA IN N_2/O_2 MIXTURES AT 1100 °C

diffusion coefficients as a function of pressure at 1100°C and an increase of D with decrease of pressure is evident. A line of slope $-\frac{1}{6}$ has been drawn through the results, corresponding to equation (4.7). The results would, however, be better described by a curve, as shown in figure 8. The oxygen pressure dependence of electrical conductivity in ceria was found to be - 1/5.7 at 987°C by Rudolph[20] and -1/5 between 1000 and 1400°C by Greener et. al.[72]. Thus the pressure dependence is consistent with the diffusion being due to oxygen vacancies formed by the reduction reaction (4.7), and not by lower valent cation impurities.

The formation of oxygen vacancy-impurity ion complexes has been observed in many fluorite systems and has been noted in ceria for the impurities: Ca^{2+} [73,74]; Gd^{3+}, Dy^{3+}, Er^{3+}, and Yb^{3+}[75]; and Sr^{2+}[76]. Vinokurov et al.[75] investigated the e.s.r. spectra of trivalent rare earth ions in ceria and concluded that both complexes and free vacancies were present. Free vacancies predominated for Gd^{3+} and were of the same order as complexes for Er^{3+}, Yb^{3+}, and Dy^{3+}. Kevane et. al.[73] studied the dielectric properties of ceria containing Ca^{2+} from 400 to 700°C and interpreted results in terms of vacancy-impurity complexes. Lay and Whitmore[74] studied dielectric and mechanical losses due to calcium-oxygen vacancy pairs in ceria from 25 to 200°C and determined a value of 19.8 k. cal. for the activation energy for vacancy jumps about the impurity ions. Solov'eva and Chebotin[76] ascribed the decrease of activation energy with increasing temperature for the ionic conductivity of CeO_2-SrO solid solutions to dissociation of a vacancy-strontium ion pair at 700-800°C. A formation energy of 14 k. cal. was calculated for this complex. Thus it is a possibility that, if the diffusion were partly due to impurities, the extrinsic part could be described by equation (4.13) rather than equation (4.10).

The activation energy for diffusion in $CeO_{1.92}$ is greater than in $CeO_{1.80}$ and this fact will be discussed in the next section. If the value for $CeO_{1.92}$ is taken as the activation enthalpy for motion of vacancies then at 0.21 atmospheres oxygen partial pressure, where the composition is close to stoichiometric, the activation enthalpy for formation of defects, or decompositoon of complexes, is about 39 k. cal. The values of the binding energy of vacancies to alter valent ions in ceria found by Lay and

Whitmore, and Solov'eva and Chebotin are much lower than this. Chebotin[77] calculated energies to form defects in ceria using a Born-type calculation. His results indicated that Schottky defects would have the lowest formation energy, 45 k. cal, with an estimated error of $\pm$ 150%. Calculations were not made for vacancy formation by reaction (4.5). Boswarva and Franklin[78] attempted the calculation of defect formation energies for oxides with the fluorite structure, but found that with oxygen vacancy formation the calculations indicated an attractive short range oxygen-oxygen potential; predicting inward collapse of the next nearest neighbour ions to a vacancy. If Chebotin's calculation is reliable it seems that an activation enthalpy of 39 k. cal to form vacancies in ceria is not unreasonable.

The above comparison of energies is arbitrary, however, because of the activation energy difference between $CeO_{1.92}$ and $CeO_{1.80}$, and because of the activation energy difference between an oxygen partial pressure of 0.21 atmospheres and 0.02 atmospheres. The former difference is discussed in the next section, and if the explanation presented there is valid then a higher activation enthalpy for motion of defects in stoichiometric CeO_2, than that in $CeO_{1.92}$, would be expected. The plot of Q_D vs. X in figure 26 predicts an enthalpy of motion at x = o of about 17 k. cal. Thus the enthalpy of formation of vacancies, or decomposition of complexes, would be 24 k. cal for 0.21 atmospheres; much closer to the figures for the binding energy of complexes quoted earlier. For 0.02 atmospheres an activation energy for diffusion of 17.4 k. cal. was found This is about equal to the activation enthalpy for motion of defects from figure 26, and thus equation (4.10) for unassociated vacancies produced by impurity cations would apply. The comparison of activation energies does not help in determining the appropriate defect formation reactions, but the fact that the activation energy for diffusion in ceria-yttria solid solutions is about the same as for ceria near stoichiometry seems to favour vacancy formation due to impurities.

The increase in activation energy with increasing oxygen partial pressure from 0.02 to 0.21 atmospheres (17.4 to 24.8 k. cal) cannot be explained in terms of part impurity control and part intrinsic vacancy formation, since this would predict a higher activation energy at 0.02, where the intrinsic vacancy concentration would be greater. Bevan and Rid

Kordis[2] found that the partial molal enthalpy of oxygen in $CeO_{(2-x)}$ changed rapidly with x approaching stoichiometry, indicating that less energy is required to create an oxygen vacancy in the oxygen-deficient state. Roberts and Markin[79] suggest that this decrease may be due to a decrease in the Madelung energy of the crystal, if the conduction processes are rapid enough to cause the excess electrons to be effectively smeared out over the whole crystal. The decrease in $-\Delta\bar{H}\ (\frac{1}{2}O_2)$ is about 20 k. cal. between $CeO_{2.0}$ and $CeO_{1.9}$ but Bevan and Kordis do not have information closer to stoichiometry than $CeO_{1.99}$. The curve of $\Delta\bar{H}\ (\frac{1}{2}O_2)$ vs x seems to increase in slope near to stoichiometry but this does not appear to be sufficient to explain the increase in activation enthalpy of formation of vacancies of about 21 k. cal calculated from the present work between 0.02 and 0.21 atmospheres oxygen pressure, where the change in x must be comparatively small. Furthermore at x = o an activation enthalpy for formation of vacancies of 118 k. cal. is predicted - much higher than any possible value from the present results.

The calculation of the pre-exponentaal factors for the three possible cases of intrinsic diffusion, extrinsic diffusion with unassociated defects, and extrinsic diffusion with associated defects may indicate which is more likely to be occurring in these results.

(i) Intrinsic diffusion. From equation (4.7)

$$D_o = (\tfrac{1}{4})^{\frac{1}{3}} .f.a^2.\nu .P_{O_2}^{-\frac{1}{6}} \quad . \exp\ ((\Delta Sm + \Delta Sf/3)\ /R)$$

For P_{O_2} = 0.21 atm.

f = 0.65

a = 5.411×10^{-8} cm.

and ν = 5×10^{13} sec^{-1}

D_o = 2.0×10^{-2} exp (Δ S/R)

(ii) Unassociated extrinsic diffusion. Equation (4.10) gives:

$$D_o = \tfrac{1}{8} . f. a^2. \nu \cdot [M_{ce}'] \quad \exp\ (\Delta S_m/R)$$

Assuming $[M_{ce}'] = 0.001$

$$D_o = 1.2 \times 10^{-5} . \exp\ (\Delta S_m/R)$$

(iii) Associated extrinsic diffusion. Equation (4.13) gives:

$$D_o = (\tfrac{1}{2})^{\frac{5}{2}} \cdot f \cdot a^2 \cdot \nu \left[V_o^{\cdot\cdot} \cdot M_{Ce}^{\prime}\right]^{\frac{1}{2}} \cdot \exp\left((\Delta S_m - \Delta S_c/2)/R\right)$$

Assuming $\left[V_o^{\cdot\cdot} \cdot M_{Ce}^{\prime}\right] = 0.001$

$$D_o = 2 \times 10^{-4} \cdot \exp\left(\sum \Delta S^1/R\right)$$

Experimentally, for single crystals and polycrystalline specimens at 0.21 atm. oxygen, $D_o = 2 \times 10^{-4}$ cm ^{2}/sec. Thus for the three cases:

(i) $\Delta S_m + \Delta S_f/3 \sim -5R$

(ii) $\Delta S_m \sim 2R$

(iii) $\Delta S_m - S_c/2 \sim 0$

Zener's[80] theory predicts that ΔS_m should always be positive for vacancy diffusion, but it has only been found valid for diffusion in closest packed metals. This theory only considers the strain dependent entropy and does not take into account the negative entropy contribution caused by increased vibrational frequencies at the saddle point of the diffusion coordinate.[111] The entropies to move vacancies in alkali halide crystals have generally been found to be positive,[112] and the migration entropy for cation diffusion in Cu_2O, CoO, and NiO were all found to be positive and of magnitude 2 - 3 R[113]. Thus it seems reasonable to assume a small positive value for ΔS_m.

The entropy to form anion defects in oxides has not been well studied. In a study of the oxidation of zirconia Smith[81] found an entropy of about 5R for vacancy formation. O'Keefe and Moore[113] found entropies of cation vacancy formation in Cu_2O, CoO, and NiO to be + 5R, - 6R, and - 7R respectively. The entropy of formation of Schottky or Frenkel defects in alkali halides vary from 3R to 5R.[112] The partial molal entropy of oxygen in CeO_2[2], $\Delta \bar{S}_{(\frac{1}{2}O_2)}$, is about -35R. This is the entropy change on adding ½ mole of oxygen to an infinite mass of oxide. Thus the entropy change associated with defect formation according to equation (4.5) is + 35R. This very large positive value for ΔS_f seems to

preclude case (i) above.

The change in viberational frequency with complex formation would not be great so that the major contribution to the entropy of formation of complexes would be configurational and ΔS_c would be less than R. Thus from the consideration of D_o values either case (ii) or case (iii) is favoured.

In conclusion the pressure dependence of diffusion coefficients for ceria favours the formation of vacancies by reduction and diffusion according to equation (4.7), while the fairly low activation energy and magnitude of D_o imply vacancy formation due to impurities and diffusion according to equation (4.10) or (4.13). In view of this contradiction, and the disagreement in the literature, it seems likely that the concentration of vacancies formed in both ways is significant in the oxygen pressure range of 0.02 to 0.21 atmospheres.

4.2.3. $CeO_{(2-x)}$ and $Ce_{(1-2x)}\ Y_{2x}\ O_{(2-x)}$.

Figure 9 shows that a substantial increase of oxygen diffusion coefficient occurs with increase of x. The diffusion coefficients for $CeO_{1.80}$ and $Ce_{0.6}\ Y_{0.4}\ O_{1.80}$ are of the order of magnitude of those found in liquids.

A similar increase of diffusion coefficient with x is found in $UO_{(2+x)}$, to about the same magnitude[37,38]. Very high oxygen diffusivities have been reported for Nb_2O_5 [82,83] but there is contradictory evidence[84] Ionic conductivities in ceria-yttria[21], and ceria-lanthana[21,23] solid solutions, with oxygen ion transport numbers close to unity, show a similar increase with x to that found in the present work,as shown in figure 20. As is generally found for solid solutions of oxides of lower valent cations with fluorite oxides, a maximum ionic conductivity occurs as x increases. The plot of log D vs x in figure 9 shows a continuous increase of the diffusion coefficient as x increases in the present work for $CeO_{(2-x)}$ and $Ce_{(1-2x)}\ Y_{2x}\ O_{(2-x)}$ and no maximum in the diffusivity occurs.

Kofstad and Hed[85] found that the tensiometric results of Bevan and Kordis[2] fitted a model assuming that the defects responsible for nonstoichiometry in ceria were singly and doubly charged interstitial cerium ions. They indicate that this is in accordance with the increase of lattice parameter with x reported by Brauer and Gingerich[6], but the increase would also arise from the larger Ce^{3+} ion with oxygen vacancies usually invoked for nonstoichiometric ceria. Furthermore Bevan[3] states that density measurements confirm the existence of anion vacancies. The very high oxygen diffusivities and marked increase with x in the present wonk would require a high concentration of oxygen vacancies increasing with x. Thus experimental results are better explained by formation of oxygen vacancies, rather than cerium interstitials, in $CeO_{(2-x)}$, as usually occurs in oxygen deficient oxides with the fluorite structure.

The activation energies for diffusion found for $CeO_{1.92}$ and $CeO_{1.80}$ only contain an activation enthalpy for motion, since the composition was held constant and the complex Ce^{3+} - oxygen vacancy would not be immobile. Electron switching can occur to change the position of the Ce^{3+} ion, effectively allowing high mobility of this entity. The co-operative movement of an electron and an oxygen vacancy would assist in the migration process since the fact that the Ce^{3+} ion is larger than the Ce^{4+} ion means a reduction in the mechanical strain due to an oxygen vacancy in the lattice. Activation entholpies for motion in $CeO_{1.92}$ and $CeO_{1.80}$ are 11.9 ± 3.9 k. cal and 3.6 ± 4.2 k. cal. respectively.

In $UO_{(2+x)}$ an activation energy of 29.7 k. cal was found for oxygen diffusion in $UO_{2.004}$ and $UO_{2.063}$[37] but this is not strictly comparable to the $CeO_{(2-x)}$ case since oxygen diffusion in $UO_{(2+x)}$ occurs via interstitials and not vacancies. By analysis of transient electrical conductivity data, activation energies for motion of oxygen vacancies in $SrTiO_3$[86] and $CaTiO_3$[87] of 6 k. cal and 13 k. cal. have been reported. Isotope exchange with $SrTiO_3$[88] gave activation energies for oxygen diffusion of 15.5 k. cal. and 29.3 k. cal. depending on the dislocation density. These values were interpreted as activation enthalpies for motion by Paladino et. al.[88] but Walters and Grace[86] suggest a contribution due to formation of vacancies. The activation energy for chemical diffusion of monovalent cations in body centered cubic sulphates,

with diffusion coefficients of similar magnitude to those of the present work, are of the order of 12 k. cal. and migration energies of 2 - 5 k. cal were calculated from these[89]. Thus, although activation energies for motion of oxygen ions in $CeO_{(2-x)}$ are very low, similar values have been reported in the literature.

In ceria-yttria polycrystalline specimens, diffusion coefficients of the same order of magnitude as in $CeO_{(2-x)}$ single crystals were found, but were associated with an activation energy of about 20 k. cal. The plot of log D vs x shown in figure 9 seems to follow the same straight line as for $CeO_{(2-x)}$. It should be noted that the diffusion coefficients for polycrystalline ceria specimens were significantly higher than for single crystals, and that the polycrystalline ceria-yttria diffusion coefficients are lower than those for polycrystalline $CeO_{(2-x)}$.

The higher activation energies for diffusion in ceria-yttria specimens could be explained by considering the binding of vacancies to immobile yttrium ions. As shown by equation (4.13)

$$Q_D = \Delta H_m - \Delta H_c/2$$

Solov'eva and Chebotin[76] calculated that ΔH_c in CeO_2 - SrO solid solutions was 14 k. cal. If the main contribution to ΔH_c is coulombic then the binding energy of oxygen vacancies to Y^{3+} ions should be less than that to Sr^{2+} ions because of the lower effective charge in the region of the substituted Y^{3+} ion in the fluorite lattice. However, using the ΔH_c value of 14 k. cal. and the ΔH_m value for $CeO_{1.92}$ of 12 k. cal, a Q_D value of about 19 k. cal. would be predicted in reasonable agreement with the value found. If this explanation were valid, a decreasing Q_D value with increasing x for ceria-yttria would be expected, since Q_D appears to decrease with x for $CeO_{(2-x)}$. The results show that Q_D for ceria-yttria solid solutions are constant to within experimental errors, suggesting that this simple explanation is not sufficient.

It should be noted that equations (4.10) and (4.13) predict that the diffusion coefficient would be proportional to x and $x^{\frac{1}{2}}$ respectively. Results reveal a continuous increase with x, but figure 23 shows that the plot of log D vs log x has a slope of 2.4. The dependence of D on x is better

described by an equation of the form D = const. x exp (x) as shown in figure 9, however.

In deriving the equations in section 4.2.1. no consideration of defect interactions was made (apart from"complex" formation). With such high concentrations of defects as encountered in the present investigation some form of interaction would be expected, and it is not surprising that the equations are not valid[13].

O'Keefe[90] considered the effect on the ionic conductivity of constraining the position of vacancies in highly defective oxides. When vacancies had one or none nearest neighbour vacancies he found that a maximum in the rate of ionic transport would be expected between x = 0.1 and x = 0.2. In ceria-yttria solid solutions this behaviour is seen for the ionic conductivity, but not for the diffusivity.

The log of the pre-exponential factors for diffusion in $CeO_{(2-x)}$ and $Ce_{(1-2x)}\ Y_{2x}\ O_{(2-x)}$ are plotted against x in figure 24, and against log x in figure 25. Within experimental errors D_o is independent of x for $CeO_{(2-x)}$ and increases with x for $Ce_{(1-2x)}\ Y_{2x}\ O_{(2-x)}$; either exponentially or proportional to $X^{2.5}$.

In the zirconia-calcia system Carter and Roth[91] mention that for ionic conductivities an exponential relationship of D_o to x has been reported in the literature, but they used a Gaussian dependence to explain the conductivity maximum.

The activation energies for oxygen diffusion in $CeO_{(2-x)}$ and $Ce_{(1-2x)}\ Y_{2x}\ O_{(2-x)}$ are plotted against x in figure 26. Within experimental errors Q_D decreases with x in $CeO_{(2-x)}$, but is constant in $Ce_{(1-2x)}Y_{2x}O_{(2-x)}$.

Within a very large scatter of results Carter and Roth[91] found the activation energy for ionic conduction in zirconia-calcia to be proportional to x.

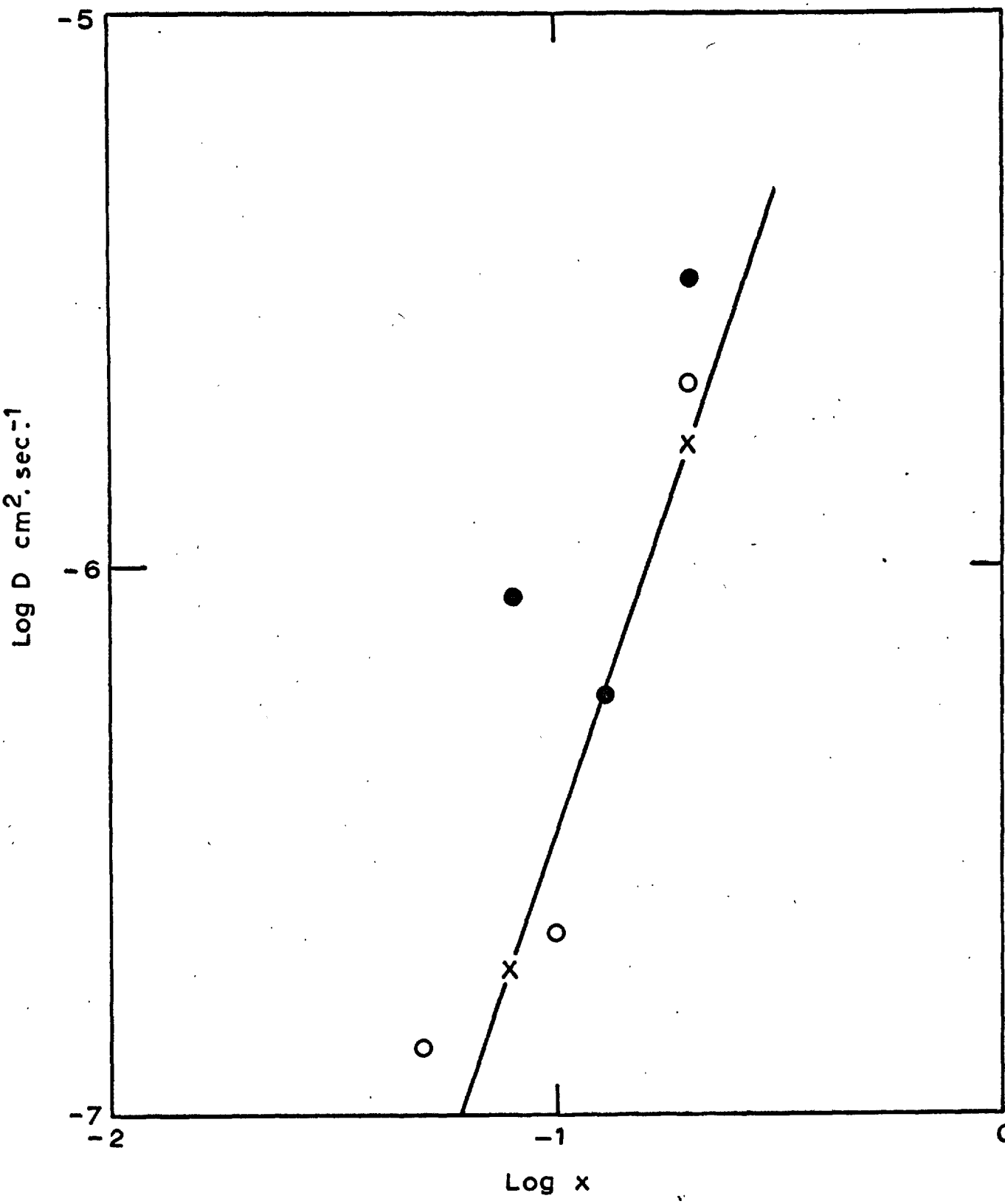

Fig.23. LOG D vs. LOG x FOR $CeO_{(2-x)}$ (S) - x, $CeO_{(2-x)}$ (P) - ● AND $Ce_{(1-2x)}Y_{2x}O_{(2-x)}$ (P) - O AT 1100°C

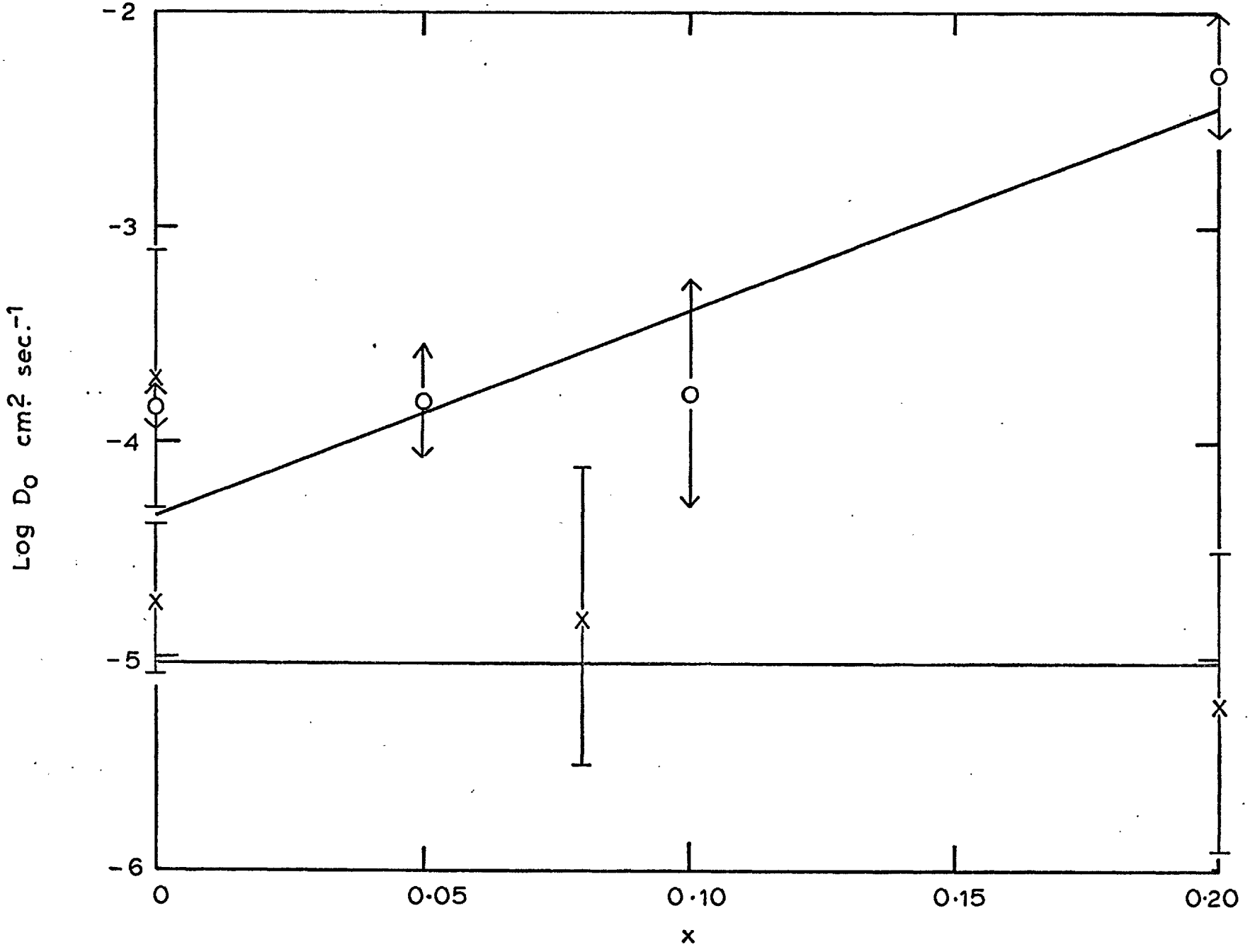

Fig.24. LOG D_o vs. x FOR $CeO_{(2-x)}$ (S) – x, AND $Ce_{(1-2x)}Y_{2x}O_{(2-x)}$ (P) – o.

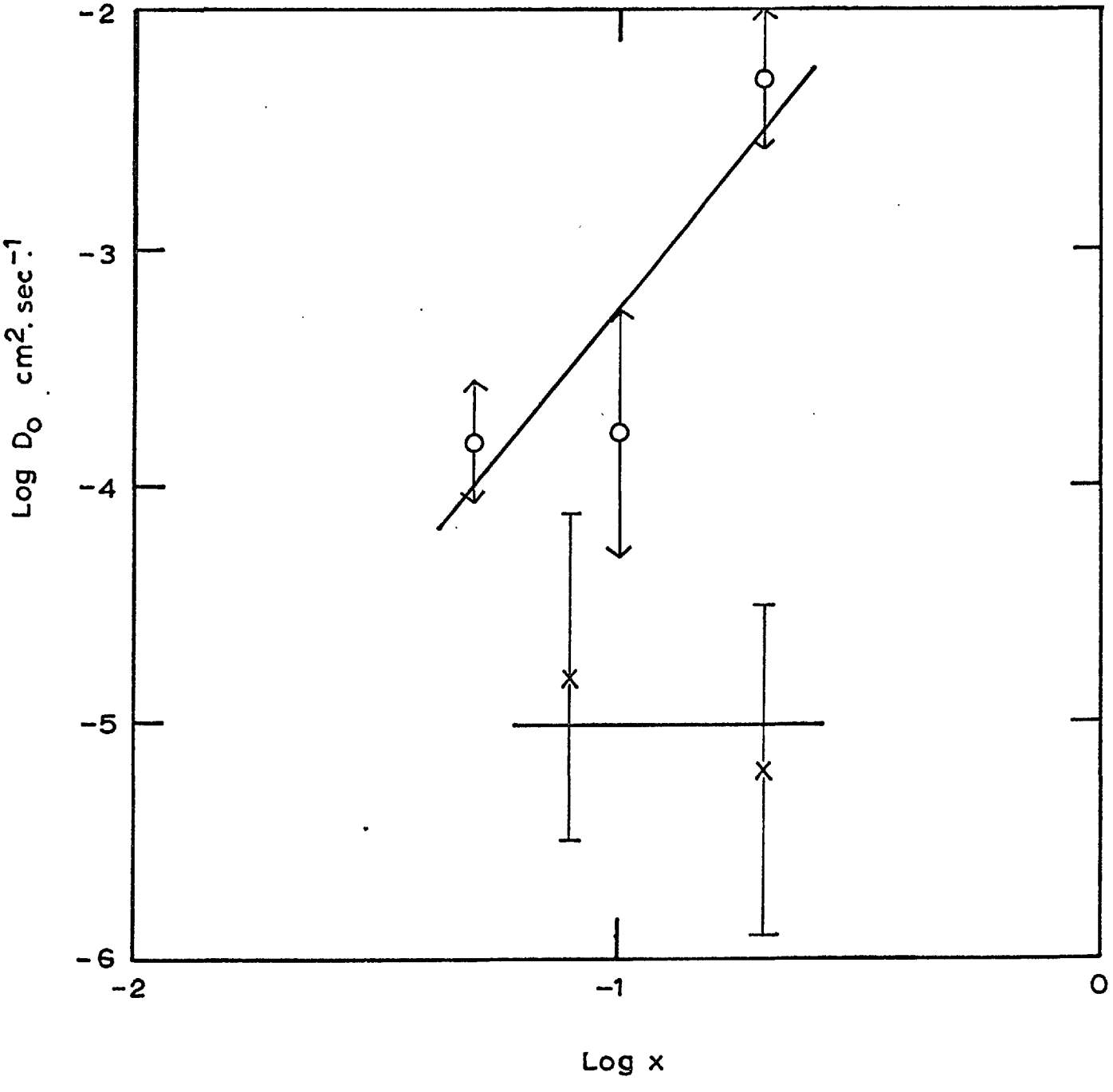

Fig.25. LOG D_o vs. LOG x FOR $CeO_{(2-x)}$ (S) -x ;
AND $Ce_{(1-2x)}Y_{2x}O_{(2-x)}$ - o .

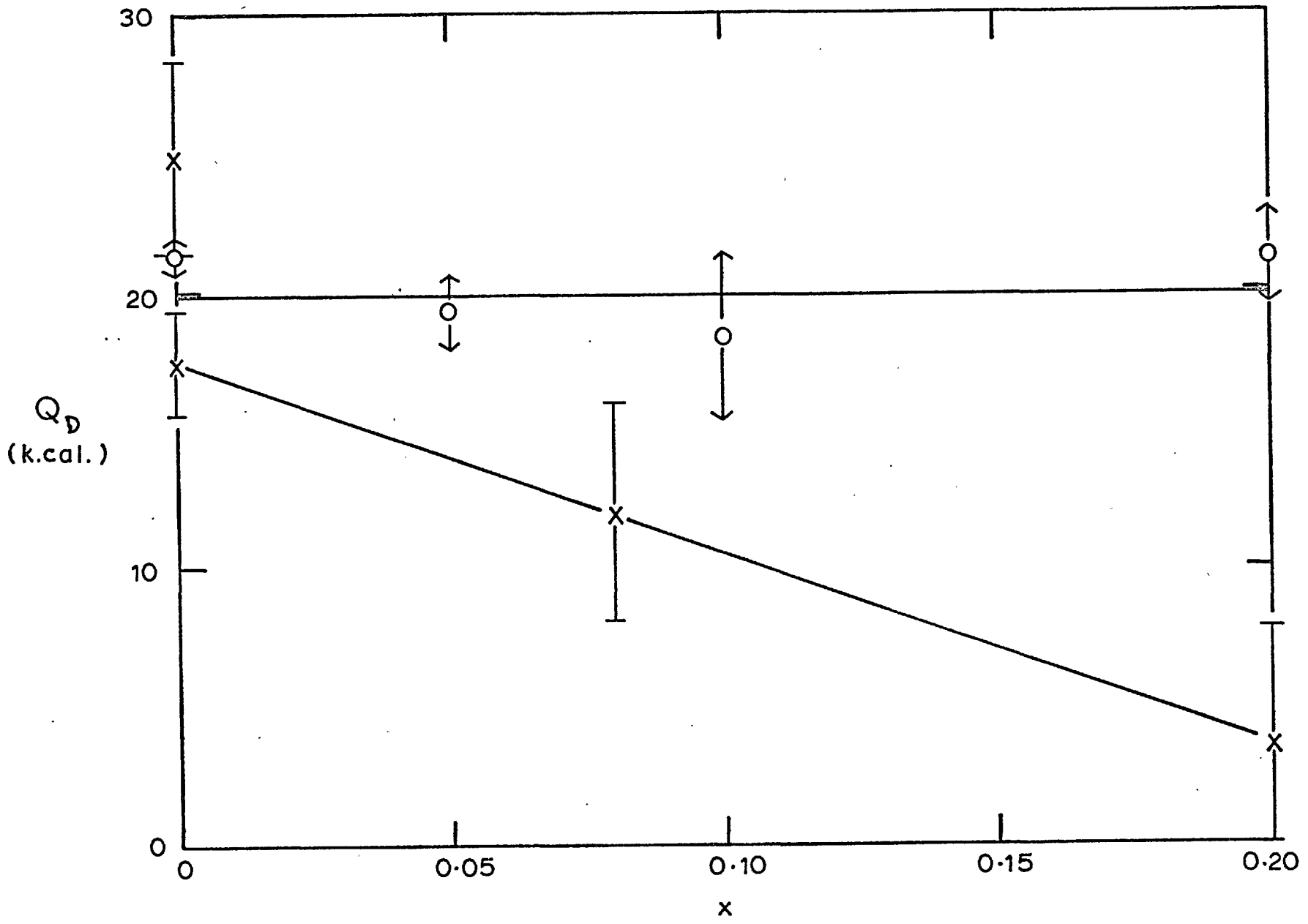

Fig.26. Q_D vs. x FOR $CeO_{(2-x)}$ (S) – x AND $CeO_{(1-2x)}Y_{2x}O_{(2-x)}$ (P) – o

If it is assumed that the vibrational frequency and entropy terms in the diffusion equations of type (4.10) or (4.13) are constant with x, the results of the present work suggest that for $CeO_{(2-x)}$ the concentration of defect giving rise to diffusion is constant with increasing x, while the activation energy to move the defect decreases with x. With defects caused by yttria addition the concentration of defects resulting in diffusion increases with x, while the activation energy remains constant. This difference in behaviour can be explained with reference to the structures involved.

Bevan and Kordis[2] found that the negative partial molal enthalpy, entropy and free energy of oxygen in fluorite $CeO_{(2-x)}$ decrease with increasing x and then pass through maxima in the range $CeO_{1.75}$ - $CeO_{1.80}$. These maxima occur in the region of intermediate low temperature phases in the system CeO_2-$CeO_{1.5}$, and were interpreted as an indication that the disordered fluorite region has similar structural entities to the ordered intermediate phases (figure 2). Atlas[59] proposed a statistical model to account for partial ordering of anion vacancies and reduced cations in a fluorite-type oxide. This model was used to derive expressions for the partial molal enthalpy, entropy, and free energy of oxygen in ceria which were used to calculate data in qualitative agreement with the experimental results of Bevan and Kordis[2]. Increasing irregularities with decreasing temperature were predicted, leading to separate intermediate phases at low temperatures. Thus defect ordering in reduced ceria in the fluorite range is indicated, and this ordering is probably similar to that occurring in the intermediate low temperature phases. No report of the effect of ordering on the high temperature x-ray diffraction of the reduced ceria fluorite solution was made by Brauer and Gingerich[6], but this work was carried out before the suggestion of ordering.

As briefly noted in chapter 1, intermediate low temperature phases in the rare-earth oxide systems correspond to a homologous series - $R_n O_{2n-2}$ - derived from the fluorite lattice according to Eyring and Holmberg[92] The two phases in the reduced system whose structures are at all well known (R_7O_{12} and C-type R_2O_3) may be considered as composed of 'strings' of Ce^{3+} ions octahedrally co-ordinated to oxygen ions, and with cube diagonals along the string vacant, as shown in figure 3. Surrounding

the MO_6 "strings" are sheaths of MO_7 polyhedra similar to those found in A - and B - type rare earth oxide structures. Hyde and Eyring[9] suggest that all of the intermediate phases are formed by aligning these "strings" in the 1,2,3, or 4 ⟨111⟩ cube directions. Hyde and Eyring postulate that these strings persist in the disordered fluorite solid solution at high temperatures, but are randomly oriented. Thornber et.al.[95] found that the structures of intermediate phases in the ZrO_2 - Sc_2O_3 system could be described in a similar manner, although linear "strings" were not found.

The structure of the reduced ceria fluorite solution may be considered as made up of a fluorite lattice with some free oxygen vacancies, but with most of the vacancies taken up in the"strings". There would be paths of easy movement of oxygen vacancies along the outside of these "strings" since co-operative movement of vacancies with electrons may occur. Thus the activation energy for diffusion will be composed of two terms: the activation energy to move the vacancies through the fluorite lattice, and a lower activation energy to move the vacancies along in the environment of the strings. As ceria is reduced, free vacancies are produced until the fluorite lattice is "saturated" with them, and then "strings" are formed. With further reduction , more of the structure becomes composed of these strings, but the concentration of free vacancies does not increase. Consequently the overall activation energy of movement of vacancies decreases as the proportion of lattice taken up by "strings", with a lower activation energy, increases.

In ceria-yttria solutions Hyde and Eyring have postulated the presence of the same type of "strings" with octahedral co-ordination of Y^{3+} ions. In this case the Y^{3+} ion ($r = 0.93\text{Å}$) is smaller than the Ce^{4+} ion ($r = 1.01\text{Å}$) so that only electrostatic energy provides the attractive force and there is an increase of mechanical stress due to the presence of an Y^{3+} ion next to a vacancy. Thus it would be reasonable to expect a higher concentration of free vacancies in ceria-yttria solutions than in reduced ceria. Furthermore the Y^{3+} ions are effectively immobile in the cation sublattice, and consequently long chains would be unlikely to be formed. There can be no significant co-operative movement of vacancies and yttrium ions contributing to the vacancy movement because of the immobility of the Y^{3+} ion, and because

co-operative movement would not assist in vacancy motion because of the smaller size of the Y^{3+} ion. Thus the diffusion occurs through the bulk in preference to along the "strings", with the activation energy of motion of free vacancies through the fluorite lattice.

As yttria is added to ceria the oxygen vacancies first produced will be unassociated. When "saturation" is reached, the vacancies will tend to form dimers across an Y^{3+} ion so that the yttrium ion has an octahedral co-ordination of oxygen ions. There will be three Y^{3+} ions and nine Ce^{4+} ions nearest neighbours to the central octahedral Y^{3+} ion so that the complex may be designated $(4Y_{Ce}' . 2\,V_O^{\cdot\cdot})$. As the concentration of yttria increases these complexes will tend to polymorize into "strings" as in $CeO_{(2-x)}$ The lower stability of the strings, and low mobility of Y^{3+} ions, will tend to produce larger concentrations of smaller complexes, rather than long strings. The vacancies at the end of strings, and associated in dimers are relatively free to take part in diffusion, while those surrounded by Y^{3+} ions within the strings are fixed in position. Consequently the diffusion rate increases continuously with x.

To explain the fact that as x increases for ceria-yttria the oxygen diffusion coefficient increases continuously while the ionic conductivity reaches a maximum and decreases, it could be assumed that the complexes can move through the lattice and contribute to diffusion but not to conduction, since they are electrically neutral. This has been invoked to explain a similar difference between diffusion and ionic conduction in NaCl[130] and LiF[131] doped with higher valent cations. Movement of the complexes would require significant mobility of the Y^{3+} ion in the cation sublattice and, in view of the low diffusion coefficients of Zr^{4+} and Ca^{2+} in zirconia-calcia solutions, this seems unlikely. A corollory of the different behaviour of ceria-yttria compositions to oxygen diffusion and ionic conductivity is that the Nernst - Einstein equation would not be valid above the maximum in the conductivity.

Support for the decrease in Q_D with increasing x in $CeO_{(2-x)}$ found in the present work can be inferred from the reported pyrophoric nature of reduced ceria[55,56]. Warmkessel and Kevane[57] stated that the composition $CeO_{1.55 \pm 0.02}$ is not pyrophoric but that for $x < 0.35$ the black reduced oxides were pyrophoric.

The reduced single crystals from the present work were not pyrophoric, although a change of colour denoted some oxidation at room temperature in the polycrystalline specimens. Thus the pyrophoric oxides must have a lower activation energy for diffusion than the present compositions for the ignition to be initiated. It can be further deduced from the pyrophoric nature of the reduced material at room temperature in air that the rate of oxygen transport cannot be reduced significantly by formation of the intermediate low temperature oxides in the CeO_2 - $CeO_{1.5}$ system (figure 2), since the initial transport must occur in these phases before the exothermic heat of solution increases the temperature with ignition.

The systems PrO_2 - $PrO_{1.5}$ and TbO_2 - $TbO_{1.5}$ are very similar to the CeO_2 - $CeO_{1.5}$ system and the same structural entities have been postulated by Hyde and Eyring[9], so that the diffusion of oxygen in these oxides. should be similar to that in ceria. The oxidation and reduction of oxides of terbium and praseodemium has been studied by Eyring and co-workers[93,94]. Mainly phase boundary reaction control was found for the oxidation and reduction reactions.

$$PrO_{1.83} + O_2 \rightleftharpoons PrO_2$$

at temperatures between 240 and 340°C[94]. The reduction of $PrO_{1.71}$ to $PrO_{1.50}$ from 700 to 970°C was the only reductuon reaction of those studied earlier[93] involving $PrO_{1.78}$, $TbO_{1.81}$ and $TbO_{1.71}$ which was largely controlled by diffusion, although even for this reduction some contribution to the rate from the interfacial reaction was suspected. The activation energy was 42 k. cal. An accurate diffusion coefficient was not obtained since the particle size was not known accurately but a value of 1.5×10^{-9} $cm.^2/sec.$ was estimated. In view of the uncertainty of these values, especially since a contribution from the phase boundary reaction was suspected, the large discrepancy between these values and those found in the present work is not surprising.

Other comparisons of activation energies and magnitudes can be made with istope exchange measurement results for $UO_{(2+x)}$[37,38,39] and results from the oxidation of slightly reduced single crystals of type - C rare earth sesquioxides[96,97,98]. For $UO_{(2+x)}$ there could be a contribution

from co-operative movement of interstitial oxygen ions and electron holes since this would aid diffusion, but the structural entities for the large range of non-stoichiometry[14] does not include "strings" such as prososed in $CeO_{(2-x)}$. For C - type rare-earth oxides there are these strings, but they are i non-intersecting and, more important, there can be no co-operative movement aiding the diffusion process. Auskern and Belle[37] found a constant activation energy for diffusion of 29.7 k. cal in UO_{2+x} for the compositions $UO_{2.004}$ and $UO_{2.063}$, and Roberts et. al.[38] found an activation energy of 30 k. cal for $UO_{2.01}$ and 23 k. cal. for $UO_{2.03}$. These compare with an activation energy of about 67 k. cal. in approximately stoichiometric UO_2. At 1200°C the magnitude of the oxygen diffusion coefficient found by Roberts et. al. for $UO_{2.03}$ was about 10^{-7} cm^2/sec. Thus the magnitude of the diffusion coefficient in $UO_{(2+x)}$ is about the same as in $CeO_{(2-x)}$ while the activation energy is much higher, and is similar to that for $Ce_{(1-2x)}$ Y_{2x} $O_{(2-x)}$. This is consistant with the diffusion in $UO_{(2+x)}$ being due to a large concentration of free interstitials with no paths for very easy movement.

The magnitude of oxygen diffusion coefficients in the C-type rare earth oxide structures of Lu_2O_3, Er_2O_3, Tm_2O_3, Ho_2O_3, Dy_2O_3, Y_2O_3 and Sc_2O_3 at 1200°C are in the region of 10^{-9} to 10^{-8} cm^2/sec[96,97,98]. The activation energies varied from 20 to 46 k. cal. In these oxides the strings in the structure would not have a very low activation energy associated with them since there can be no effective co-operative movement, so that the higher activation energy is understandable. Since there can be few free vacancies with all of the oxygen "vacancies" in the structure taken up in the non-intersecting strings, the diffusion coefficient is much lower than in $CeO_{(2-x)}$.

4.2.4. Thoria-yttria.

The thoria-yttria results are compared with the oxygen diffusion coefficients calculated from the ionic conductivity data at 15 mole % $YO_{1.5}$ of Lasker and Rapp[26] in figure 21. This seems to confirm that the present results are of the correct order of magnitude. In the last section (4.2.3.) it was pointed out that for ceria-yttria solid solutions the Nernst-Einstein

equation would not be valid, and would tend to give lower diffusion coefficients at high yttria concentrations, than those determined in diffusion measurements. At 15 mole % $YO_{1.5}$ the ionic conductivity of thoria-yttria solutions is at the peak of a fairly broad maximum, so that if the oxygen diffusion results are due to both free and bound vacancies while the ionic conductivity is only produced by free vacancies, then the slightly higher oxygen diffusion coefficient from the present work is explained. This explanation would require a higher activation energy for the results of this work, but a lower value is found, as shown in figure 21. Furthermore if this explanation were correct, the activation energy for diffusion would increase with x, whereas in fact it decreases from 22 k. cal. for 10 mole % $YO_{1.5}$ to 18 k. cal for 15 mole% $YO_{1.5}$. The activation energy for ionic conduction shcws a similar decrease from 25 to 23 k. cal.[27] This indicates that in thoria-yttria the vacancies bound in complexes with Y^{3+} do not contribute significantly to the overall diffusion process.

4.2.5. Zirconia-yttria.

Figure 21 shows good agreement between the magnitude of single crystal results with the ionic conductivity for polycrystalline specimens[34]. The diffusion results of Simpson and Carter[32] for zirconia-calcia are shown for comparison.

The polycrystalline results of the present work showed a lower diffusion coefficient and higher activation energy than the single crystals. The difference in nominal composition of the polycrystalline specimens (15 mole % $YO_{1.5}$) and single crystals (15.6 mole % $YO_{1.5}$) was consistant with the lattice parameter difference. In this composition region the conductivity goes through a sharp maximum while the activation energy goes through a pronounced minimum[27,34], so that the difference in the two sets of results could be explained by the polycrystalline results being just on the low side of the maximum occurring at about 15.6 mole % $YO_{1.5}$. In this composition region there is a phase boundary between the two phase region of distorted fluorite structure ZrO_2 and fluorite solid solution, and the single

phase solution. A second phase was seen under the microscope for the polycrystalline specimens while no second phase was associated with the single crystals and the difference between the two types of specimen may be caused by this.

All of the single crystal diffusion results were obtained in N_2-O_2 mixtures except for one in a CO - CO_2 mixture.. The diffusion coefficient for the run in CO - CO_2 mixtures fell on the good straight line Arrhenius plot for the other results so that there was no difference between the diffusion results with the two experimental conditions.

The single crystal specimens were cooled from the melting point in about six hours so that, as explained in section 2.1.2. (ii), the cation sublattice would contain defects appropriate to a temperature of about 2000°C. To see what effect these imperfectly defined cation defects had on the oxygen diffusion results, a single crystal was cut with [100] faces and fired at 1400°C in air for seven days. The diffusion coefficient from this specimen was approximately the same as the other specimens so that the effect of cation defects cannot be significant.

4.2.6. Effect of Pores on Diffusion.

The polycrystalline ceria specimens of preparation 1 had 10% unconnected porosity with half the pores elongated of size 20 x 50μ around the grains and half as 10 μ spheres within the grains. The polycrystalline ceria specimens of preparation 2 had 20 % porosity, with at least some connected pores of spherical diameter about 20μ. Tigure 11 shows that these large differences in pore structure had no appreciable effect on the oxygen diffusion coefficient at 0.21 atmospheres oxygen pressure.

One of the zirconia-yttria single crystals developed a fine crack before the exchange measurements, but gave oxygen diffusion coefficients in good agreement with the other specimens.

These results indicate that gaseous diffusion with phase boundary exchange along the cracks or pores, and surface diffusion down the crack and pores, do not occur fast enough to affect the exchange experiment

results in these materials.

4.2.7. Effect of Grain Boundaries on Diffusion.

Enhanced oxygen diffusion was observed in all ceria specimens containing grain boundaries. Figure 6 shows the enhancement in single crystal aggregates (B = bicrystals) and figure 11 shows that polycrystalline specimens in air have higher diffusivities than single crystals (shown in figure6). Polycrystalline $CeO_{(2-x)}$ specimens also revealed a similar enhancement of diffusion in CO - CO_2 mixtures, as shown in figure 9.

Proton activation experiments revealed grain boundary enhancement of diffusion by an increase of silver grain density in an exposed autoradiograph. Figure 15 shows that the penetration along the grain boundary occurred very much more rapidly than bulk diffusion into the crystals. Thus the grain boundary diffusion rate is orders of magnitude greater than the rate of bulk diffusion.

Other workers have reported enhanced oxygen diffusion along grain boundaries in the oxides MgO[50], CoO[58] Al_2O_3[99] and BeO[100, 101] Tien[132] found that below 1000°C the ionic conductivity in $Zr_{0.84}$ $Ca_{0.16}$ $O_{1.84}$ was higher for finely polycrystalline material than for specimens with larger grains. This was interpreted as due to enhanced grain boundary conduction which become insignificant above 1000°C. No enhanced grain boundary diffusion has been reported for oxygen in other fluorite oxides, and for oxygen in zirconia-calcia Simpson and Carter[32] specifically reported no observed increase of diffusion coefficienn for polycrystalline specimen over that for single crystals from 800 to 1100°C.

Grain boundaries may be paths for rapid diffusion due either to the crystalline misorientation, or to voids and impurities at the interface. The latter would be expected to be important for the single crystal aggregates and large voids were observed. In section 4.2.6 it was shown that voids do not have a significant effect on the diffusivity of ceria so that the contribution from these must be small in the aggregates, but the affect of segregated impurities may be more important. From a curvature in the Arrhenius plot for conductivity in zirconia-yttria Bauerle and Hrizo[120] concluded that two processes with different activation energies were

contributing to the overall rate of conduction. They suggested that this was either due to formation of an yttrium-oxygen vacancy complex with a trapping energy of 11.2 k. cal. and an activation energy of motion of free vacancies of 15.8 k. cal, or due to a high resistance grain boundary layer with an activation energy for conduction of 27 k. cal. and a bulk activation energy of 15.7 k. cal. They proposed that for the latter case a segregation of yttrium ions at the grain boundary would producet the lower conductivity.

A segregation of thoria at grain boundaries has been reported in thoria-yttria by Jorgenson and Anderson[103]. The present results could be explained in terms of formation of complexes, as described earlier, but the second proposal could also apply. If such a segregation did occur then single crystals would be expected to have a higher diffusivity of lower activation energy than polycrystalline specimens. In the present work a higher diffusivity with lower activation energy was found for single crystals of zirconia-yttria, but this can be explained by a small composition difference. Examination of Simpson and Carter's[32] figure 2 showing the oxygen diffusion coefficient Arrhenius plot for zirconia-calcia reveals that their individual results do show higher diffusivities with lower activation energy for the single crystals than for the polycrystalline specimens. Similarly the conductivity composition plot of Carter and Roth[91] for zirconia-yttria solutions show a tendency to higher conductivities with single crystals. Thus the proposed grain boundary segregation in zirconia- and thoria- based solutions would retard diffusion. In ceria-yttria it has been found that the rate of diffusion increases with yttria content so that any grain boundary yttrium ion segregation would lead to enhanced diffusion.

In $CeO_{(2-x)}$ the enhancement of diffusion in polycrystalline specimens is seen down to $CeO_{1.80}$ (figure 9). The large concentration of electrons, relatively free to move through the crystal, would preclude the formation of significant space charges at grain boundaries as found in ionic compound crystals[104,105,106] Thus no significant contribution to the enhanced grain boundary diffusion in ceria can arise from space changes at boundaries.

The rapid diffusion down the grain boundary in ceria shown by figure 15, followed by bulk diffusion from the boundary and interfaces into

the specimen, is consistant with the requirements of the Fischer[107] analysis that the grain boundary region have negligible capacity for absorbing material compared with the grain bulk. For diffusion of anions in alkali halides Laurent and Benard[108] found that the grain boundaries had considerable capacity. Oishi and Kingery[99] found that the oxygen diffusion coefficient in polycrystalline Al_2O_3 decreased with time because of the contribution of the grain boundary capacity to the overall uptake at small times. Thus if the capacity had been significant in the present work the separation of D and K using the graphical method, shown in appendix 3, would have been in error for polycrystalline specimens. The fact that the grain boundary capacity is not significant is further shown by the equal activation energy for diffusion in single crystals and polycrystalline specimens[109].

4.3 Surface Exchange Coefficients.

4.3.1. Introduction.

The following steps may be rate controlling for the exchange process:

(i) Transport of gas molecules to the specimen surface.
(ii) Adsorption on the surface.
(iii) Rearrangement of adsorbed molecules on the surface.
(iv) Desorption of the product molecules.
(v) Transport of the molecules produced away from the surface.

The rate of mass transfer, K^*, for a gas flowing past a solid sphere may be calculated, assuming laminar flow, using the equation[110]

$$\frac{K^* d}{D_{AB}} = 2.0 + 0.6\,(Sc)^{\frac{1}{3}}\,(Re)^{\frac{1}{2}} \qquad \ldots\ldots(4.14)$$

where $Sc = \dfrac{\mu}{\rho D_{AB}}$

$Re = \dfrac{d u \rho}{\mu}$

d is the diameter of the solid sphere,

D_{AB} is the gas diffusion coefficient,

ρ is the gas density,

μ is the vistosity,

and u is the velocity of flow.

For oxygen at 1000°C, using data from Perry's "Chemical Engineers Handbook" a gas velocity of 0.95 cm/sec. (from a flowrate of 160 ml/min. through the $\frac{3}{4}$ inch reaction tube), and a particle diameter of 0.1 cm., a K^* value of about 10 cm/sec is obtained. Experimental results gave a maximum surface exchange coefficient of the order of 10^{-3} cm/sec so that steps (i) and (v) cannot be rate determining. This conclusion is supported by the variation of K with ceria-yttria composition shown in figure 10.

If step (iii) were rate controlling no dependence of K on oxygen pressure would be expected. In figure 7 the K values for ceria in air are higher than in an oxygen partial pressure of 0.02 atm. Comparing the results obtained with single crystal cubes having the original cube surfaces (the highest K value for air and the two values at lower temperatures for p_{O_2} = 0.02 atm.) a difference in log K of 0.85 at 960°C is found. This gives a reaction order of 0.83. It is later suggested that the results imply that the same defect entity controls both the rate of surface exchange and the diffusion rate. If this is so then an increase of surface exchange for a decrease of oxygen partial pressure from 0.21 atm to 0.02 atm. would occur due to the change in defect concentration in the solid. If the increase in diffusion coefficient of 0.2 (for log D) is added to the change of log K with oxygen pressure then a reaction order of approximately unity is obtained. This eliminates step (iii) as a rate determining step; leaving either adsorption or desorption as the rate controlling processes.

A dependence of the surface exchange rate on both gas composition and solid composition can be explained in terms of active surface sites. With a limited concentration of active surface sites, exchange can only occur when a gas molecule approaches a site with suitable orientation and energy. With a change in composition of the solid the concentration of sites, and thus the exchange rate, will alter. With a change of concentration of gas molecules the probability that a molecule striking the surface will have suitable orientation and energy for adsorption will alter.

The variation of log K with x, shown in figure 10 for ceria-yttria, shows very similar behaviour to that of log D with x, shown in figure 9. This could mean that the same defect entity is responsible for both diffusion and adsorption - desorption. Thus in ceria-yttria the concentration of free vacancies, or vacancies at the ends of "strings" increases with x, leading to an increase in both D and K. In $CeO_{(2-x)}$ it was postulated that the concentration of free vacancies remains constant, but that lengthening of the "strings" decreases the activation energy for diffusion so that D increases exponentially with x. If this explanation is correct, the surface exchange coefficient should be independent of x in $CeO_{(2-x)}$

The gas mixture changes from N_2 - O_2 to CO - CO_2 for the two K values shown in figure 10 for $CeO_{(2-x)}$, and a different adsorption - desorption process would apply in each case. A different adsorption process could also be expected in a predominantly CO_2 mixture to that in a predominantly CO mixture. The effect of changing the CO/CO_2 ratio can be gauged by comparing the results for $CeO_{1.92}$ with those for $CeO_{1.80}$. At low temperatures, where K was low enough to affect the exchange process for $CeO_{1.92}$, the K values were the same, as shown in figure 7. The fact that K was too large to be observed in $CeO_{1.92}$ at high temperatures, but could be obtained for $CeO_{1.80}$, is consistent with a constant K value and increasing rate of diffusion for the two compositions. The effect of changing from N_2 - O_2 mixtures to CO - CO_2 mixtures was seen in zirconia-yttria single crystals. Figure 14 shows a significant increase of K with this change. If this increase of about 0.5 in log K is subtracted from the log K value for $CeO_{1.80}$ in figure 10, then the difference in K values between ceria in air and $CeO_{1.80}$ is much less than the corresponding difference in D values. This supports the proposition that K is constant with x in the region where the structural "strings" take up all of the "vacancies" formed by reduction.

4.3.2. Comparison with other work.

The phase boundary reaction rate was found to play a part in the overall kinetics of gaseous exchange of isotopically enriched oxygen with zirconia-calcia[32], thoria[25] CdO[114], Sm_2O_3[115], Nd_2O_3[115] and TiO_2[133] at high temperatures. As mentioned earlier, in section 4.2.3,

the reduction and oxidation of oxides of praseodemium and terbium[93,94] were found to be partly rate controlled by the phase boundary reaction For the oxidation of $UO_{2.01}$ to $UO_{2.13}$ in the temperature range 900 to 1400°C in CO - CO_2 mixtures a phase boundary control mechanism also applied.[116].

The isotopic exchange of oxygen with oxides at low temperatures, where solid diffusion does not occur to a significant extent has been studied for many oxides[117, 118] including ceria[119, 120]. The catalytic properties of ceria-lanthana solid solutions to oxidation of CO were studied by Rienaker and Wu[121]

In figure 27 the K values from the present work are compared with published surface exchange coefficients. The figures in brackets are; reference numbers. In the published coefficients there was a considerable scatter; similar to that found in the present results. As mentioned previously, the ceria single crystals had a lower exchange coefficient with roughened surfaces. This could be explained in terms of either a less reactive crystalline face being exposed, or a more reactive natural surface being removed. Both these effects would predict a lower exchange coefficient in polycrystalline specimens than in single crystals, and the reverse was found. If the grain boundaries enhance surface exchange, as they have been seen to increase the diffusion coefficient, then this may explain the higher surface exchange rates for polycrystalline specimens. For polycrystalline specimens with rough surfaces the surface exchange rate was too high to affect exchange so that the K value was higher than for well polished specimens, as would be expected from the greater surface area. Obviously the surface preparation (mechanical and chemical) plays a very important part in the rate of surface exchange, and more work needs to be done on this aspect of experiments. In exchange experiments where diffusion of oxygen is important, techniques used in many lower temperature adsorption and catalysis studies, such as high temperature out gassing and vacuum evaporation[122] cannot be used.

In spite of this scatter it can be seen from figure 27 that the magnitude of results are in agreement with other work on similar oxides. A striking feature of this figure is that the exchange coefficients for

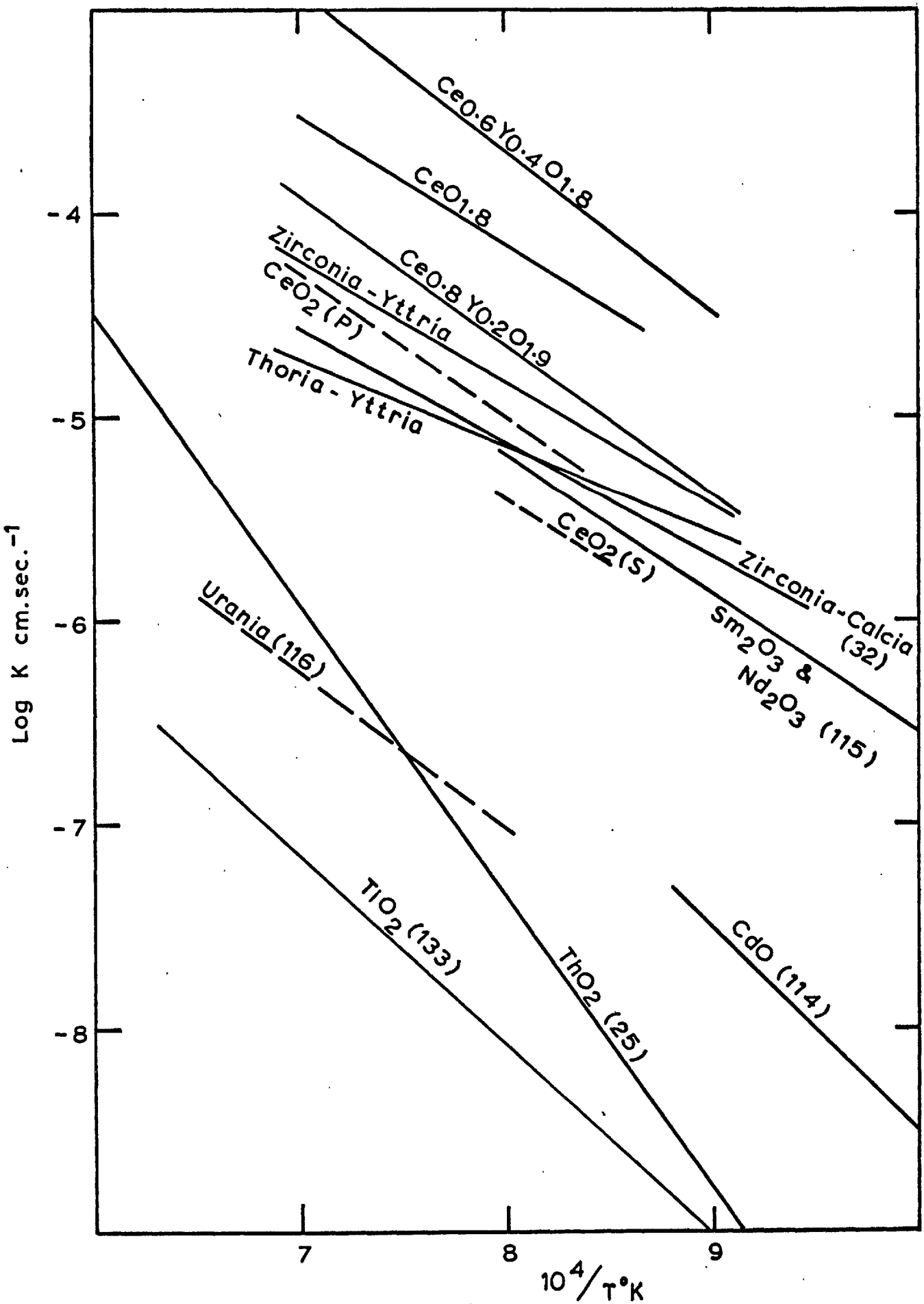

Fig.27. SURFACE EXCHANGE COEFFICIENTS

these oxides have about the same relationship to each other as the diffusion coefficients shown in figure 28*. This adds weight to the hypothesis in the present work that the surface active entity is the same as that controlling diffusion. There are three facts which show that this is a real correlation, and not an artifact of the calculation of K through Q.

Firstly, if the values of K obtained were artificial, then K should not only vary in the same way as D with x in the present results, but also in the same way with change of oxygen pressure. In fact for ceria in N_2-O_2 mixtures the K values varied in the opposite way to D with change of pressure.

Secondly, the K values calculated for urania were obtained using a different technique, but still fit in well with the general pattern.

Thirdly, as shown below, oxygen adsorption on ceria at low temperatures, where the rate of diffusion was too low to affect exchange rates, extrapolate to give similar values of the surface exchange coefficients at the temperatures of the present work.

The exchange results of Sasanov et al.[119] and Antoshin et al.[120] were in reasonable agreement. The results were quoted in the form of rates of exchange, in moles of oxygen cm^{-2} sec^{-1}, with activation energies of 29 k. cal and 16 k. cal respectively. Sasanov et. al found the order of reaction with respect to oxygen of 0.84, in good agreement with the present results. Antoshin et al state that the reaction was first order.

The surface exchange coefficient is related to the rate constant, k for the surface reaction by $K = k.d_o$, where d_o is the thickness of the solid layer in contact with the gas. The rate constant is equal to the

* Figures in brackets are reference numbers. For Nd_2O_3 the equation for D given by Stone et al.[115] does not fit their Arrhenius plots. $D = 1.9 \times 10^{-7}$ exp (-13.5 k. cal. /RT) gives good agreement with their data.

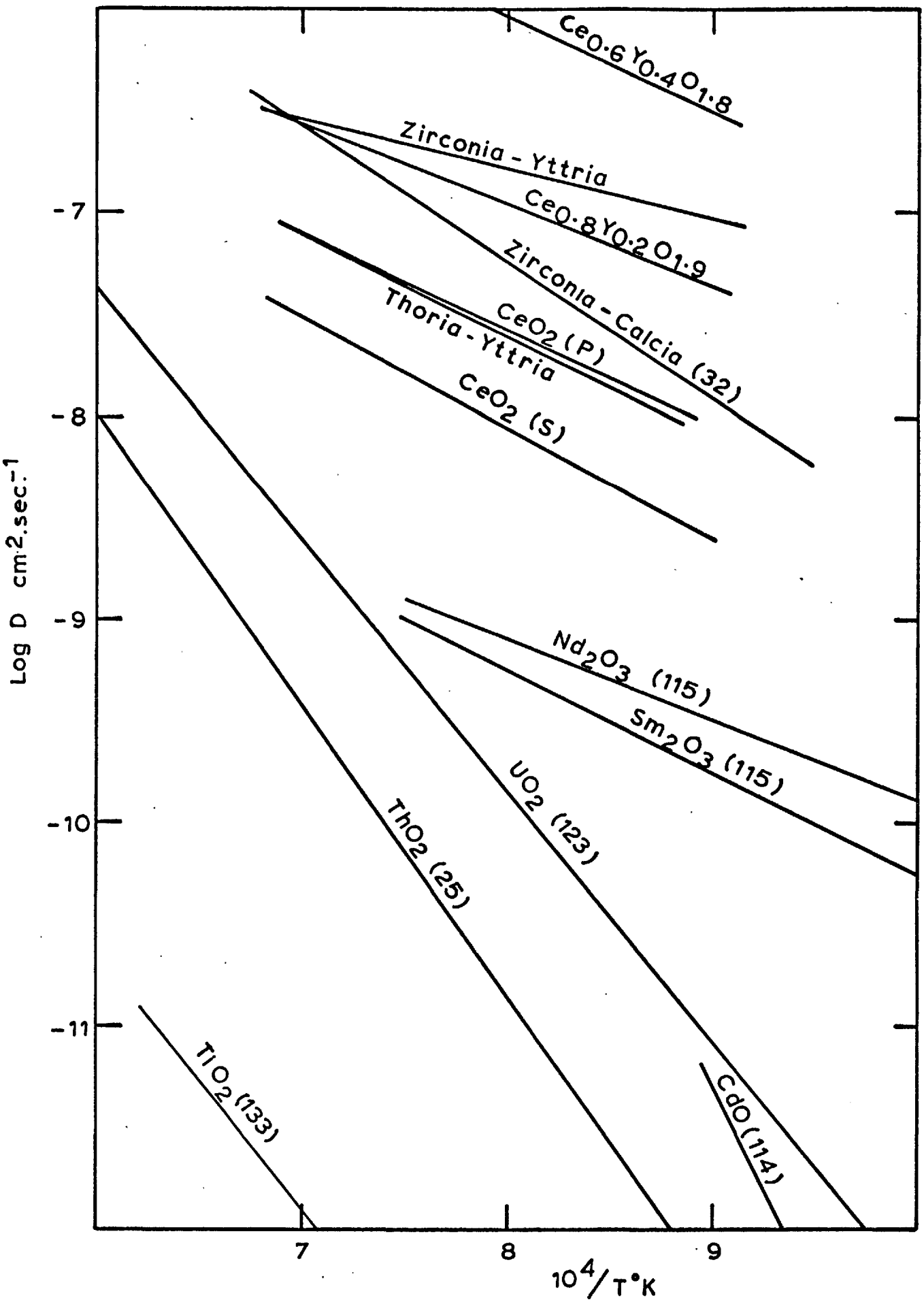

Fig.28. DIFFUSION COEFFIENTS

rate multiplied by the ratio of the total surface area to the total number of moles of oxygen in the system[118]. Neither publication gives sufficient information to convert rates to k values, but in an earlier paper[124] Antoshin et al. quote a specific surface area of 29 m^2/g, and amount of oxygen in the gas phase of 0.0489g, and in the solid surface of 0.34×10^{-3} g/cm^2. Assuming a sample weight of 10g, using their activation energy and rate of 10^{13} atoms cm^{-2} sec. at 420°C, and putting d_o the lattice parameter, a K value of the order of 10^{-8} cm sec^{-1} is obtained at 1000°C. Assuming similar quantities the higher activation energy of Sasanov et al. result in a K value of about 10^{-6} cm sec^{-1} at 1000°C. The figures give confidence that the surface exchange coefficients found in the present work are about of the right magnitude, and in particular do not appear to be too low.

Rienacker and Wu[121] studied the catalytic oxidation of carbon monoxide on ceria-lanthana solid solutions up to 800°C. They found a decrease of catalytic activity with addition of lanthana. They assumed that ceria was a p-type semiconductor while lanthana was n-type, and the process of adsorption proceeded according to the mechanism

$$e^+ + CO \rightleftharpoons CO^+ \text{ (surf)}$$

The change of conduction from p- to n- type therefore reduced the catalytic activity. These results and proposed mechanism do not agree with the present work, but Vinokurov et al.[75] and Kevane et al.[73] found that CeO_2 undergoes a p- to n-type transition on heating through 800°C, so that the conditions are not strictly comparable. The fact that the lower temperature isotope exchange does not give exact agreement of K values when entropolated to the temperatures of the present results is therefore not unreasonable.

As shown in section 4.3.1 the results of the present work seem to indicate that the same defect entities control the surface exchange reaction as control diffusion, and this is supported by the similarity of the patterns of Arrhenius plots for K and D shown in figures 27 and 28. Furthermore the surface exchange coefficient is not increased as much with reduction from CeO_2 to $CeO_{1.80}$ as with addition of yttria, as explained in section 4.3.1, so that the process depends on the presence

of oxygen vacancies rather than electrons. If it is assumed that the active surface site is associated with a free oxygen vacancy, then the process occurring when a gas molecule approaches the surface could be:

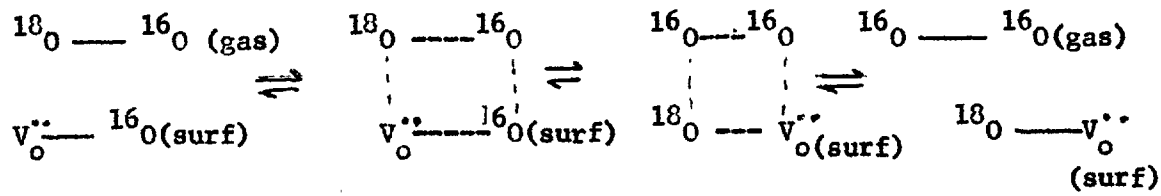

Haul and Just[114] explained their oxygen diffusion results in CdO by the formation of oxygen vacancies and unchanged cadmium ions. They found that the surface exchange coefficients increased with decreasing oxygen pressure and with addition of Li_2O to the CdO. Both effects could be explained by the variation of oxygen vacancy concentration and the scheme proposed above.

4.4. Applications.

The high rate of transport of oxygen ions in ceria solid solutions would make them useful as solid electrolytes at high oxygen potentials. But with reduction the ionic transport number would decrease and in a fuel cell this would probably preclude their use. Another problem is that the mechanical strength of the reduced material is low[125]. The maximum in the ionic conductivity as the yttria concentration is increased is not significantly higher for ceria-yttria than in zirconia-yttria.

The present work has shown that the surface reactions should be considered in the rate of the transport process in fuel cells. This varies in a similar manner to the diffusion process, but is enhanced in polycrystalline materials by having roughened surfaces.

The high electron and oxygen mobilities in $CeO_{(2-x)}$ would make it a useful material for electrodes in fuel cells.

It seems unlikely that oxides with much higher oxygen diffusivity than those studied in the present work will be found[1], but in oxyfluorides such as those in the system CeF_2 - CeO_2[126], the Ce-F bond would be stronger than the Ce-O bond, perhaps leading to an increased rate of oxygen transport

4.5 Suggestions for further work.

The present work has given surface exchange coefficients which contain occasional results widely varying from the general behaviour. It is concluded that the surface preparation technique was not sufficiently reproducible. Further work is required on the preparation of surfaces for experiments where both surface exchange and diffusion contribute to the overall rate. Chemical polishing with a solution containing hydrofluoric acid would possibly give rise to some improvement

Dislocations were found to enhance oxygen diffusion rates in $SrTiO_3$[127], MgO[50], and ZnO[128], and this effect was not studied in the present work.

Oxygen diffusion rates have been shown to depend on crystal orientation in Nb_2O_5[51] and BeO[129], and the influence of crystal orientation on the oxidation of metals is well known[134] but little is known of the effect of crystal orientation on adsorption and catalysis of oxides. Investigations such as the present work, where diffusion and surface exchange rates are obtained simultaneously, provide a good opportunity to study the effect of crystal orientation on these properties.

Oxygen exchange with oxy-fluorides could also be studies to indicate whether more rapid transport occurs.

The present work showed that in ceria-yttria fluorite solutions the oxygen diffusion rate increased continuously with yttria concentration. The ionic conductivity goes through a maximum in the same composition region, and this difference in behaviour has not been explained. Further work on the variation of oxygen diffusion coefficient with addition of lower valent cations to fluorite oxides, to determine whether this is a general phenomenon, would be of use. The cation diffusivities in ceria-yttria solutions could be measured to show whether co-operative movement of vacancies and cations would cause the difference in behaviour.

Conclusions.

1. Isotopic exchange of ^{18}O with fluorite structure oxides showed that the surface exchange process, as well as the diffusion process, contributed to the overall rate of exchange. Diffusion coefficients and surface exchange coefficients were determined in polycrystalline (P) and single crystal (S) specimens of CeO_2 (S and P) $CeO_{(2-x)}$ (S and P) $Ce_{0.9}Y_{0.1}O_{1.95}$ (P), $Ce_{0.8}Y_{0.2}O_{1.90}$ (P), $Ce_{0.6}Y_{0.4}O_{1.80}$ (P), $Th_{0.9}Y_{0.1}O_{1.950}$ (P), $Th_{0.85}Y_{0.15}O_{1.925}$ (P), $Zr_{0.844}Y_{0.156}O_{1.920}$, (S), and $Zr_{0.85}Y_{0.15}O_{1.925}$ (P).

2. Specimens containing grain boundaries revealed enhanced diffusion over single crystals. Proton activation of ^{18}O exchanged specimens with grain boundaries, followed by autoradiography, confirmed that rapid diffusion occurred down grain boundaries.

3. A continuous increase of D with x in $CeO_{(2-x)}$ and $Ce_{(1-2x)}Y_{2x}O_{(2-x)}$ was observed and explained in terms of proposed structural entities in the fluorite solutions.

4. Results may be explained by free vacancies controlling both the diffusion and surface exchange processes for the fluorites studies. The The Arrhenius plots for diffusion coefficients and exchange coefficients for oxides where both are known show very similar patterns of behaviour, indicating that this may be generally the case in such oxides.

REFERENCES.

1. B.C.H. Steele, B.E. Powell and P.M.R. Moody, Proc. Brit. Ceram. Soc., No. 10, 87 (1968)
2. D.J.M. Bevan and J. Kordis, J. Inorg. Nucl. Chem., 26, 1509 (1964)
3. D.J.M. Bevan, J. Inorg. Nucl. Chem. 1, 49 (1955)
4. G. Brauer and H. Gradinger, Z. anorg. u. allg. Chem., 277, 87 (1954)
5. G. Brauer and K. Gingerich, Angew. Chem., 69, 480 (1957)
6. Idem., J. Inorg. Nucl. Chem., 16, 87 (1960)
7. G. Brauer, K.A. Gingerich and U. Holtsmidt, Ibid, p.77
8. F.A. Kuznetsov, V.I. Belyi and T.N. Rezukhina, Dokl. Akad. Nauk, S.S.S.R., 139, 1405 (1961)
9. B.G. Hyde and L. Eyring, Rare Earth Research III (1965) L. Eyring (ed.) (Proc. Fourth Conf. (1964)) p. 623.
10. D.J.M. Bevan, W.W. Barker and R.L. Martin, Ibid., p. 441.
11. M. Hoch and H.S. Yoon, Ibid., p. 665.
12. W.W. Barker and A.F. Wilson, J. Inorg. Nucl.Chem., 30, 1415 (1968)
13. J.S. Anderson, Adv. in Chem. Series, 39, 1 (1963)
14. G.G. Libowitz, "Mass Transport in Oxides", Ed. J.B. Watchman, Jr. and A.D. Franklin; (Proc. of a Symposium (1967) U.S. Dept. of Comm., N.B.S. Special Publ., 296, 109 (1968)
15. H. Rickert, "Emf Measurements in High Temperature Systems" (Proc. of symp., Nuffield Research Group, I.C. London, (1967), I.M.M., London (1968) p.59.
16. G. Amsel, G. Beranger, B. de Gelas and P. Lacombe, J. Appl. Phys., 39, 2246 (1968)
17. J.F. Marin and P. Contamin, J. Nucl. Mat., 30, 16 (1969)
18. U. Croatto, Ric. Sci., 13, 830 (1942)
19. U. Croatto and A. Mayer, Gaz. Chim. It., 73, 199 (1943)
20. J. Rudolph, Z. Naturforsch., 14a, 727 (1959)
21. A.D. Neuimin and S.F. Pal'guev, Trudy Inst. Electrochem., Urals Acad. Sci., 2, 185 (1961)
22. A.D. Neuimin, S.F. Pal'guev and V.N. Chebotin, Ibid,, 4, 79 (1963)
23. T. Takahashi and H. Iwahara, Denki Kagaku, 34, 254 (1966)
24. I.V. Vinokurov and V.A. Ioffe, Fiz. Tverd. Tela., 11, 257 (1969)
25. H.S. Edwards, A.F. Rosenberg and J.T. Bittel, G.E. Tech. Doc. Rep. No. ASD-TDR-63-635 (1963)
26. M. Lasker and R. Rapp, Z. Phys. Chem. (N.F.) 49, 198 (1966)
27. B.C.H. Steele and C.B. Alcock, Trans. Met. Soc. A.I.M.E., 233, 1359 (1965)

28. A. Madeyski and W.W. Smeltzer, Mat. Res. Bul. 3, 369 (1968)
29. J. Debuigne and P. Lehr., Compt. Rend. 256, 1113 (1963)
30. C.T. Rosa and W.C. Hagel, J. Nucl.Mat., 27, 12 (1968)
31. D.L. Douglass, "Corrosion of Reactor Materials", Vol. 2, I.A.E.A. Vienna (1962) p.223.
32. L.A. Simpson and R.E. Carter, J. Am. Ceram. Soc., 49, 139 (1966)
33. W.D. Kingery, J. Pappis, M.E. Doty, and D.C. Hill, J. Am. Ceram. Soc., 42, 393 (1959)
34. D.W. Strickler and W.G. Carlson, J. Am. Ceram. Soc., 47, 122 (1964)
35. J.M. Dixon, L.D. La Grange, U. Merton, C.F. Miller and J.T. Porter, II, J. Electrochem. Soc., 110, 276 (1963)
36. J. Belle and B. Lustman, "Kinetics of High Temperature Processes". Ed. Kingery, (Proc. of Conf. (1958)) Wiley, N.Y. (1959) p.44.
37. A.B. Auskern and J. Belle, J. Pyys Chem., 28, 171 (1958)
38. L.E.J. Roberts, V.J. Wheeler and Perrin, A.E.R.E. Harwell, cited by J. Belle, J. Nucl. Mat. 30, 3 (1969)
39. J.F. Marin and P. Contamin, J. Nucl. Mat., 30, 16 (1969)
40. C.J. Hardy, S.R. Buxton, and H.M. Lloyd. Oak Ridge National Laboratory Report, ORNL - 4000, (August 1967)
41. B.C.H. Steele, Ph.D. thesis, University of London, (1966)
42. P. Duwez, F.H. Brown, Jr., and F. Odell, J. Electrochem. Soc., 98 356 (1951)
43. S. Darken and R.W. Gurry, "Physical Chemistry of Metals", Mc. Graw-Hill (1953) p.446
44. W.H. Rhodes and R.E. Carter, J. Am. Ceram. Soc., 49, 244 (1966)
45. O. Kubaschevski and B.E. Hopkins, "Oxidation of Metals and Alloys", Butterworth Scientific Pub., (1953) p.20
46. J. Crank, "Mathematics of Diffusion", Clarendon Press, Oxford (1956)
47. R. Haul, G. Dumbgen and D. Just, Z. phys. Chem. (N.F) 31, 309 (1962)
48. M. O'Keefe, J. Appl. Phys., 37, 2007 (1966)
49. R.H. Condit and J.B. Holt, J. Electrochem. Soc., 111, 1192 (1964)
50. J.B. Holt and R.H. Condit, Mat. Sci. Res. 3, 13 (1966)
51. J.S. Sheasby and B. Cox, J. Less-Common Metals, 15, 129 (1968)
52. F.J. Norton, J. Appl. Phys., 29, 1122 (1958)
53. Betteridge and Rhys, First International Congress of Metal Corrosion (London (1961)) (1962), p.186.
54. W.C. Hagel, Trans. Met. Soc. A.I.M.E., 236, 179 (1966)
55. N.E. Topp, "Chemistry of the Rare Earths", (Elsevier Pub. Co. (1965)) p.87.

56. F.A. Kuznetsov, V.I. Belyi, T.N. Rezukhina, and Ya. I. Gerasimov, Proc. Acad. Sci. U.S.S.R., 139, 642 (1961).
57. B.M. Warmkessel and C.J. Kevane, J. Am. Ceram. Soc., 51, 663 (1968).
58. J.B. Holt, Proc. Brit. Ceram. Soc., 9, 157 (1967).
59. L.M. Atlas, J. Phys. Chem. Sol., 29, 91 (1968).
60. C.E. Birchenall, "Mass Transport in Oxides" Ed. Watchman and Franklin (Proc. of a Symp. (1967)),U.S. Dep. of Commerce, N.B.S. Special Publication 296, p.119 (1968)
61. P.J. Koros and J.B. King, Trans. Met. Soc. A.I.M.E., 224, 299 (1962)
62. J.R. Manning, "Diffusion Kinetics for Atoms in Crystals", D. Van Nostrand Co., Inc. (1968)
63. F.A. Kroger and H.J. Vink, Solid State Physics, 3, 307 (1956).
64. E. Zintle and U. Croatto, Z. anorg. u. allg. Chem., 242, 79 (1939)
65. A.D. Neuimin and S.F. Pal'gnev, Transactions of the Institute of Electrochemistry of the Urals Branch of the Academy of Sciences, U.S.S.R. No. 3 (1962)
66. A.D. Neuimin and S.F. Pal'guev, Doklady Acad. Nauk, S.S.S.R., 143, 1388 (1962).
67. W. Noddack and H. Walch, Z. phys. Chem., 211, 194 (1959)
68. R.N. Blumenthal and B.A. Pinz, J. Appl. Phys., 38, 2376 (1967).
69. E.L. Holverson and C.J. Kevane, J. Chem. Phys., 44, 3692 (1966).
70. R.C. Linares, J. Phys. Chem. Sol., 28, 1285 (1967)
71. T.R. Griffiths, Inorganic Chemistry Department, University of Leeds, Private communication.
72. E.H. Greener, J.M. Wimmer and W.M. Hirthe, "Rare Earth Research", Vol. 2, Edited by K.S. Vorres, (Gordon and Breach, N.Y. (1964))p.539.
73. C.J. Kevane, E.L. Holverson and J.B. Armstrong, Fifth Rare Earth Reaearch Conference, (Aug 30 - Sept. 1 (1965)) p.43.
74. K.W. Lay and D.H. Whitmore, ibid. p.55.
75. I.V. Vinokurov, Z.N. Zonn and V.A. Ioffe, Sov. Phys. - Sol. State, 9, 2659 (1968).
76. L.M. Solov'eva and V.N. Chebotin, Trans. (No.9) of the Inst. of Electrochem., Urals Acad. Sci. Electrochem. of Molten and Solid Electrolytes, Vol. 6 (Consultants Bureau (1968)), p.100.
77. V.N. Chebotin, ibid. (No. 7, 1967) p.137.
78. I.M. Boswava and A.D. Franklin, "Mass Transport in Oxides", (Proc. of a a Symposium (1967), U.S. Dep. of Comm., N.B.S. Special Publication 296, Ed. Watchman and Franklin, p.25.

79. L.E.J. Roberts and T.L. Markin, Proc. Brit. Ceram. Soc., 8, 201 (1967)

80. C. Zener, "Imperfections in Nearly Perfect Crystals," Ed. W. Schockley, J. Wiley, N.Y. (1952) p.289.

81. T. Smith, J. Electrochem Soc., 112, 560 (1965).

82. D.L. Douglass, I.A.E.A. Corrosion of Reactor Materials, Conference (Salzberg, 1962), Proc. Vol. 2, 223 (1962).

83. J.S. Sheasby, W.W. Smeltzer, and A.E. Jenkins, J. Electrochem. Soc. 115, 338 (1968)

84. W.K. Chen, and R.A. Jackson, J. Chem. Phys., 47, 1144 (1967).

85. P. Kofstad and A.Z. Hed, J. Am. Ceram. Soc., 50, 681 (1967).

86. L.C. Walters and R.E. Grace, J. Phys. Chem. Sol., 28, 245 (1967).

87. W.L. George and R.E. Grace, J. Phys. Chem. Sol., 30, 889 (1969).

88. A.E. Paladino, L.G. Rubin and J.S. Waugh, J. Phys. Chem. Sol., 26 391 (1965).

89. A. Bengtzelius, A. Kuist and U. Trolle, Z. Naturforsch., 23a, 2040 and 2042 (1968).

90. M. O'Keefe, article to be published in proceedings of the conference, "The Chemistry of Extended Defects in Non-Metallic Solids", held in Phoenix, Arizona. (1969).

91. R.E. Carter and W.L. Roth, G.E. Research Lab. Rep. No. 63 - RL - 3479 M (1963).

92. L. Eyring and B. Holmberg, Adv. in Chem. Series, 39, 46 (1963)

93. U.E. Kuntz and L. Eyring, "Kinetics of High-Temperature Processes", W.D. Kingery, Ed., John Wiley and Sons. Inc., N.Y. (1959) p.50.

94. B.G. Hyde, E.E. Gørver, U.E. Kuntz and L. Eyring, J. Phys. Chem, 69, 1667 (1965).

95. M.R. Thornber, D.J.M. Bevan and J. Graham, Acta Cryst., B24, 1183 (1968).

96. M.F. Berard and D.R. Wilder, J. Appl. Phys., 34, 2318 (1963)

97. C.D. Wirkus, M.F. Berard, and D.R. Wilder, J. Am. Ceram. Soc., 50, 113 (1967).

98. M.F. Berard, C.D. Wirkus, and D.R. Wilder, J. Am. Ceram. Soc. 51, 643 (1968).

99. Y. Oishi and W.D. Kingery, J. Chem. Phys., 33, 480 (1960).

100. S.B. Austerman, R.A. Meyer, and D.G. Swarthart, A.E.C. Res. and Dev. Rept. NAA-SR-6427 (1961).

101. S.B. Austerman and R.A. Meyer, ibid, NAA-SR-7637. (1962)

102. J.E. Bauerle and J. Hrizo, J. Phys. Chem. Sol., 30, 565 (1969).

103. P.J. Jorgenson and R.C. Anderson, J. Am. Ceram. Soc., 50, 553 (1967).

104. J.D. Eshelby, C.W.A. Newey, P.L. Pratt, and A.B. Lidiard, Phil. Mag. 3, 75, (1958).
105. R.W. Whitworth, ibid, 15, 305 (1967).
106. K.G. McQuhae, Ph.D. thesis, University of London March 1969.
107. J.C. Fischer, J. Appl. Phys. 22, 74 (1951)
108. J.F. Laurent and J. Benard, J. Phys. Chem. Sol. 7, 218 (1958).
109. G.C. Kuczynski, Bull. Soc. Franc. Céram. 80, 45 (1968)
110. C.O. Bennett and J.E. Myers, Momentum, Heat, and Mass Transfer", p.345.
111. P. Wynblatt, J. Phys. Chem. Sol., 30, 2201 (1969).
112. L.W. Barr and A.B. Lidiard, "Defects in Ionic Crystals", to be published in Volume 10 of Physical Chemistry - An Advanced Treatise (Academic Press).
113. M. O'Keefe and W.J. Moore, J. Chem. Phys. 36, 3009 (1962).
114. R. Haul and D. Just, J. Appl. Phys., 33, Suppl., 487 (1962).
115. G.D. Stone, G.R. Weber, and L. Eyring, "Mass Transport in Oxides" (Proc. of Symp. (1967)) U.S. Dept. of Commerce, N.B.S. Spec. Publ. 296, (1968), p.179
116. R.E. Carter and K.W. Lay, General Electric Research and Development Report No. 68 - C - 381 (1968)
117. E.R.S. Winter, Disc. Farad. Soc. 8, 231 (1950).
118. G.K. Boreskov, Advances in Catalysis 15, 285 (1964).
119. L.A. Sazanov, V.D. Sokolovski, and G.K. Boreskov, Kin. i Kataliz 7, 521 (1966).
120. G.V. Antoshin, Kh. M. Minachev, and R.V. Dimitriev, Russ. J. Phys. Chem. 41, 1587 (1967).
121. G. Rienaker and Y. Wu, Z. anorg. u. allg. Chem., 315, 121 (1962).
122. J.M. Thomas and W.J. Thomas, "Introductuon to the Principles of Heterogeneous Catalysis", (Academic Press, N.Y. and London (1967)p.69
123. J. Belle, J. Nucl. Mat. 30, 3 (1969)
124. K.M. Minachev and G.V. Antoshin, Doklady Akad. Nauk S.S.S.R., 161, 122 (1965).
125. Akopov and Polubayarinov, Refractories (Trans. of Ogneupori) 1965 196.
126. J.P. Besse and M. Capestan, Bull. Soc. Chim. France. 1968 (8) 3095
127. A.E. Paladino, L. G. Rubin, and J.S. Waugh, J. Phys. Chem. Sol. 26 391 (1965)
128. W.J. Moore and E.L. Williams, Disc. Farad. Soc. 28, 86 (1959).
129. C.F. Cline and H.W. Newkirk, J. Chem. Phys. 49, 3496 (1968)
130. D. Mapother, H.N. Crooks, and R. Maurer, J. Chem. Phys. 18, 1231 (1950).

131. T.G. Stoebe and P.L. Pratt, Proc. Brit. Ceram. Soc. No. 9, 181 (1967).

132. T.Y. Tien, J. Appl. Phys. 35, 122 (1964)

133. R. Haul and G. Dumbgen, J. Phus. Chem. Sol. 26, 1 (1965).

134. K.R. Lawless. "The Oxidation of Metals" Energetics in Metallurgical Phenomena. Ed. Mueller Vol. 1 (1965), (Gordon and Breach, N.Y.)

Appendix 1

Treatment of Mass Spectrometer Results.

The M.S.3 mass spectrometer produced recorder charts such as those shown in figure 29 and 30 for $N_2 - O_2$ mixtures in run 49 and $CO - CO_2$ mixtures in run 31 respectively. The recorder incorporated a range change device so that peak heights in ranges 1X, 3X, 10X, and 30X could be measured in one sweep of the mass range.

Each gas sample was mass scanned two, three, or four times. The peak heights were measured and gave results as shown in tables 4 and 5 and the percentage ^{18}O calculated for the gas as follows:

$N_2 - O_2$

$$^{18}O = \tfrac{1}{2}(h_{34}) + h_{36}$$

$$^{16}O = h_{32} + \tfrac{1}{2}(h_{34})$$

$CO - CO_2$

$$^{18}O = \tfrac{1}{2}(h_{30}) + \tfrac{1}{2}(h_{46}) + h_{48}$$

$$^{16}O = \tfrac{1}{2}(h_{28} - N.h_{32}) + \tfrac{1}{2}(h_{29}) + h_{44} + h_{45} + \tfrac{1}{2}(h_{46})$$

$$\% \, ^{18}O = \frac{^{18}O}{^{16}O + \, ^{18}O}$$

h_M is the peak height for mass number M minus the background M peak. No significant contribution from ^{17}O was found in $N_2 - O_2$ mixtures. In the $CO - CO_2$ mixtures any air leak into the gas holder during transfer to the mass spectrometer gave a h_{32} peak. This peak was generally very small but was multiplied by a factor N (previously determined from h_{28}/h_{32} for air as 4.5) and subtracted from the h_{28} peak to allow for N_2 leaked in

The % O_2 or CO/CO_2 ratio in the gases was calculated from the peak heights as shown after the tables.

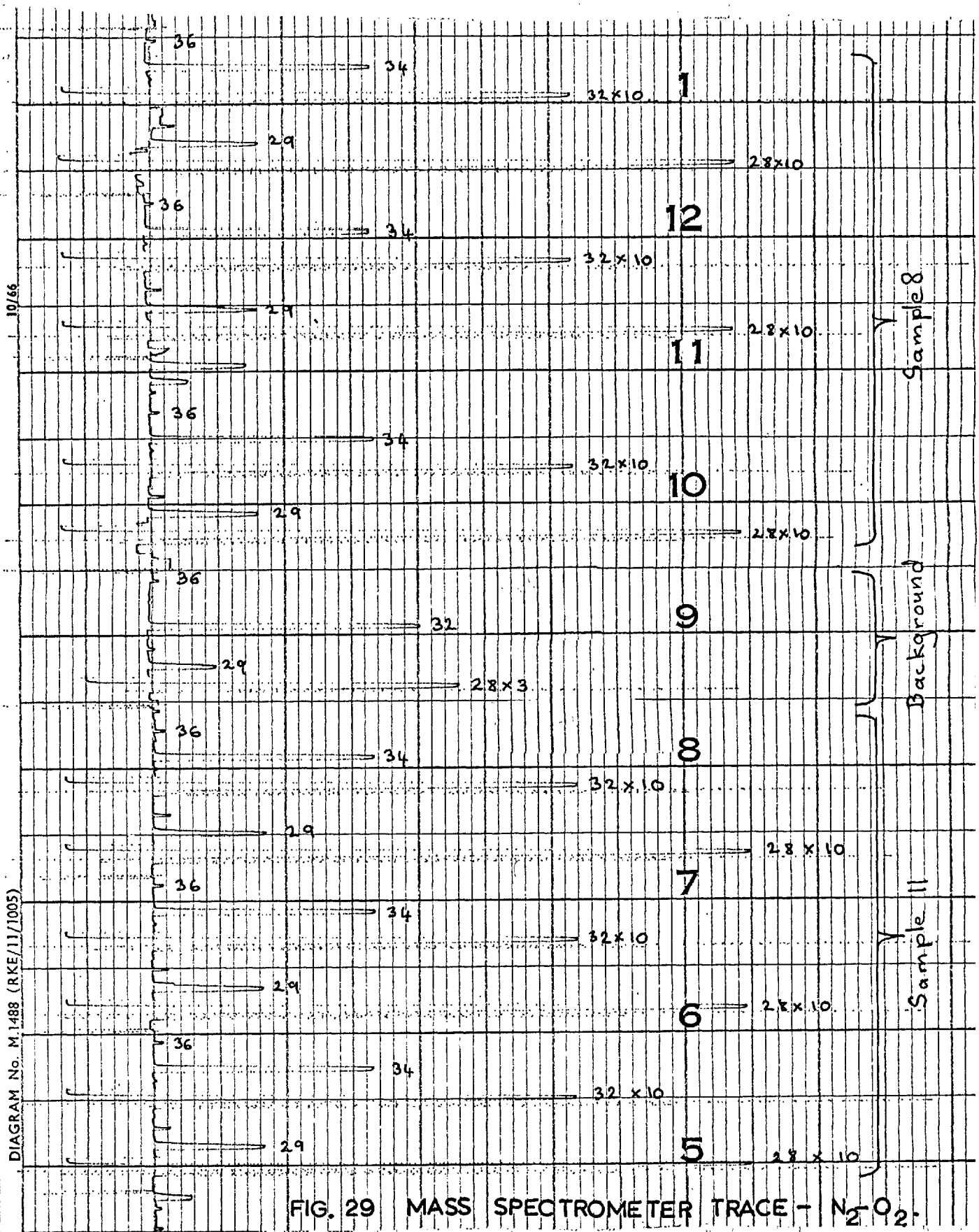

FIG. 29 MASS SPECTROMETER TRACE - N_2 O_2.

Table 4.

Peak heights from figure 29 for run 49.

$Ce_{0.6}Y_{0.4}O_{1.80}$ T = 1148°C

Sample.	Peak heights. h_{28}	h_{32}	h_{34}	h_{36}	^{16}O	^{18}O	$\%^{18}O$	$\frac{h_{28}}{h_{32}+h_{34}+h_{36}}$
(11) (i)	515	384	16.5	0.8	372	8.65	2.27	1.13
(ii)	512	386	16.7	0.8	374	8.75	2.28	1.12
(iii)	516	386	16.7	0.8	374	8.75	2.28	1.13
Back-ground	84.	20.2	-	0.4				
(8) (i)	511	385	16.8	0.8	373	8.80	2.30	1.11
(ii)	505	384	16.8	0.7	372	8.80	2.31	1.10
(iii)	509	383	16.8	0.7	371	8.80	2.32	1.11
Back-ground.	86	20.4	-	0.3				

The percentage oxygen in the gas was found by comparing the ratio $h_{28}/(h_{32} + h_{34} + h_{36})$ with that for run 1 where, from the gases added $\%N_2 / \%O_2 = 0.89$

Run 1: $h_{28}/(h_{32} + h_{34} + h_{36}) = 1.5$, $\%N_2/\%O_2 = 0.89$

Run 49: $h_{28}/(h_{32} + h_{34} + h_{36}) = 1.2 \pm 1$, $\therefore \%N_2/\%O_2 = 0.71$.

Therefore $\%O_2 = 58\%$

and $P_{O_2} = \frac{258}{760} \times 0.58 = 0.20$ atm.

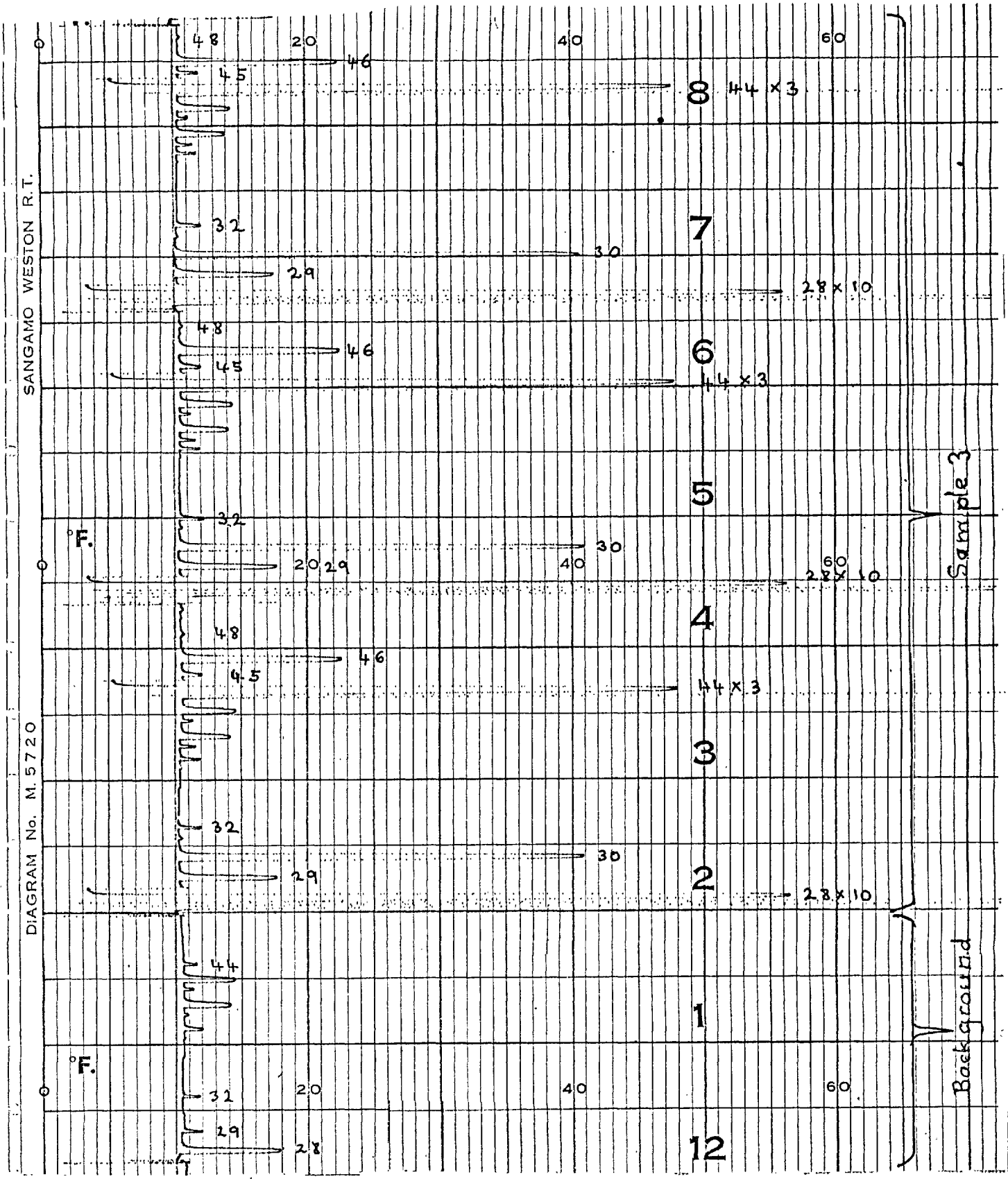

FIG. 30 MASS SPECTROMETER TRACE - $CO-CO_2$.

Table 5.

Peak heights from figure 30, for run 31

$Th_{0.9}\ Y_{0.1}\ O_{1.95}$, T = 1149°C

Sample.	Peak heights								$h_{32} \times \frac{16_O}{N}$		^{18}O	$\%^{18}O$	h_{28}/h_{44}
	h_{28}	h_{29}	h_{30}	h_{32}	h_{44}	h_{45}	h_{46}	h_{48}					
Back-ground	7.8	1.6	-	1.5	1.0	-	-	-					
(3)													
(i)	531	7.5	30.6	1.8	128.1	1.6	12.1	0.2	1	400	21.55	5.10	4.1
(ii)	528	7.5	30.7	1.8	127.8	1.5	12.0	0.2	1	398	21.55	5.12	4.1
(iii)	526	7.4	30.5	1.9	127.4	1.6	12.0	0.2	2	395	21.45	5.15	4.1

In previous runs with addition of mixtures from the gas handling system of accurately known CO/CO_2 ratio it was found that $CO/CO_2 = 2 \times h_{28}/h_{44}$. Thus $CO/CO_2 = 8.2$

Appendix 2.

Computer Programs.

Fortran IV programs were developed to obtain Mt/M_∞ as a function of $(Dt/\ell^2)^{\frac{1}{2}}$ for finite rate of the gas-solid interface reaction during exchange with specimens of geometry approximating to infinite plane sheets and spheres.

(1) Infinite Plane Sheet Geometry.

Equation (2.5) is the expression for the uptake of gas by an infinite plane sheet, assuming that a first order surface exchange reaction contributes to the overall rate. This is:

$$Mt/M_\infty = 1 - \frac{2(1+\alpha)}{\alpha} \sum_{a=1}^{\infty} \frac{\exp(-q_a^2 Dt/\ell^2)}{T^2 + q_a^2 + T + 2/\alpha}$$

where q_a is the non-zero, positive root of $\tan q_a = q_a/T$

$T = Q\, q_a^2 - 1/\alpha$

$Q = DS/K$

K = surface exchange coefficient, cm/sec.

S = surface to volume ratio.

ℓ = half thickness of sheet.

α = ratio of number of moles of solute in gas to number of moles in solid.

t = elapsed time

The Fortran IV computer program for solution of this equation is set out in table 6. Plots of Mt/M_∞ vs. $(Dt/\ell^2)^{\frac{1}{2}}$ produced by this program are shown in figure 31 for $\lambda = 0.57$ and various Q values. (λ is the final fractional uptake $= \frac{1}{1+\alpha}$)

(2) Spherical Geometry

Equation (2.4) is the expression for the uptake of gas by a sphere, assuming that a first order surface exchange reaction contributes to the overall rate. This is:

TABLE 6. PLANE SHEET

```
      DIMENSION VQ(8),SQDTR(40),NOR(40),SUM(40),AMOM(40)
      PI=3.1416
      VLAM=0.57
      ALF=(1./VLAM)-1.
      SPR=2.*(1.+ALF)/ALF
      READ (5,2002) (VQ(IQ),IQ=1,8,1)
 2002 FORMAT (10X,F5.2)
      WRITE (6,2002) (VQ(IQ),IQ=1,8,1)
      DO 9 IQ=1,8,1
      VNOR=0.
      SQDTR(1)=0.025
      DO 25 IZ=1,40,1
      AMOM(IZ)=0.
      NOR(IZ)=0.
      SUM(IZ)=0.
   25 CONTINUE
      DO 44 IN=1,20,1
      VN=IN-1
      DIF=(1./(VQ(IQ)*ALF))**0.5-(VN+0.5)*PI
      IF (ABS(DIF).LE.1.0) GO TO 24
   44 CONTINUE
      VN=-1.0
      DIF=0.0
   24 AQA=((VNOR+0.5)*PI)
      B=-1.
      IF (VNOR.EQ.VN) B=-(ABS(DIF))/10.
      Z=10000000.
   10 B=-B/2.
    1 AQA=AQA+B
      REM=Z
      ALS=TAN(AQA)
      T=(VQ(IQ)*AQA**2)-1./ALF
      ARS=AQA/T
      Z=ALS-ARS
      IF (T.GE.0.) GO TO 100
      IF ((REM*REM)**0.5.LT.0.0001) GO TO 3
      IF ((Z*Z)**0.5.GT.(REM*REM)**0.5) GO TO 10
      GO TO 1
  100 AQA=((VNOR+0.5)*PI)
      B=1.0
      IF (DIF.LT.0.0) B=(ABS(DIF))/4.
      GO TO 104
  101 AQA=((VNOR+0.5)*PI)
  102 B=1.0
  104 Z=10000000.
  110 B=-B/4.
  111 AQA=AQA+B
      REM=Z
      ALS=TAN(AQA)
      T=(VQ(IQ)*AQA**2)-1./ALF
      ARS=AQA/T
      Z=ALS-ARS
      IF ((REM*REM)**0.5.LT.0.0001) GO TO 3
      IF((Z*Z)**0.5.GT.(REM*REM)**0.5) GO TO 110
      GO TO 111
    3 NOO=0
      WRITE (6,1000) AQA,REM
 1000 FORMAT (5X,3HXA=,F7.4,4X,F14.12)
      VNOR=VNOR+1.
```

TABLE 6 (Cont.)

```
      SQA=AQA**2
      DO 4 IN=2,40,1
      SQDTR(IN)=SQDTR(IN-1)+0.025
      FUNC=EXP(-SQA*SQDTR(IN)**2)
      FUNC=FUNC/(T*T+AQA**2+T+2./ALF)
      IF (FUNC*SPR.LT.0.001)GO TO 30
      SUM(IN)=SUM(IN)+FUNC
      NOR(IN)=NOR(IN)+1
      IF (NOR(IN).GT.20) GO TO 30
      GO TO 4
   30 NOO=NOO+1
      IF (NOO.EQ.39) GO TO 500
    4 CONTINUE
      IF (T.GT.0.) GO TO 101
      GO TO 24
  500 DO 501 NS=2,40,1
      AMOM(NS)=1.-(SPR*SUM(NS))
  501 CONTINUE
      WRITE (6,1010) VQ(IQ),ALF,VLAM
 1010 FORMAT (1H1,21HPLANE SHEET DIFFUSION // 6X,2HQ=,F4.1,3X,
     16HALPHA=,F6.4,2X,7HLAMBDA=,F4.2 / 6X,12H(DT/R*R)**.5,2X,5HMT/MI
     2 9X,11HNO OF ROOTS)
      WRITE (6,1011) (SQDTR(IW),AMOM(IW),NOR(IW), IW=2,40,1)
 1011 FORMAT (8X,F6.4,6X,F6.4,9X,I2)
    9 CONTINUE
      STOP
      END
```

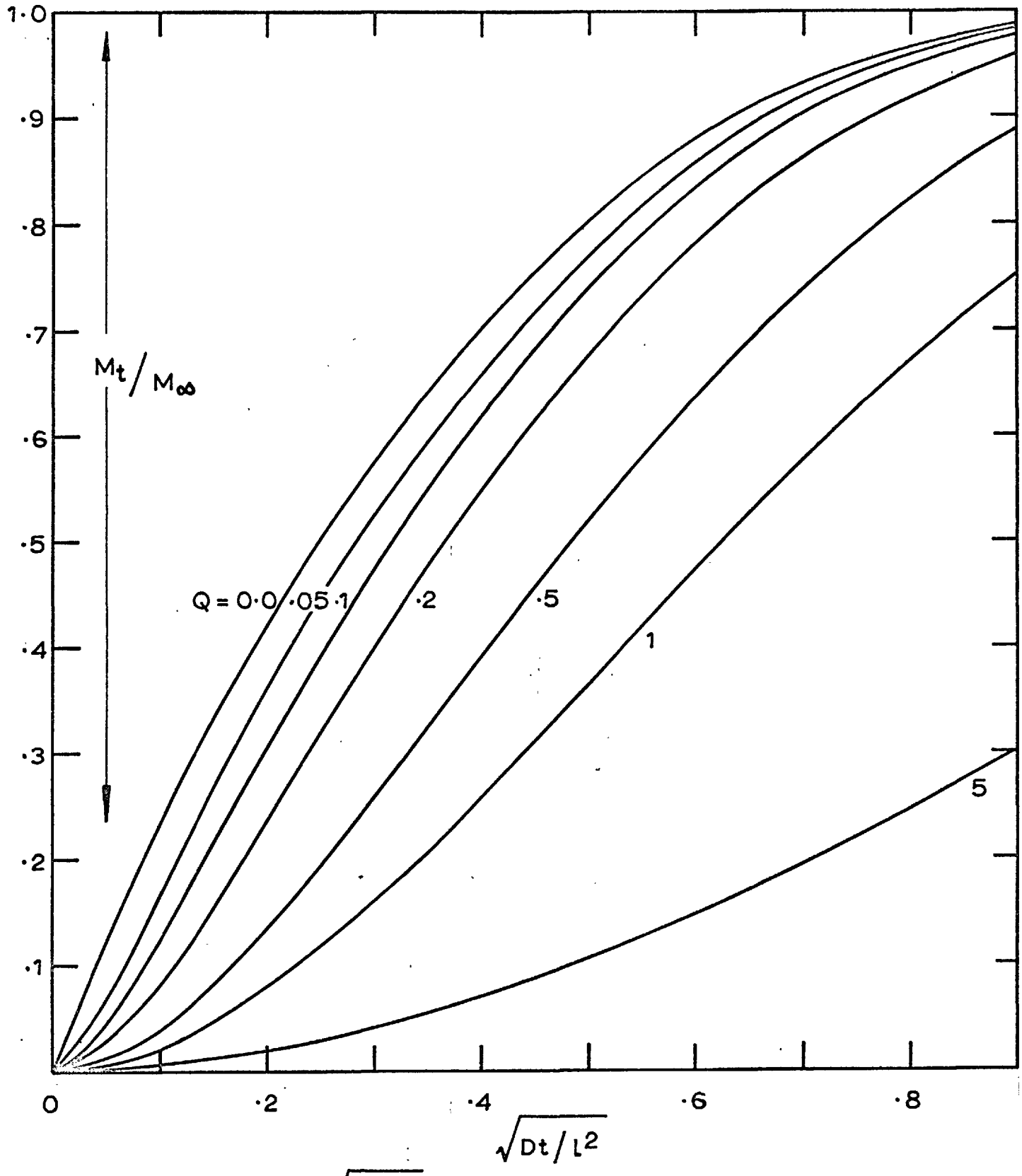

Fig. 31. M_t / M_∞ vs. $\sqrt{Dt/l^2}$ FOR PLANE SHEET GEOMETRY.

$\lambda = 0{\cdot}57.$

$$Mt/M\infty = 1 - \frac{2(1+\alpha)}{3\alpha} \sum_{a=1}^{\infty} \frac{q_a^2 \exp(-q_a^2 Dt/r^2)}{F(q_a^2 Q/9 + 1/\alpha) + F^2 + q_a^2 E^2 - 2E/\alpha}$$

where q_a is the non-zero, positive root of $\tan q_a = q_a E/F$

$$E = 1/\alpha - Q\, q_a^2/9$$

$$F = 1/\alpha + Q\, q_a^2\, (3/Q - 1)\, /9$$

The Fortran IV computer program for the solution of this equation is set out in table 7. Figure 32 shows plots of $Mt/M\infty$ vs. $(Dt/r^2)^{\frac{1}{2}}$ for λ = 0.19 and various Q values obtained using this program.

TABLE 7. SPHERE

```
C  PROGRAM TO FIND MT/MI AS A FUNCTION OF (1)SQDTR (2) ALPHA (3) Q - VALUES
      DIMENSION  VQ(6),SQDTR(22),NOR(22),SUM(22),AMOM(22)
      READ (5,1100)(VQ(IQ),IQ=1,6,1)
 1100 FORMAT (10X,F4.1)
      WRITE (6,1100) (VQ(IQ),IQ=1,6,1)
      PI=3.1416
      VLAM=0.19
      ALF=(1./VLAM)-1.
      SPR=2.*(1.+ALF)/(3.*ALF)
      X=1./ALF
      SQDTR(1)=0.025
      DO 9 IQ=1,6,1
      DO 31 IZ=1,22,1
      NOR(IZ)=0.0
      AMOM(IZ)=0.0
      SUM(IZ)=0.0
   31 CONTINUE
      VNOR=0.
C     FIND VALUE FOR QA
   24 AQA=((VNOR+0.5)*PI)
      B=-1.0
      Z=10000000.
   10 B=-B/2.
    1 AQA=AQA+B
      REM=Z
      ALS=TAN(AQA)
      Y=VQ(IQ)*(AQA**2)/9.
      F=X-Y+(AQA**2)/3.
      E=X-Y
      ARS=AQA*E/F
      Z=ALS-ARS
      IF ((REM*REM)**0.5.LT.0.0001) GO TO 3
      IF ((Z*Z)**0.5.GT.(REM*REM)**0.5) GO TO 10
      GO TO 1
C  CALCULATE SUMS FOR THIS VALUE OF QA
    3 NRR=0
      VNOR=VNOR+1.0
      DO 5 IN=2,21,1
      SQDTR(IN)=SQDTR(IN-1)+0.025
      SQA=AQA**2
      FUNC=(SQA*EXP(-SQA*SQDTR(IN)**2))/(F*(X+Y)+F*F+SQA*E*E-2.*E/ALF)
      IF (FUNC*SPR.LT.0.001) GO TO 30
      NOR(IN)=NOR(IN)+1
      SUM(IN)=SUM(IN)+FUNC
      IF (NOR(IN).GT.20) GO TO 30
      GO TO 5
   30 NRR=NRR+1
      IF (NRR.EQ.20)GO TO 6
    5 CONTINUE
      GO TO 24
    6 DO 7 NS=2,21,1
      AMOM(NS)=1.-(SPR*SUM(NS))
    7 CONTINUE
C  WRITE OUT VALUES OF MT/MI FOR EACH ALPHA AND Q
      WRITE (6,1001) VQ(IQ),ALF,VLAM
 1001 FORMAT(1H),5X,30HSOLUTION OF DIFFUSION EQUATION / 6X,2HQ=,F4.1,
     13X,6HALPHA=,F6.4,2X,7HLAMBDA=,F4.2 // 6X,12H(DT/R*R)**.5,
     2 2X,5HMT/MI,9X,11HNO OF ROOTS)
      WRITE (6,1002)(SQDTR(IW),AMOM(IW),NOR(IW), IW=2,21,1)
 1002 FORMAT (8X,F6.4,6X,F6.4,9X,I2)
    9 CONTINUE
      STOP
      END
```

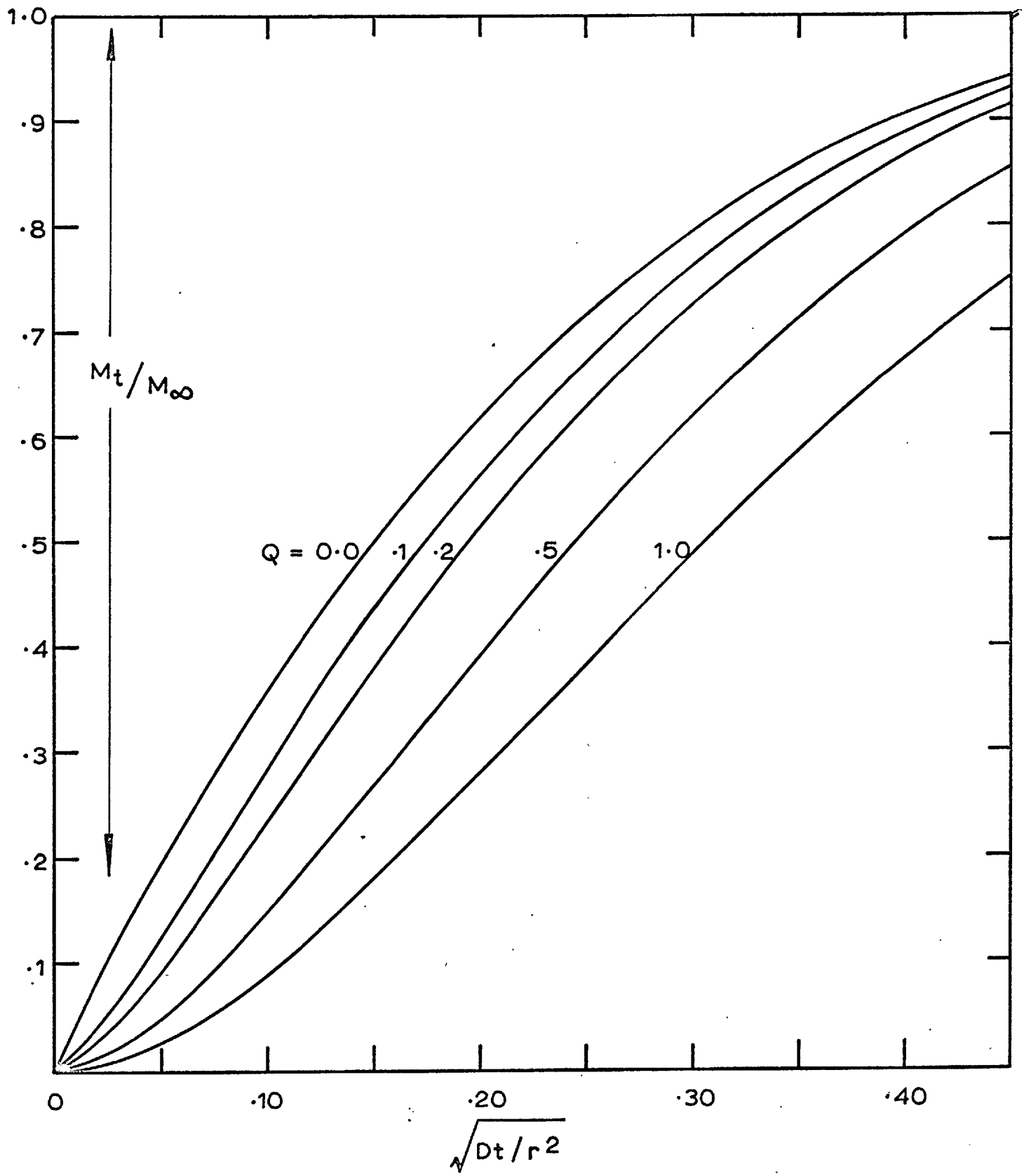

Fig.32. M_t / M_∞ vs. $\sqrt{Dt/r^2}$ FOR SPHERICAL GEOMETRY.

$\lambda = 0.19$.

Appendix 3

Sample Calculation.

Run 49 $Ce_{0.600}\ Y_{0.400}\ O_{1.800}$ fired in $P_{O_2} = 0.21$ at 1148°C

Weight of sample = 0.1878g.

Shape. - cube.

Molecular weight for one mole of oxygen = 164.8

Fraction of oxygen in the gas = 0.58.

Gas pressure during run = 258 torr

Volume of gas handling system = 180 ml.

Change in pressure due to expansion = 153 torr.

Room temperature = 22°C

Time (min)	$z\%^{18}O$
Zero - 5	4.90
Zero	4.90
5	3.19
10	2.73
16	2.53
20	2.44
30	2.31
40	2.28
50	2.25
60	2.23

Moles of oxygen in gas, $Ng = \frac{180}{22,400} \times \frac{273}{295} \times \frac{153}{760} \times 0.58 = 8.70 \times 10^{-4}$ moles.

Moles of oxygen in solid, $Ns = \frac{0.1878}{164.8} = 1.14 \times 10^{-3}$ moles

$\alpha = \frac{N_g}{N_S} = 0.763,$

Final fractional uptake, $\lambda = \frac{1}{1+\alpha} = 0.567$

Total number of moles of O^{18} = Ng x fraction ^{18}O in gas - N_S x fraction ^{18}O natural

$= (8.70 \times 10^{-4} \times 0.049) + (1.14 \times 10^{-3} \times 0.002)$

$= 4.49 \times 10^{-5}$ moles.

Total number of moles of $^{16}O = (8.70 \times 10^{-4} \times 0.951) + (1.14 \times 10^{-3} \times 0.998)$

$= 1.97 \times 10^{-3}$

Mole fraction $^{18}O = \frac{4.49 \times 10^{-5}}{2.01 \times 10^{-3}}$

$= 0.0224$

Number of moles of ^{18}O taken up by solid at infinite time,

$M\infty = N_s \times (\text{fraction } ^{18}O - \text{natural } ^{18}O)$

$= 1.14 \times 10^{-3} \times (0.0224 - 0.0020)$

$= 2.32 \times 10^{-5}$

For time 5 minutes.

Mt = (Initial fraction O^{18} - Fraction O^{18} at time) x moles of O^{18} in gas.

$= 0.0171 \times 8.70 \times 10^{-4}$

$= 1.49 \times 10^{-5}$

$M_t/M_\infty = 0.641$

This Mt/M∞ value is that for a cube. O'Keefe[48] has published a solution for the diffusion equation for a rectangular parallelepiped, which reduced to that of a cube. If $(Mt/M\infty)_{\underline{\underline{III}}}$ is the fractional uptake for the cube, and $(Mt/M\infty)_{\underline{I}}$ the fractional uptake for a plane sheet.

$$(Mt/M\infty)_{\underline{I}} = 1 - \sqrt[3]{1 - (Mt/M_\infty)_{\underline{\underline{III}}}}$$

In table 8 values of $(Mt/M\infty)_{\underline{\underline{III}}}$ and the derived values for $(Mt/M\infty)_{\underline{I}}$ are given;

Table 8. Calculations for run 49

			Q = 0.00		Q = 0.05		Q = 0.1	
Time	$(M_t/M_\infty)_{III}$	$(M_t/M_\infty)_I$	$(Dt/\ell^2)^{\frac{1}{2}}$	Dt/ℓ^2	$(Dt/\ell^2)^{\frac{1}{2}}$	Dt/ℓ^2	$(Dt/\ell^2)^{\frac{1}{2}}$	Dt/ℓ^2
5	0.641	0.290	.126	1.59×10^{-2}	.160	2.56×10^{-2}	.190	3.61×10^{-2}
10	0.815	0.430	.204	4.16	.240	5.77	.271	7.35
16	0.889	0.519	.260	6.76	.294	8.63	.327	10.7
20	0.923	0.574	.298	8.90	.335	11.2	.366	13.4
30	0.970	0.689	.390	15.2	.425	18.0	.456	20.8
40	0.982	0.738	.435	18.9	.470	22.1	.500	25.0
50	0.992	0.800	.498	24.8	.531	28.2	.562	31.6

The diffusion equation for plane sheet geometry with finite phase boundary reaction rate was used to produce plots of M_t/M_∞ vs. $(Dt/\ell^2)^{\frac{1}{2}}$ as shown in Appendix 2. Typical plots for $\lambda = 0.57$ and a series of Q values are shown in figure 31.

Table 8 shows values of Dt/ℓ^2 found using different Q values. These are plotted against time in figure 33, The straight line plot going through the origin is used to obtain D/ℓ^2 and Q.

$$D/\ell^2 = 9.26 \times 10^{-5} \text{ sec}^{-1}$$

$$Q = 0.05$$

ℓ^2 can be obtained from the weight, and density of the specimen, obtained from tables 1 and 9.

$$\text{Volume} = \frac{\text{weight}}{\text{density}} = \frac{0.1878}{5.56} = 3.37 \times 10^{-2} = (2\ell)^3$$

$$\ell = 0.166 \qquad \ell^2 = 2.76 \times 10^{-2}$$

$$D = 2.56 \times 10^{-6} \text{ cm}^2/\text{sec.}$$

$$K = \frac{D \times S}{Q}$$

$$S = \frac{\text{surface}}{\text{anea}} = \frac{3}{\ell}$$

$$K = \frac{2.56 \times 10^{-6} \times 3}{0.05 \times 0.166}$$

$$= 9.26 \times 10^{-4} \text{ cm/sec.}$$

From figure 33 it can be seen that the maximum error occurs through the estimation of the appropriate Q value. The scatter of points about the straight line is not very great and of the three Q values drawn, $Q = 0.05$ gives a better straight line through the origin than $Q = 0.00$ and $Q = 0.1$. An estimate of the possible error from choice of the incorrect Q value can be obtained by drawing a straight line through the origin for the other Q values, and finding the difference from the selected value.

For $Q = 0.00$

$$D/\ell^2 = 7.91 \times 10^{-5} \text{ sec}^{-1}$$

$$D = 2.18 \times 10^{-6} \text{ sec}^{-1}$$

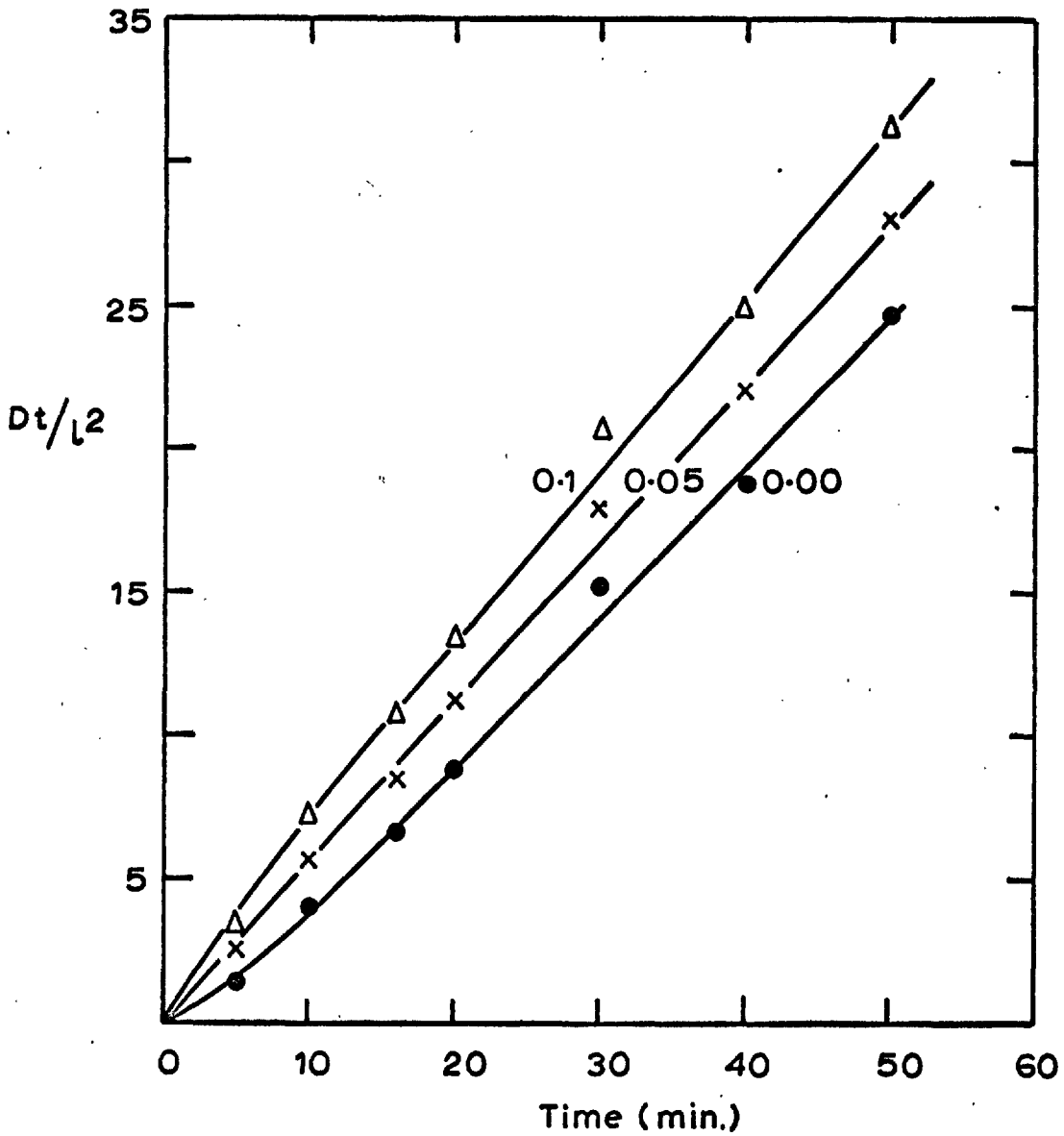

Fig.33. Dt/l^2 vs. t FOR RUN 49

For Q = 0.1

$D/\ell^2 = 1.07 \times 10^{-4}$

$D = 2.95 \times 10^{-6}$ cm^2/sec.

$K = 5.31 \times 10^{-4}$ cm/sec.

Thus $D = 2.6 \pm 0.4 \times 10^{-6}$ gives an estimated error of $\pm$ 15%. The error in K is seen to be much greater than this - $\pm$ 50%.

Appendix 4.

Tabulated Results.

The results of exchange experiments are set out in tables 9 and 10. Table 11 contains additional information required to calculate the exchange parameters for the discs of thoria-yttria.

Table 9 lists details of specimens, equilibrium and exchange gases, and the results for log D and log K of each ran. The symbols under geometry are explained at the back of the table. The equilibrium and exchange gases are designated EQ and EX respectively. The higher oxygen pressure gases were N_2-O_2 mixtures and the lower ones were CO-CO_2 mixtures. N_g is the number of moles of oxygen in the gas. λ is the final fractional uptake ($\lambda = \frac{1}{1+\alpha}$).

Table 10 lists the results of mass spectrometer analyses of the gas samples taken for each run and the Mt/M_∞ ratio calculated for each sample. For the cubic specimens the Mt/M_∞ value is that calculated for the equivalent plane sheet solution (i.e. (Mt/M_∞) I of appendix 3. Times are in minutes.

Table 11 contains the dimensions of the thoria-yttria discs.

Table 9 Details and results of exchange experiments.

Run	Sample	Geom	Wt.(g)	T°C	$-\log Po_2$ EQ	EX	n_g x10^{-4}		-log D	-log K
1	$Th_{0.850}Y_{0.150}O_{1.925}$	P,t	0.7733	998	0.68	0.68	11.8	0.72	7.34	5.35
2	$Th_{0.850}Y_{0.150}O_{1.925}$	P,t	0.8723	875	0.68	0.80	6.10	0.85	7.72	7.16
3	CeO_2	S,sp, **	0.0668	990	0.68	0.68	10.2	0.28	7.98	5.62
4	CeO_2	S,c,**	0.0554	911	0.68	0.68	10.2	0.24	8.33	5.55
5	CeO_2	S,c	0.0599	957	0.68	0.70	10.75	0.26	7.94	5.17
6	$Th_{0.850}Y_{0.150}O_{1.925}$	P,t	0.3252	1009	0.68	0.68	10.2	0.56	7.41	5.22
7	$Th_{0.850}Y_{0.150}O_{1.925}$	P,t	0.3744	1081	0.68	0.70	11.1	0.57	7.19	5.79
8	CeO_2	S,c	0.0619	1115	0.68	0.54	15.1	0.19	7.63	-
9	CeO_2	S,sp,**	0.1004	1184	0.68	0.66	9.50	0.38	7.49	-
10	CeO_2	S,c, **	0.0920	890	0.68	0.66	9.50	0.36	8.50	6.09
11	CeO_2	S,sp,*,**	0.0912	1101	0.30	0.29	23.1	0.19	7.95	5.63
12	CeO_2	S,sp,*,**	0.1069	1105	1.70	1.55	1.03	0.86	7.54	6.02
13	CeO_2	S,c	0.0407	1099	1.00	0.89	4.84	0.33	7.69	4.56
15	CeO_2	S,c	0.0320	1005	1.70	1.51	0.97	0.66	7.71	5.85

Table 9 cont.

Run	Sample	Geom.	Wt.(g)	T°C	EQ	EX	$n_g \times 10^{-4}$	λ	-logD	-logK
16	CeO_2	S,c	0.0449	904	1.70	1.54	0.92	0.74	8.01	6.20
17	Blank			1100		0.68				
18	$CeO_{1.92}$	S,c	0.0631	1089	12.5	12.7	11.1	0.24	6.74	-
19	$CeO_{1.92}$	S,c	0.0593	974	14.8	15.2	9.66	0.26	6.94	-
20	$CeO_{1.92}$	S,c	0.0734	895	17.7	18.2	7.92	0.34	6.94	-
21	$CeO_{1.92}$	S,c	0.0475	855	19.4	19.4	8.12	0.25	7.21	4.71
22	$CeO_{1.80}$	S,c	0.1085	1130	15.9	15.6	7.60	0.43	5.82	3.73
23	$CeO_{1.80}$	S,c	0.0646	1015	18.3	17.2	7.47	0.32	5.87	4.11
24	$CeO_{1.80}$	S,c	0.0632	912	21.1	19.4	7.49	0.31	5.86	4.40
25	$CeO_{1.80}$	S,c	0.0536	1086	16.3	16.0	7.50	0.28	5.68	3.49
26	CeO_2	M,c	0.2555	1140	0.68	0.60	11.8	0.56	7.30	--
28	$Th_{0.900}Y_{0.100}O_{1.950}$	P,t	0.9552	990	15.0	16.4	6.90	0.85	7.71	5.36
29	$Th_{0.900}Y_{0.100}O_{1.950}$	P,t	0.6148	908	16.4	17.8	7.10	0.77	7.72	5.12
30	$Th_{0.900}Y_{0.100}O_{1.950}$	P,t	1.4131	1097	13.3	14.0	7.39	0.88	7.29	5.04

Table 9 cont.

Run	Sample	Geom	Wt.(g)	T°C	-log Po_2 EQ	-log Po_2 EX	n_g x10^{-4}	χ	-logD	-logK
31	$Th_{0.900}Y_{0.100}O_{1.950}$	P,t	0.9160	1149	12.3	13.7	7.15	0.84	7.05	4.47
32	CeO_2	M,c,	0.3543	924	0.68	0.85	6.55	0.76	8.12	-
33	CeO_2 Prep. 1	P,c,*	0.0481	988	0.68	0.64	10.8	0.21	7.85	-
34	CeO_2 Prep. 1	P,c,*	0.1093	988	0.68	0.66	10.2	0.38	7.55	-
35	CeO_2 Prep. 1	P,c,*	0.1120	1081	0.68	0.66	9.75	0.40	7.28	-
36	$CeO_{1.92}$ Prep 1	P,c,*	0.1331	915	17.3	17.3	7.40	0.50	6.38	-
37	$CeO_{1.92}$ Prep 1	P,c,*	0.1029	1011	14.5	14.5	6.61	0.47	6.15	-
38	$Zr_{0.844}Y_{0.156}O_{1.920}$	S,c	0.1391	1002	0.68	0.68	9.59	0.54	6.78	4.76
39	$Zr_{0.844}Y_{0.156}O_{1.920}$	S,c	0.1196	850	0.68	0.69	9.58	0.50	6.99	5.36
40	$Zr_{0.844}Y_{0.156}O_{1.920}$	S,c	0.1536	1151	0.68	0.69	9.02	0.57	6.52	4.23
41	$Zr_{0.844}Y_{0.156}O_{1.920}$	S,c	0.1449	950	15.9	16.5	7.34	0.61	6.82	4.52
43	$Zr_{0.850}Y_{0.150}O_{1.925}$	P,c	0.0497	1157	0.68	0.74	8.05	0.33	6.94	4.47
44	$Zr_{0.850}Y_{0.150}O_{1.925}$	P,c	0.0436	837	0.68	0.77	7.80	0.30	7.88	5.42
45	$Zr_{0.850}Y_{0.150}O_{1.925}$	P,c	0.0347	1010	0.68	0.80	7.12	0.28	7.22	4.70

Table 9 cont.

Run	Sample	Geom	Wt.(g)	T°C	$-\log Po_2$ EQ	$-\log Po_2$ EX	n_g x10^{-4}	λ	-log D	-log K
46	$Ce_{0.900}Y_{0.100}O_{1.950}$	P,c	0.0792	1148	0.68	0.62	10.4	0.31	6.75	4.03
47	$Ce_{0.900}Y_{0.100}O_{1.950}$	P,c	0.0944	838	0.68	0.68	9.49	0.37	7.58	5.18
48	$Ce_{0.900}Y_{0.100}O_{1.950}$	P,c	0.0768	1008	0.68	0.72	8.66	0.34	7.13	5.48
49	$Ce_{0.600}Y_{0.400}O_{1.800}$	P,c	0.1878	1148	0.68	0.70	8.70	0.57	5.59	3.03
50	$Ce_{0.600}Y_{0.400}O_{1.800}$	P,c	0.1517	849	0.68	0.74	8.06	0.53	6.46	4.48
51	$Ce_{0.600}Y_{0.400}O_{1.800}$	P,c	0.1626	1012	0.68	0.80	7.29	0.58	5.88	3.30
52	CeO_2 Prep. 2.	P,c	0.1136	944	0.68	0.76	7.84	0.45	7.81	5.17
53	CeO_2 Prep. 2	P,c	0.0788	1157	0.68	0.78	7.16	0.39	7.02	4.33
54	$Ce_{0.80}Y_{0.200}O_{1.900}$	P,c	0.1162	856	0.68	0.85	6.50	0.52	7.28	5.24
55	$Ce_{0.800}Y_{0.200}O_{1.900}$	P,c	0.1064	1154	0.68	0.80	7.19	0.47	6.53	3.87
56	$Ce_{0.800}Y_{0.200}O_{1.900}$	P,c	0.1018	1009	0.68	0.82	6.95	0.47	6.96	4.60
57	$CeO_{1.87}$ Prep 2.	P,c	0.0713	1102	14.0	14.0	6.64	0.37	6.24	-
58	$CeO_{1.80}$ Prep 2	P,c	0.1289	1108	15.9	15.6	5.80	0.54	5.48	3.15
60	$Zr_{0.844}Y_{0.156}O_{1.920}$	S,c	0.2549	982	0.68	0.89	5.89	0.77	6.60	4.66

P - Blycrystalline M - Multicrystal c - cube * - surface ground on 400# corundum

S - Single crystal Sp - Sphere t tablet ** - surface sand blasted

Table 10

Details of exchange experiments.

Run	Time	$\%O^{18}$	Mt/M_{∞}	Time	$\%O^{18}$	Mt/M_{∞}	Time	$\%O^{18}$	Mt/M_{∞}
1	0	8.85		15	8.01	.130			
	5	8.56	.047	30	7.40	.225			
2	0	19.90		120	19.47	.026	300	18.56	.080
	30	19.83	.004	180	18.87	.062			
	60	19.71	.011	240	18.70	.072			
3	0	6.74		45	6.57	.095	120	6.37	.205
	15	6.69	.028	60	6.51	.127			
4	0	6.68		120	6.46	.047	240	6.39	.067
	60	6.53	.033	180	6.40	.065			
5	0	6.59		120	6.18	.090	300	5.93	.154
	30	6.45	.020	180	6.14	.099			
	60	6.29	.064	240	5.96	.144			
6	0	6.48		30	5.54	.268	90	4.66	.518
	15	5.90	.165	62	5.04	.410	120	4.43	.581
7	0	8.31		45	6.55	.370	120	5.17	.660
	15	7.25	.222	60	6.20	.443	150	4.89	.719
	30	6.95	.286	90	5.65	.560	180	4.61	.777
8	0	6.41		30	6.11	.087	90	5.91	.159
	15	6.19	.064	60	6.00	.125	120	5.85	.181
9	0	6.17		45	5.52	.286	120	5.24	.409
	15	5.74	.190	60	5.40	.339			
	30	5.63	.242	90	5.31	.378			
10	0	6.21		90	6.07	.021	195	6.01	.031
	30	6.14	.010	120	6.06	.022	240	5.99	.035
	60	6.11	.015	150	6.04	.025	300	5.93	.044
							360	5.92	.046

Table 10 cont.

Run	Time	%O^{18}	Mt/M_{∞}	Time	%O^{18}	Mt/M_{∞}	Time	%O^{18}	Mt/M_{∞}
11	0	1.999		45	1.968	.090	125	1.942	.166
	15	1.983	.047	60	1.962	.108	150	1.934	.197
	30	1.975	.070	90	1.950	.142			
12	0	36.1		45	27.2	.288	105	21.5	.475
	15	32.0	.131	60	26.2	.320	120	21.0	.489
	30	30.7	.176	90	24.0	.392			
13	0	8.15		60	7.62	.070	105	7.34	.115
	15	7.95	.025	75	7.54	.084	120	7.19	.140
	30	7.84	.040	90	7.40	.105			
15	0	39.5		60	33.2	.090	105	28.7	.164
	47	36.6	.043	75	31.4	.119			
16	0	43.7		58	40.6	.033	106	39.2	.050
	15	42.8	.010	70	40.4	.035	115	39.6	.044
	47	41.2	.025	90	40.1	.039			
17	0	7.91		30	8.02		60	7.79	
	19	7.91		45	7.99		96	8.13	
	23	7.93		47	7.92				
18	0	7.66		45	6.50	2.92	75	6.25	.396
	15	6.85	.180	60	6.40	.330	90	6.24	.405
	30	6.52	.285	65	6.32	.365			
19	0	6.07		35	5.33	,200	76	5.07	.304
	15	5.44	.165	45	5.16	.265			
	30	5.35	.194	60	5.08	.299			
20	0	5.57		30	4.54	.240	60	4.40	.288
	5	5.17	.079	35	4.51	.250			
	15	4.78	.171	50	4.50	.255			

Table 10 cont.

Run	Time	$\%o^{18}$	Mt/M_{∞}	Time	$\%o^{18}$	Mt/M_{∞}	Time	$\%o^{18}$	Mt/M_{∞}
21	0	3.93		17	3.78	.059	40	3.66	.109
	10	3.84	.033	30	3.71	.086	45	3.65	.114
22	0	11.92		10	8.80	.269	20	8.15	.382
	5	10.01	.124	15	8.39	.324			
23	0	0.800		15	0.711	.199	60	0.626	.553
	5	0.757	.081	20	0.689	.251			
	10	0.725	.154	50	0.624	.569			
24	0	5.64		15	5.11	.118	40	4.26	.310
	5	5.45	.040	20	4.95	.160	50	4.39	.358
	10	5.28	.077	30	4.71	.232	60	4.50	.420
25	0	2.188		10	1.801	.338	20	1.694	.544
	5	1.949	.174	15	1.757	.406	30	1.662	.670
26	0	22.6		15	19.2	.100	30	17.9	.150
	5	20.8	.050	21	18.5	.124	36	17.7	.158
	10	19.6	.089	25	18.3	.131	40	17.6	.156
28	0	7.44		30	5.27	.329	120	3.29	.676
	15	5.93	.246	75	3.97	.566			
29	0	7.09		45	5.40	.318	90	4.66	.458
	15	6.05	.195	60	5.16	.362			
	30	5.69	.263	75	4.79	.431			
30	0	6.81		20	4.13	.437	50	2,92	.635
	5	5.54	.207	30	3.56	.530	60	2.65	.679
	10	4.82	.324	40	3.27	.578	70	2.55	.695
31	0	6.70		15	4.04	.490	30	3.31	.623
	5	5.12	.291	20	3.78	.539	35	3.12	.660
	10	4.52	.402	25	3.51	.587	40	3.03	.675
32	0	30.1		95	21.4	.149	180	19.0	.200
	30	24.4	.094	120	20.3	.171	210	18.4	.215
	60	22.6	.126	150	19.9	.181	240	17.7	.232

Table 10 cont.

Run	Time	$\%O^{18}$	Mt/M_∞	Time	$\%O^{18}$	Mt/M_∞	Time	$\%O^{18}$	Mt/M_∞
33	0	8.26		120	7.51	.172	241	7.41	.193
	59	7.80	.100	179	7.43	.190			
	89	7.73	.114	209	7.46	.181			
34	0	8.05		15	7.51	.064	40	7.07	.123
	5	7.71	.040	20	7.40	.078	50	7.01	.131
	10	7.56	.058	30	7.20	.105	60	6.89	.150
35	0	7.96		15	7.16	.095	30	6.79	.146
	5	7.58	.043	20	6.95	.124	35	6.84	.139
	10	7.34	.071	25	6.90	.130	40	6.69	.161
36	0	6.46		15	4.33	.312	30	4.02	.390
	5	5.08	.174	20	4.16	.351	35	3.96	.406
	10	4.56	.265	25	4.06	.379	40	3.91	.423
37	0	2.83		15	1.93	.354	30	1.76	.492
	5	2.16	.149	20	1.88	.390	35	1.71	.551
	10	1.99	.319	25	1.79	.464	40	1.67	.612
38	0	7.83		6	7.54	.025	12	7.33	.044
	2	7.72	.010	8	7.44	.033	15	7.15	.059
	4	7.60	.020	10	7.35	.040	20	6.92	.080
39	0	7.76		16	7.55	.019	50	7.12	.060
	6	7.72	.004	20	7.50	.024	60	7.11	.062
	10	7.67	.008	40	7.17	.054			
40	0	7.56		6	6.70	.074	15	6.00	.141
	2	7.23	.027	8	6.58	.085	20	5.80	.164
	4	6.94	.051	10	6.43	.099	25	5.49	.200
41	0	5.78		16	4.87	.099	40	4.08	.207
	5	5.39	.039	20	4.74	.114	53	3.98	.224
	10	5.00	.084	30	4.44	.154			
43	0	7.25		15	6.63	.099	40	6.33	.155
	5	7.05	.029	20	6.53	.116			
	10	6.81	.066	30	6.43	.136			

Table 10 cont.

Run	Time	δ^{18}	Mt/M	Time	$\%O^{18}$	Mt/M	Time	$\%O^{18}$	Mt/M
44	0	7.19		40	6.96	.036	80	6.84	.058
	10	7.14	.009	60	6.92	.044			
	31	7.05	.025	70	6.94	.040			
45	0	7.20		20	6.78	.079	50	6.56	.125
	5	7.14	.009	30	6.69	.098	60	6.48	.144
	10	7.05	.026	40	6.60	.116	70	6.36	.174
46	0	4.24		15	3.88	.110	30	3.69	.182
	5	4.07	.050	20	3.78	.147	35	3.62	.211
	10	3.97	.080	25	3.73	.165	40	3.56	.240
47	0	4.76		20	4.61	.030	50	4.48	.059
	5	4.74	.005	30	4.60	.034	60	4.52	.051
	10	4.71	.010	40	4.50	.055	70	4.47	.062
48	0	5.08		20	5.03	.011	50	4.93	.031
	10	5.07	.004	30	4.98	.020	60	4.88	.044
	15	5.00	.015	40	4.91	.036			
49	0	4.90		16	2.53	.519	40	2.28	.738
	5	3.19	.290	20	2.44	.574	50	2.25	.800
	10	2.73	.430	30	2.31	.689			
50	0	5.19		6	4.86	.044	13	4.59	.081
	2	5.10	.011	8	4.73	.061	17	4.46	.101
	4	4.95	.031	10	4.68	.069	20	4.36	.118
51	0	5.59		10	3.54	.301	25	2.83	.525
	3	4.69	.109	15	3.23	.379	30	2.80	.537
	6	4.04	.206	20	3.01	.446	35	2.73	.569
52	0	4.38		45	4.10	.052	90	4.00	.073
	15	4.24	.025	60	4.09	.055	105	3.99	.075
	30	4.14	.045	75	4.07	.059	120	3.96	.081

Run	Time	$\%O^{18}$	Mt/M_{∞}	Time	$\%O^{18}$	Mt/M_{∞}	Time	$\%O^{18}$	Mt/M_{∞}
53	0	4.52		30	4.00	.115	60	3.70	.199
	10	4.20	.068	40	3.91	.139	70	3.61	.227
	20	4.05	.104	50	3.76	.180	80	3.65	.215
54	0	5.06		15	4.88	.025	40	4.59	.067
	5	4.97	.011	20	5.76	.041	50	4.59	.067
	10	4.93	.018	30	4.74	.044	60	4.61	.065
55	0	3.89		10	3.32	.125	25	2.92	.238
	3	3.88	.001	15	3.13	.174	30	2.86	.259
	5	3.54	.074	20	2.96	.224	35	2.79	.284
							40	2.72	.310
56	0	3.87		10	3.61	.055	25	3.41	.100
	3	3.77	.020	15	3.53	.071	30	3.37	.110
	6	3.37	.029	20	3.47	.085	35	3.32	.122
57	0	5.05		10	3.83	.314	20	3.75	.345
	3	4.32	.160	13	3.80	.324	25	3.71	.361
	6	3.97	.261	16	3.74	.349	30	3.67	.380
58	0	3.46		9	2.02	.436	18	1.85	.561
	3	2.46	.245	12	1.90	.518	21	1.74	.696
	6	2.20	.346	15	1.81	.606			
60	0	4.37		12	3.57	.090	24	2.95	.176
	3	4.04	.035	17	3.23	.135	27	2.85	.193
	7	3.86	.055	21	3.12	.150	30	2.78	.208

Table 11

Dimension of Thoria-Yttria Specimens

Run No.	Sample	Thickness cm	Diameter cm
1	$Th_{0.85}Y_{0.15}O_{1.925}$	0.122	1.043
2	$Th_{0.85}Y_{0.15}O_{1.925}$	0.141	1.030
6	$Th_{0.85}Y_{0.15}O_{1.925}$	0.077	0.772
7	$Th_{0.85}Y_{0.15}O_{1.925}$	0.102	0.732
28	$Th_{0.90}Y_{0.10}O_{1.950}$	0.104	1.160
29	$Th_{0.90}Y_{0.10}O_{1.950}$	0.131	0.841
30	$Th_{0.90}Y_{0.10}O_{1.950}$	0.136	1.206
31	$Th_{0.90}Y_{0.10}O_{1.950}$	0.133	1.001

Appendix 5

$CeO_{(2-x)}$ Dissociation Pressures.

Figure 34 shows the dissociation pressure vs. x data of Bevan and Kordis[2] for $CeO_{(2-x)}$ at different temperatures. These were obtained by equilibration with CO - CO_2 or H_2 - H_2O mixtures and thermogravimetry.

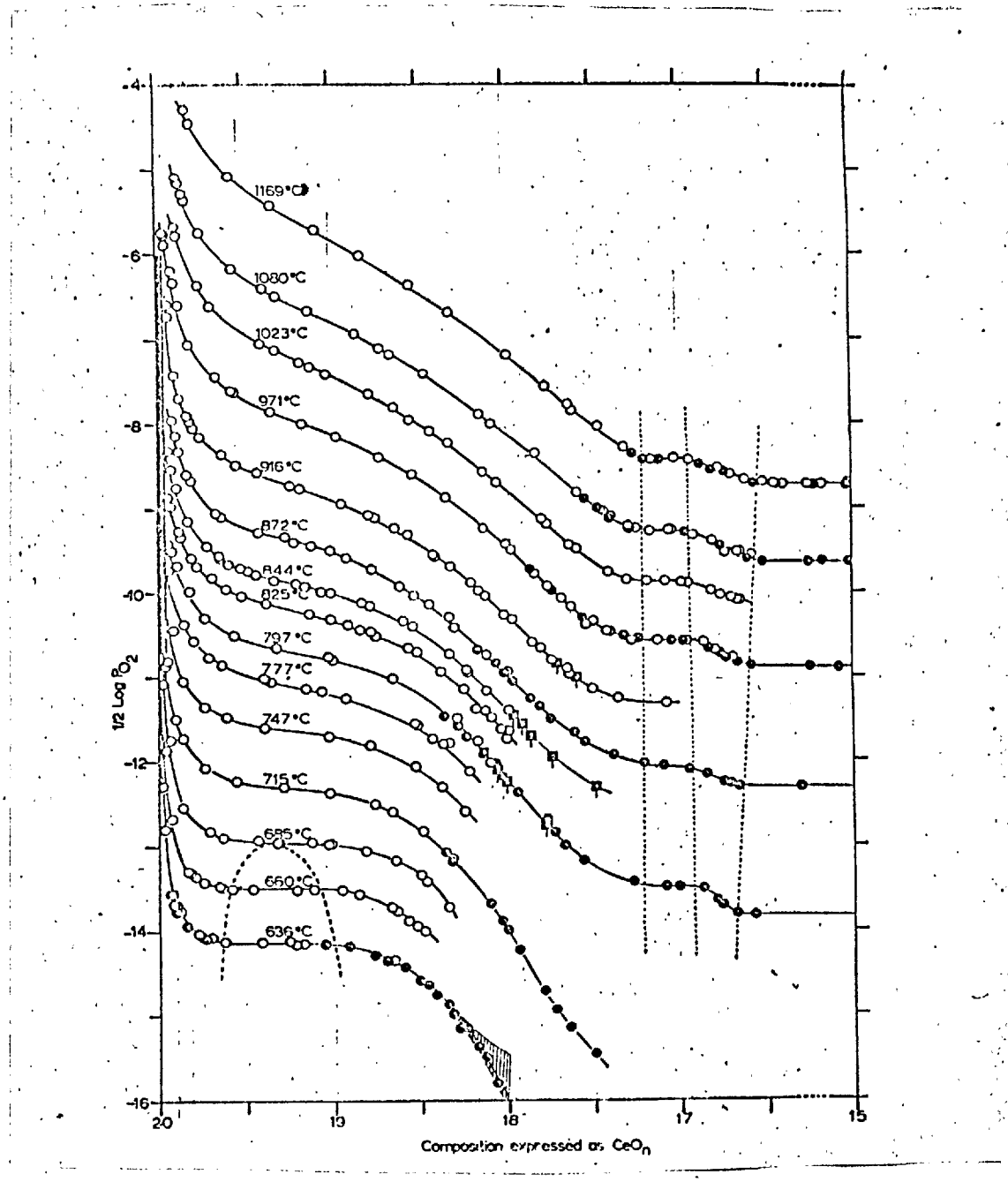

Fig. 34. Dissociation pressures vs. x in $CeO_{(2-x)}$.

ACKNOWLEDGEMENTS.

Advice, discussions, and helpful criticism from my supervisor, Dr. B.C.H. Steele, has been invaluable to me in this project, and I would like to express my sincere gratitude to him. I would also like to thank Professor F.D. Richardson for providing space within the Nuffield Research Group for me to do this work. Discussion and advice from members of the Group have been of help throughout my project.

I have much appreciated the ready co-operation of the staff at Imperial College with experimental problems and up keep of equipment. In particular I would like to thank Dr. White of the single crystal growing unit for supplying the ceria single crystals.

During innumerable visits to the Central Electricity Research Laboratories, Leatherhead, I have been greatly aided by the help and co-operation of Mr. A.C. Smith and his colleagues in the analytical chemistry section, in providing and maintaining their A.E.I. M.S.3. mass spectrometer for my use. I have much pleasure in thanking them.

Thanks are also due to the Chemistry Division of A.E.R.E., Harwell, for making available ^{18}O enriched water so that my work could be started while waiting for the arrival of enriched gases from Israel.

The position of Research Assistant in the Department of Metallurgy, sponsored by the Ministry of Defence, provided the financial support for this project.

J. T. Lloyd.